TITLE OF THE PROJECT: OPTIMAGRID SOE2/P2/E322

GT 2: Definition and Modeling

DELIVERABLE: D7 Micro – Grid computer models

ABSTRACT

In this deliverable a brief description of the study cases is given which will be modeled in Working Program GT3. In addition, the software used in each case is explanained briefly.

The test cases are installations or microgrids with a typology similar to some of the test cases analyzed in Deliverables 2 and 3 of Working Program GT2. A total number of six microgrids will be modeled, which are listed below:

1. Model of Microgrid at Walqa Technological Park,
2. Model of Microgrid at Sangüesa (CENER installations),
3. Model of Microgrid at Port of Bayonne,
4. Model of Rural Microgrid for Irrigation Pumping,
5. Model of Industrial Area with Small Workshops and Industrial Stores,
6. Model of AICIA microgrid facility.

CONTENTS

INDEX OF ILLUSTRATIONS

INDEX OF FIGURES

INDEX OF TABLES

1 INTRODUCTION

In this deliverable those study cases are introduced which will be modeledduring Optimagrid project. In the first deliverables of Working Program GT2 a database of SUDOE industrial areas and a quantitative and qualitative description of the test cases to analyze were developed. A total number of six microgrids will be modeled, which are listed below:

1. Model of Microgrid at Walqa Technological Park
2. Model of Microgrid at Sangüesa (CENER installations)
3. Model of Microgrid at Port of Bayonne
4. Model of Rural Microgrid for Irrigation Pumping
5. Model of Industrial Area with Small Workshops and Industrial Stores
6. Model of AICIA microgrid facility

For each one of the test cases a simple description of the area to model is done. After that the model of the cases is described or at least the way to set up the model. The final part of this deliverable contains a review of the software tools which will be used to develop the models.

This deliverable represents and introduction to Working Program GT3 with the results and analysis made by Working Program GT2.

2 MODEL OF MICROGRID AT WALQA TECHNOLOGICAL PARK

Walqa Technology Park (hereafter Walqa), located in Cuarte (Huesca), is home to many R & D centers specialized in new technologies, among which is the Foundation for the Development of New Hydrogen Technologies in Aragon (FHA) whose main objective is the development of new technologies related to hydrogen, renewable energies and promoting the incorporation of Aragon to economic activities consistent in the use of hydrogen as an energy carrier.

Illustration 1. Aerial view of Walqa

The micro grid presented in this document is integrated within the ITHER project (Infrastructure for Hydrogen Generation with Renewable Energy), belonging to FHA. The ultimate aim is to create a solid infrastructure with different renewable power generation technologies, allowing a laboratory for hydrogen production by electrolysis.

This section shows the different generators and systems that make up the micro grid Walqa. The section is divided into three main parts, wind, solar and electrical distribution connection.

2.1 Renewable Energy

2.1.1 Wind Power

The small wind farm consists of three wind turbines which 635kW of total power. The turbines are from "repowering", as currently on the market of first use is very difficult to find these kind of turbines, whit power less than 1 MW. In particular the generators installed are:

- Vestas V29, 225 kW.
- Enercon E33, 330 kW.
- Lagerway L80, 80 kW.

Figure 1. Characteristics of the wind turbines

As you can see the 3 turbines chosen have very different technical features to enhance the research orientation of FHA, having different types of generators and allowing greater flexibility in testing.
The distribution of these turbines along Walqa could be seen in the image below.

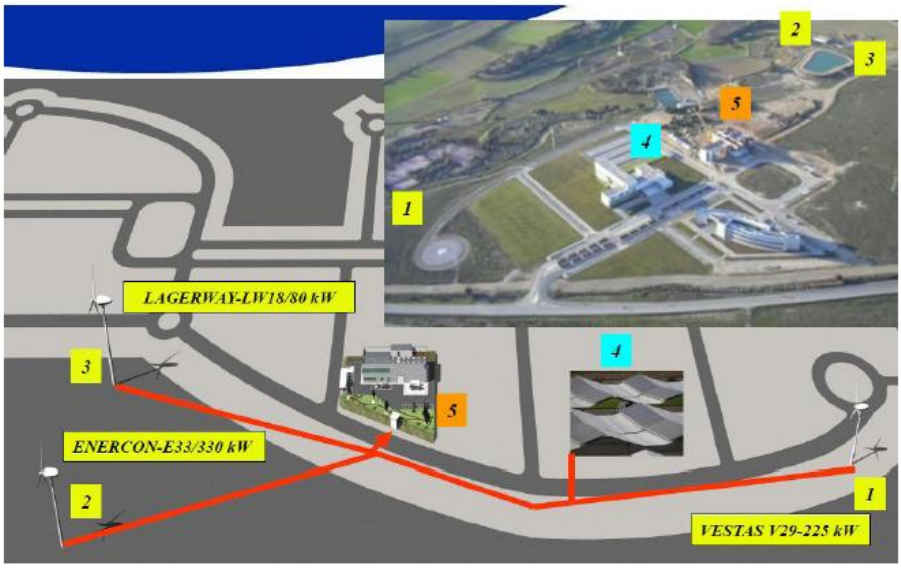

Figure 2. Situation of the wind park in Walqa

2.1.2 PV Installation

The microgrid also includes a section of photovoltaic generation. The PV installation has an installed peak power of 100kW, distributed as follows:

- 60 kW fixed plate peak power, installed in a carport at Walqa.
- 20 kW peak power in an ADES solar tracker.
- 10 kW peak power in a Mecasolar solar tracker.
- 10 kW peak power in 2 Deger solar trackers.

Figure 3. Characteristics of the solar installation

Just as the wind farm, there are various tracking technologies and also different solar panel technologies. This only reinforces the research orientation of FHA.
The 3 technologies of PV panels are:

- Polycrystalline (12 % efficiency)
- Monocrystalline (14 % efficiency)
- Heterogeneous junction (Sanyo; 17 % efficiency)

There are two tracking methods implemented:

- Calendar or astronomical tracking
- Maximum luminosity follow up

2.1.3 Interconnection center

Finally, the project has an interconnection center with motorized medium voltage cells. With a PLC and a SCADA, we can choose at any time to sell the generated electricity or to send power to the workshops of FHA to generate hydrogen by electrolysis in the laboratory. A general diagram of the installation, location and interconnection of different generators can be seen in the following pictures.

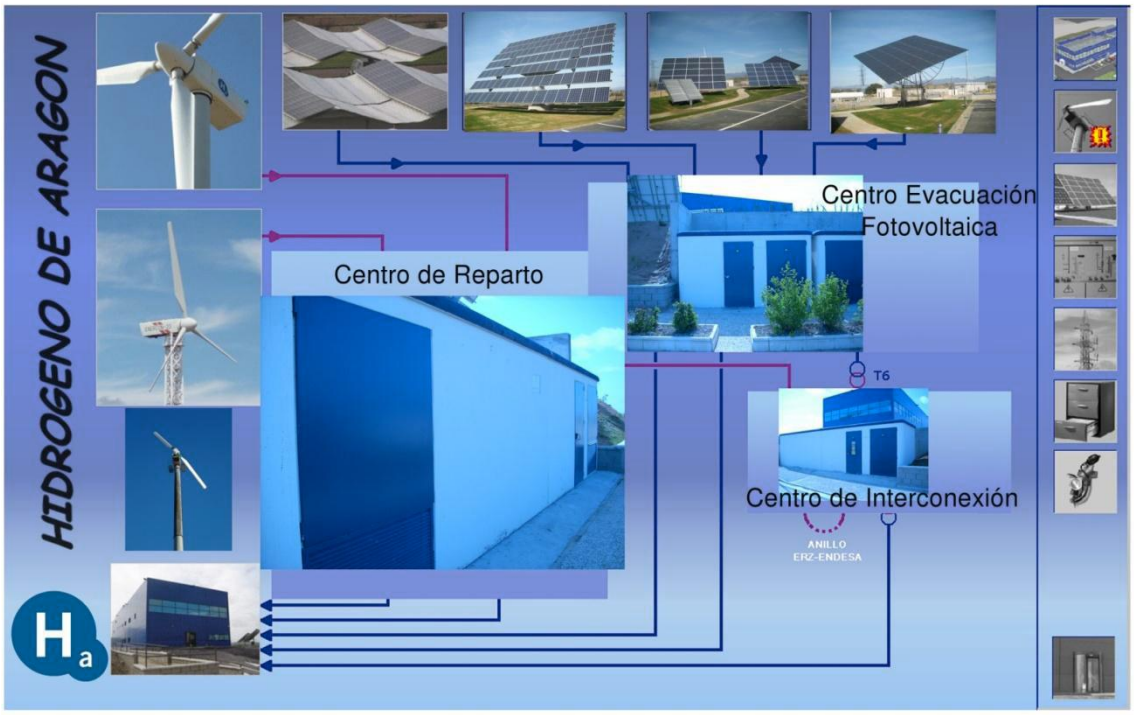

Figure 4. General diagram of ITHER project

In Figure 4 we could see the interconnection between the different elements of the installation. In Figure 5 we see the placement of the distribution centers of energy and evacuation.

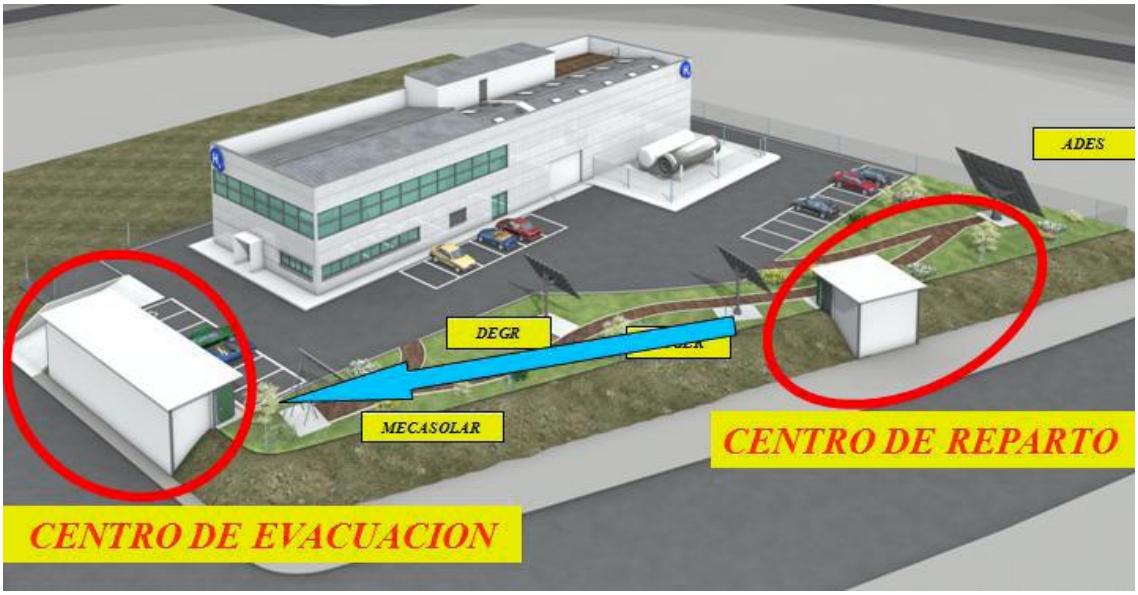

Figure 5. Situation of the distribution centers

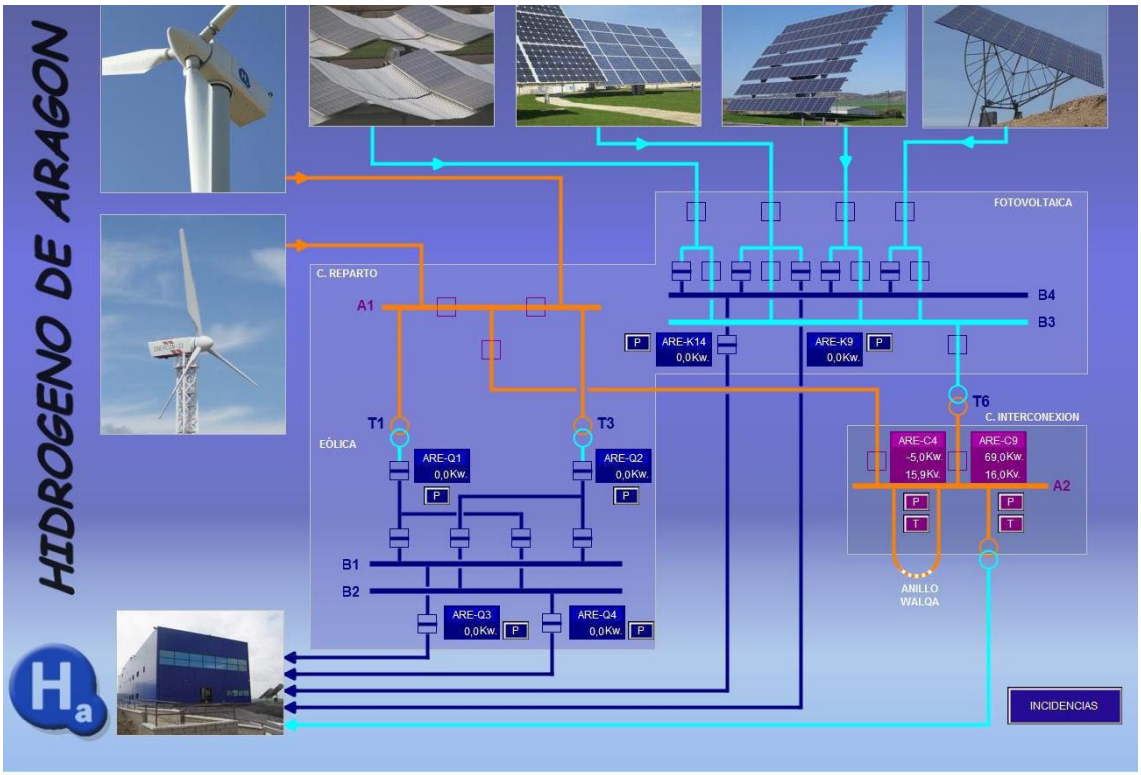

Figure 6. General view of all systems of the Project

2.2 Hydrogen production

The system to produce hydrogen in Walqa has the capacity to produce 25 kg of hydrogen every day at two pressure levels, 200 bar and 350 bar. The system is used to manage the renewable energy production at Walqa and to serve as fuel for sustainable mobility.
The main stages of the installation are:

- Production and purification
- Buffer storage
- Compression
- High pressure storage
- Dispenser
- SCADA

2.2.1 Production and purification

Hydrogen is produced by water electrolysis in an alkaline electrolyzer (Lurgi-IHT technology). The electrolyzer has a discharge pressure of 32 bar which involves an important energy saving in the next stage of hydrogen compression. The electric consumption is close to 70 KW with a discharge flow of 10 Nm3/h and 99,7% (vol) of purity.
In order to use the hydrogen in a fuel cell, the hydrogen purity is increased in the purification unit (99,999% vol), meanwhile the oxygen is vented to the atmosphere.

Illustration 2. Electrolyzer at Foundation for Hydrogen in Aragón installations.

2.2.2 Buffer storage

There is a first buffer hydrogen storage at 30 bar after the purification unit where the hydrogen is stored for the fuel cells and different hydrogen demands of the workshops and for keeping a constant pressure in the compressor inlet. This storage contains up to 120 Nm3 of hydrogen at 30 bar. This storage can be filled with merchant gas at convenience.

Illustration 3. Hydrogen Buffer

2.2.3 Compression

The compression stage is comprised by a Hofer diaphragm compressor which increases the pressure from 30 bar to 350 bar in two stages, with a intermediate pressure of 100 bar. The compressor must be oil free in the mechanical parts that are in contact with the hydrogen so that the hydrogen flow is not contaminated when crosses each stage. After each compression stage, the hydrogen flow must be refrigerated to reduce the temperature so as to keep the hydrogen temperature in safe operation ranges and increase the efficiency of the unit. The maximum amount of hydrogen that can be compressed is 10,9 Nm3/h at 30 bar in the compressor suction head.

Illustration 4. Hydrogen compressor

2.2.4 High pressure storage

The hydrogen store is composed of high pressure stain steel cylinders in a steel bank. In the first stage of operation, the high pressure hydrogen storage will be close to 25 Kg. The cascade is formed by 18 cylinders with 6 bottles for each stage.

Illustration 5. Hydrogen storage system

2.2.5 Dispenser

The FTI International dispenser is able to fill buses and cars at 350 or 200 bar with a touch screen interface to select the fill pressure and visualize operation parameters. The dispenser is provided with two WEH TK 16 y TK 25 nozzles. There is no precooling neither communications interface with the vehicle.

The filling rate depends highly on the ambient temperature. Hereby, if the ambient temperature is higher than 30ºC, the dispenser supplies hydrogen with a low filling rate in order to keep the temperature inside the vehicle tank below 85ºC. This filling rate could vary between 0.2 and 0.6 Kg/min.

Illustration 6. Dispenser at hydrogen station at Walqa

2.2.6 SCADA

The station is controlled by a master PLC which oversees the installation for a safe operation and will be also used to record and send all the important operation parameters such as pressures, temperatures, flows, time of fillings or electric consumptions so that these results can be analyzed in order to optimize the installation and to improve future designs of hydrogen stations.

2.3 Walqa microgrid model

For the moment any model of Walqa microgrid has been developed. The intention is to create the models during the GT3 of OPTIMAGRID project using HOMER to make the sizing and MATLAB for the physical model.
The operation of the microgrid will be based in the model on a system with renewable energy production (wind and solar), energy consumption of the Walqa buildings, the connection of the microgrid with the real grid in a physical point and the hydrogen and some other systems like electrochemical batteries and supercapacitors as energy management systems to control and optimize the renewable energy resources at the microgrid.

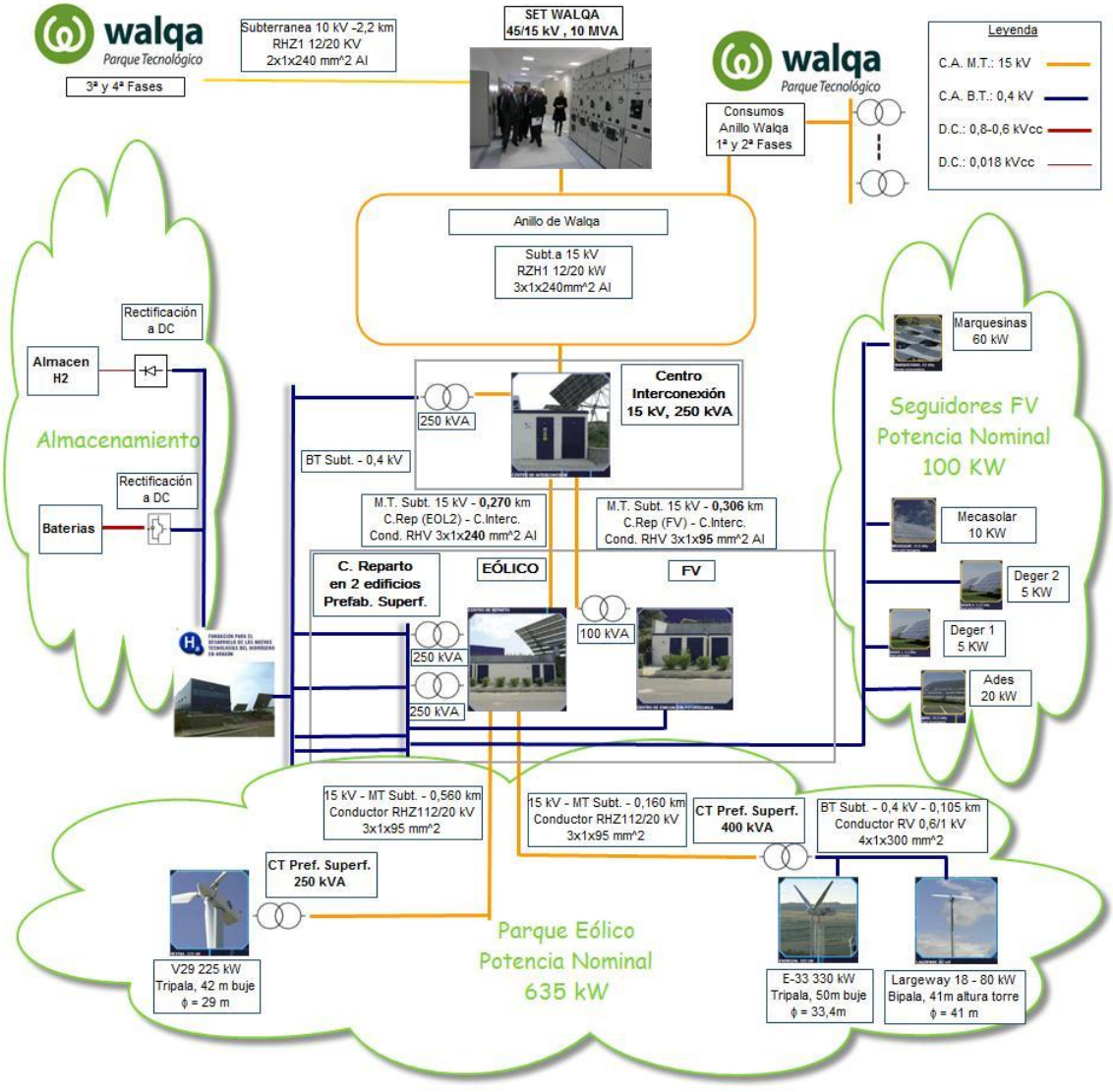

Figura 7. Walqa microgrid

3 MODEL OF MICROGRID AT SANGÜESA (CENER INSTALLATIONS)

3.1 Description of the real microgrid

The microgrid located in LEA (Laboratorio de Ensayo de Aerogeneradores, Wind turbine test laboratory, CENER, Sangüesa) is oriented to the industrial application. Currently, it can supply part of the electrical demand of LEA and part of the lighting of the industrial estate. This microgrid can work either connected to the main grid or isolated.
The microgrid is comprised of the following elements:

- A low voltage distribution network, where a series of distributed energy sources are interconnected to provide electricity and heat for a group of consumers.
- A local communication infrastructure
- A hierarchical control and management system
- Energy storage systems
- Smart consumption and load controllers
- A central controller that manages the microgrid, which gives the set point to the controllers of all the other equipment, such as the generation sources, the energy storage systems and smart loads.

The main targets of the installation are the following.

- To manage the available generated power at every moment so the supply to the loads is always guaranteed
- To optimize the use of renewable energies to cover the loads, promoting the energy independence of LEA
- To protect the existing equipments from faults coming either from the grid or from the microgrid itself
- To be able to send the energy excess to the main grid, so the microgrid does not operate as an independent entity but as an active part of the grid
- To be used as a test bench for new equipments, generation systems, energy storage and strategies for microgrid control and protection

Based on these objectives, the microgrid currently has the following equipment at its disposal:

- Equipment (all of them include the connection, control and ancillary equipment)
  - 25 kWp photovoltaic installation

  - Full-converter type 20 kW nominal power **wind turbine**

- 55 kVA rated power **diesel** genset generating set

- Lead-acid gel technology **battery bench**, able to supply 50 kW uninterruptedly for 2 hours

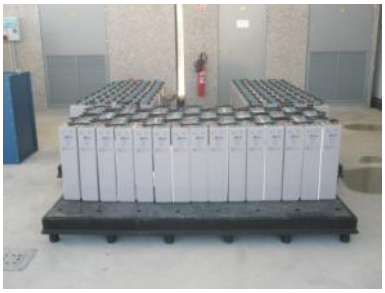

- **Vanadium flow battery** with capacity to provide 50 kW for approximately 4 hours

- Loads
  - LEA (lighting of one building)

- Industrial estate (public lighting)

- 120 kVA three-phase programmable **loads** bank (resistance and inductance)

- Electrical installation
- Energy management and control system

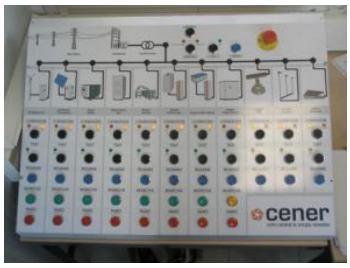

Operation modes

- Standard
  - Grid connected. The external grid provides voltage and frequency references
  - Isolated. The microgrid generates voltage and frequency references through the storage systems
- Test bench
  - Testing different systems
  - Simulation of electric consumptions
  - Different energy management strategies

3.2 Description of the System

The tool described in this report comprises a combination of mathematical and electrical models simulating the behavior of each of the components installed in the microgrid, and hence, the microgrid. This tool has enabled the development and validation of the code for the control/management of the microgrid.
The platform used to model these systems was Matlab/Simulink, with the help of some toolboxes and an accelerating system (C language compiler), allowing to carry out long time simulations in short periods of time.
This simulation platform will enable the forecast at all time about the behavior of the system facing any event. At the same time, it will be possible to analyze the system response after the implementation of new generation or storage systems, as well as to define the overall control system and management strategy.
This model of the CENER microgrid in Sangüesa consists of the following equipments:

- Energy storage systems
  - Lead-acid battery bank
  - Flow battery

- Power generation systems
  - Wind turbine
  - Photovoltaic system
  - Diesel power generator

- Loads supplied by the microgrid
  - Lighting of one of CENER's buildings
  - Public lighting in the industrial area of Rocaforte
  - Programmable loads bank

- Electric system
  - Electric grid
  - Power transformer
  - Connection to the grid
  - Switches
  - Wattmeters

- Control systems
  - Management system of the microgrid
  - Control panel for the switches

Needless to say, this is a first step for the construction of a precise model. Therefore, each of the models has to be tuned and its performance has to be validated against the real performance of each component.
The next figure shows a general scheme of the overall model.

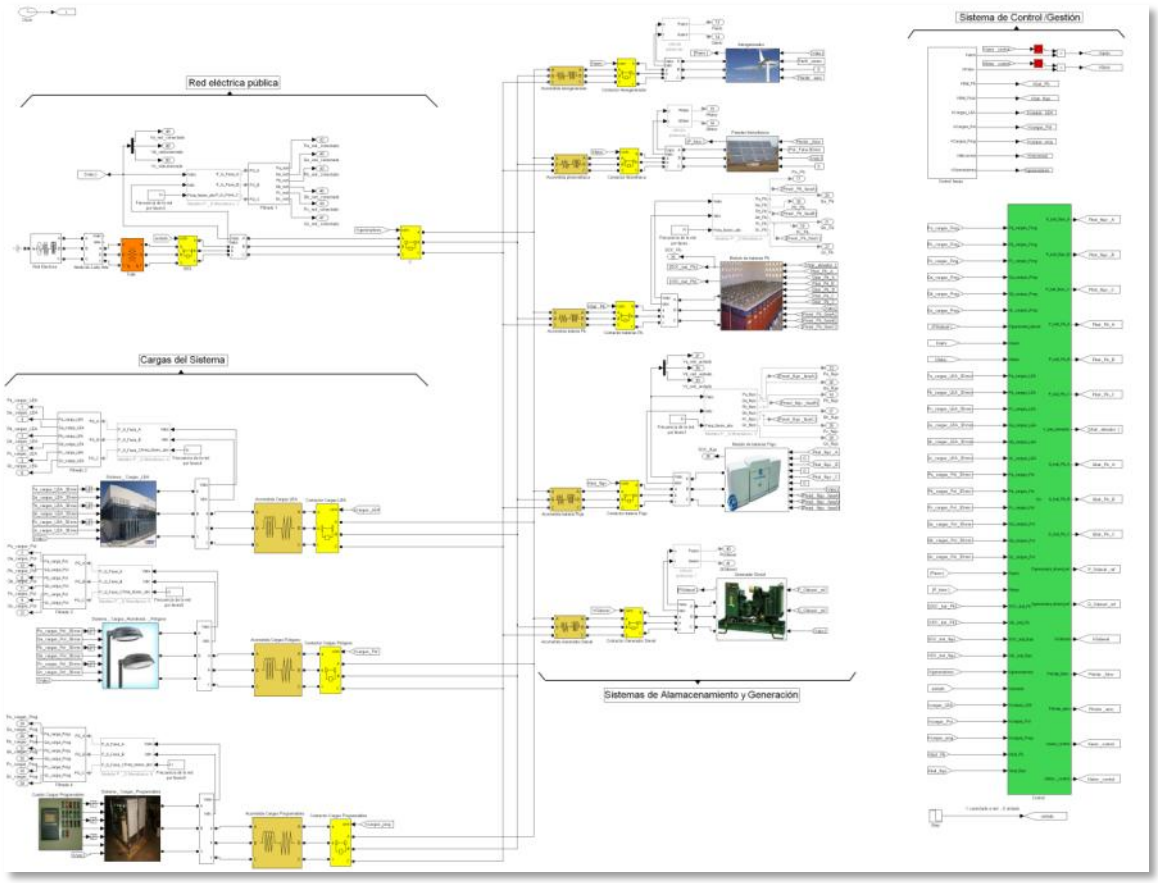

Figure 8. Overview of the model

As we can see, the model is divided in four different parts. First of all, we can find the external electric grid. The second one includes the loads to be supplied from the microgrid. Third, the energy storage systems and the power generation systems, while the last one comprises the lines control panel and the microgrid management control.

Microgrid working modes

Before the description of the different models, the logic used for the management of the system is depicted. There are two working modes available for the system: the first one considers the microgrid connected to the external electric grid through the power transformer (Connected mode), and the other one consists on working isolated from the electric grid, while one of the energy storage systems generates its own grid (Island mode).

Broadly speaking, while the microgrid remains connected to the external grid (Connected mode), the performance for every *t* instant is the following.

- If the generation through the renewable systems is greater than the consumption of the loads, the exceeding energy will be absorbed by the energy storage systems provided that they have enough capacity. Otherwise, this energy will be delivered to the grid so it can be used by other consumers.
- If the generation through the renewable systems is lower than the consumption of the loads, this part will be supplied by energy storage systems provided that their SOC (state of charge) is within the acceptable range. Otherwise, the electric grid will be who will meet the loads.
- All in all, the main target is that the consumption of the loads will be met by the elements within the microgrid, avoiding if possible the consumption from the external electric grid.
- It is worth mentioning that the management strategy is not the same for all of the storage systems in the microgrid. For this specific working mode, the objective is the maximum SOC in the lead-acid batteries, so in case of working in island mode, the maximum energy is available. The strategy for the flow battery is

different, because although it is interesting a rather high SOC, a margin is also interesting for its purpose when working in island mode.

If a fault in the external electric grid occurs, or by any other reason the microgrid changes to island mode, the performance of the system will be as follows.

- The flow battery, through its converter, will create an electric grid providing the needed references of voltage and frequency for the rest of the systems. This energy storage system, will act as a system stabilizer, that is, it will absorb or deliver the power excess or shortfall in every moment, derived from the instant unbalances between generation and demand.
- If the renewable generation is greater than the consumption of the loads, the management system will use this excess to charge the lead-acid batteries. Whenever the batteries are not able to absorb this energy, the flow battery itself will absorb it. In the extreme case that the flow battery is not able to do this, the power coming from the renewable sources will be limited, even stopping this generation when the SOC limits are reached.
- On the other hand, if the consumption of the loads is greater than the power generated by the renewable systems, this energy need will be met in first place by the lead-acid batteries if the SOC is enough, and in second place by the flow battery. If both SOC low limits are reached, then the diesel generator will be switched on.
- Once the diesel generator is working, it will meet the loads trying at the same time to charge the batteries. This energy excess to be stored will not be very far, as the aim is to avoid any fossil energy consumption if possible, trying to charge the batteries from the renewable systems. Therefore, the future work will be focused on how to manage this and other particular cases of behavior through weather forecasts.

3.3 Models of the components

In this chapter the models of the main components of the microgrid are detailed, giving a clear idea of the performance of each of them.

Components of the microgrid

- Electrical system:

For this group of models, the models from the Simpower library have been used. Then, different parameters have been fixed in order to adjust the performance to the required one.

- Electrical grid.

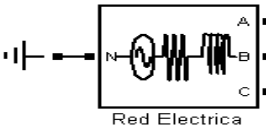

This model is used to simulate the external electrical grid. Some data have been introduced to make it similar to the real medium voltage grid, in order to validate its performance later.

- Power transformer.

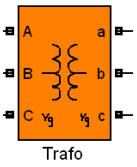

The parameters fixed in this model (magnetizing resistance and inductance, winding resistance and inductance, nominal values) are the ones given by the manufacturer of the transformer installed in the real microgrid.

- Connections.

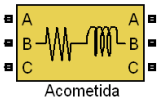

The objective of this model is to simulate the performance of each of the connections of the different equipments. It is intended to study the influence of the transient phenomena.

- Switches.

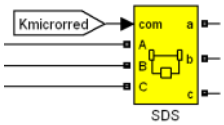

This model is used as a power contactor, enabling the connection and disconnection of each component whenever the control system or the control panel requires so.

- Voltage and current meters.

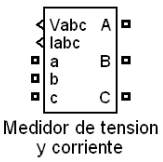

The lectures taken by this multimeter are used to calculate the instant power generated or absorbed by the different systems comprising the microgrid, as well as to examine the response of the different electrical and electronic systems in the microgrid.

- Power meters.

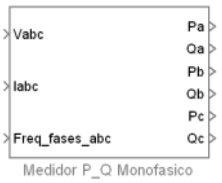

In the case of the power meters, two models have been used in our microgrid model. One of them (three-phase meter) was taken from the Simpower library and the other one (single-phase meter) was fully developed by CENER in order to fulfill all the requirements of the simulation platform. The single-phase meter is used for the storage systems, the loads and the electrical grid, given that the power amplitude, offset and sign can differ among phases. On the other hand, the Simpower meter is used for the balanced three-phase systems, like the wind turbine, PV system and the diesel generator.

- Generation systems:
  - Wind turbine of 20 kW.

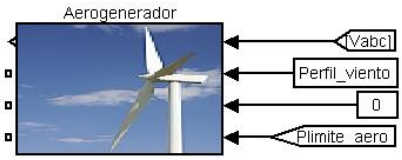

The model created comprises a full converter topology wind turbine. It includes a permanent magnet multipole synchronous machine of 20 kW connected to a converter, together with a 12.8 m diameter wind turbine, a wind turbine control system and an algorithm for the maximum power point tracking (MPPT) with a limiter of the power generated by the wind turbine.
The input variables for the model are the ones shown in the picture:

Perfil_viento: It involves a data file of wind measures obtained from a meteorological station at 30 m height. The time interval in this case is 0.2 s, giving a very realistic response of the wind turbine because of its mechanical system inertia. In the future, the wind speed is expected to be introduced in real time from an anemometer.
Plimite aero: This variable expresses a limit of the energy capture. It is essential to have the ability to limit the power captured by the wind turbine in certain moments, due to the characteristics of the installation. This setpoint value comes from the components control and forces the machine to restrict the generated power, acting over the pitch of the blades.
0: This input indicates the reactive power required to the machine. Actually, it is obtained through a cos phi setpoint.
Vabc: Through this variable, the converter is synchronized with the electrical grid, so the P and Q delivered by the converter coincide with the reference ones. This input variable is used in most of the equipments comprising the microgrid, and consequently it is not described hereafter.
Listed below are some of the components included in the wind turbine model:

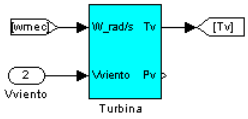

Wind turbine: This model is parameterized with the values given by the manufacturer. Wind speed and mechanical speed of the machine are the input variables, while the mechanical torque applied to the synchronous generator is the output variable, taking into account that a gearbox is not available.

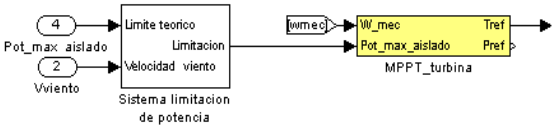

MPPT algorithm and power limiting system: The MPPT algorithm sends to the generator a torque reference calculated from the rotating speed of the machine. According to this reference, the machine accelerates or brakes in relation with the difference between the reference torque and the torque coming from the turbine. This way, the machine is gradually autoregulated, absorbing the maximum energy available from the wind. Finally, the power limiting system acts when the control system needs so.

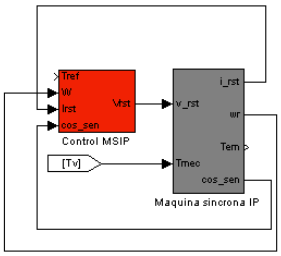

Generator and Control: The multipole synchronous generator was created through a series of mathematical equations defining its electrical and mechanical performance. As can be seen from the picture, the inputs are the reference voltages coming from the control, so the machine generates the reference torque dictated by the MPPT algorithm, and the Tmec, corresponding to the mechanical torque applied to the generator rotor by the turbine.

The output variables coming from the generator are the rotating speed of the rotor and the electromagnetic torque of the machine, together with the induced currents in the machine. Also, we get the cos_sen variable, needed to drive a precise control of the torque in the machine.

Finally, the generated energy is delivered to the grid through the grid side of the converter (inverter). This inverter, common in most of the equipments, is analyzed later in the report.

- Photovoltaic system of 25 kW.

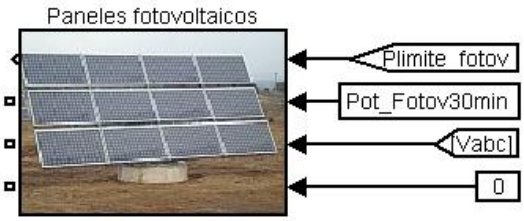

For the building of this PV system model, a curve of a real PV system and the inverter model have been used. As shown in the figure, the model comprises the following inputs described below.

Plimite_fotov: This variable is sent by the control agent to the PV system, with the aim of limiting the power generated when working in island mode. In fact, this setpoint is sent to the converter of the PV system, who will modify the MPPT algorithm moving the working point to a more inefficient one, thus reducing the generated power.

0: This input indicates the reactive power required to the machine.

Pot_Fotov30min: Here, the input variable is a data file with the generated power from a real 25 kW PV system. Consequently, this power signal is introduced in the model and delivered through the invertir to

the microgrid. In future models, the input variable will be the solar radiation, trying to adjust the behavior to the real system.

- Diesel generator of 48 kW.

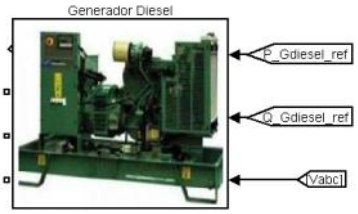

The diesel generator model includes an internal combustion engine, directly linked to a synchronous generator, and through this, to the electrical grid. Listed below are the input variables of the model.

P_Gdiesel_ref: Reference of active power that the generator must deliver to the grid.

Q_Gdiesel_ref: Reference of reactive power that the generator must deliver to the grid.

Both the P and Q references are sent by the microgrid management control when, working in island mode, the batteries are discharged and the renewable resource is low. Otherwise, this equipment will remain disconnected.

In the next figure the internal part of the model is depicted, where we can see the combustion engine connected to the synchronous generator.

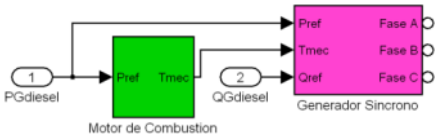

The model strategy consists on the introduction of a reference power into the combustion engine, so through its control body it regulates the fuel feed valve, controlling the torque applied to the synchronous generator and hence the active power. The reference for the reactive power is introduced in the synchronous generator model.

- Energy storage systems:
  - Lead-acid batteries.

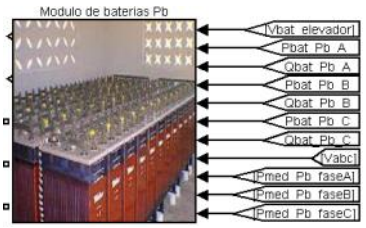

The bank of lead-acid batteries is able to supply 50 kW during 2 hours (50% DoD). Its performance within the microgrid is fundamental when working in island mode, since the autonomy of the microgrid depends on its SOC.

The model is mainly comprised of the bank of batteries and a bidirectional converter, capable to withstand unbalancing among phases and even inverse flows of charge.

The strategy of the model is explained below.

Pbat_Pb_A….: This input includes the references of P and Q that the converter should meet independently for each phase. These phase values can differ in their value or direction.

Pmed_Pb_faseA…: These are parameters measured with the power meters and used within the battery model to decide the charge/discharge power, in relation to the total power and the output voltage. Logically, depending on this power the SOC will vary accordingly.

In the next figure, the block of the bank of lead-acid batteries is shown.

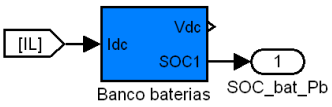

As can be seen, the input signal corresponds to the current, either entering or coming out depending on the power balance by phase, and thus charging or discharging the batteries. The output variables are the output voltage, varying in relation to the SOC, and the SOC itself.

- Flow battery of 50 kW.

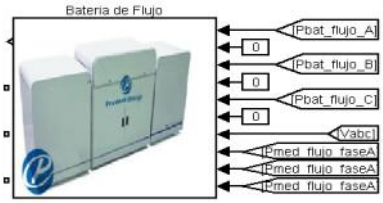

The flow battery is the most important element in the microgrid according to the strategy of the control system. As mentioned before, this is the system in charge of establishing the grid when the microgrid is working in island mode. This system is capable to provide 50 kW during 4 hours. Like the bank of batteries, it is connected to the grid through a bidirectional converter able to govern each phase in an independent manner. Therefore, the flow battery permits two working modes, either connected to the grid under P and Q setpoints, or generating its own grid.

All in all, when working in connected mode, the performance is similar to the one for the batteries, but when working in island mode its aim is to generate the grid damping the power unbalancing in each phase.

The strategy of the model is explained below.

Pbat_flujo_A….: This input, if working in island mode, includes the references of P and Q that the converter should meet independently for each phase. These phase values can differ in their value or direction.

0: This input indicates the reactive power by phase required to the battery.

Pmed_flujo_faseA…: These are parameters measured with the power meters and used within the battery model to decide the charge/discharge power, in relation to the total power and the output voltage. Logically, depending on this power the SOC will vary accordingly.

The next figure shows the block corresponding to the electrochemical part of the flow battery:

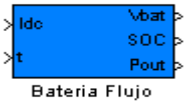

As can be seen, the input signal corresponds to the current, either entering or coming out depending on the power balance by phase, and thus charging or discharging the batteries. The output variables are the output voltage, varying in relation to the SOC, the SOC itself and the power entering or coming from the flow battery.

- Loads covered by the microgrid:
  - Lighting system of the CENER building in Sangüesa.

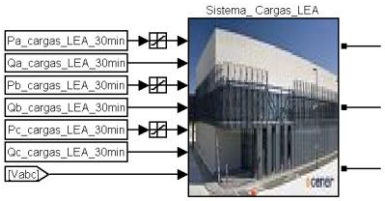

The procedure followed to model these loads, mostly being luminaries of the building, consisted on the register of the consumption of the loads. Thanks to these measures and through data processing software, both the active and reactive power consumption along the day was calculated. Then, the P and Q data by phase was separated.

- Public lighting system of the Rocaforte industrial area in Sangüesa.

The modeling of the public lighting consumption was performed in the same way as for the previous case.

- Bank of programmable loads.

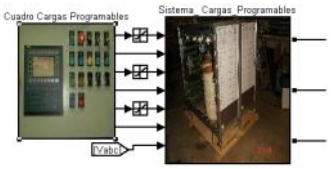

The bank of programmable loads involves a series of resistances and coils, that according to the input variables, consume the required active and reactive power.

- Control systems:

  - Microgrid management system.

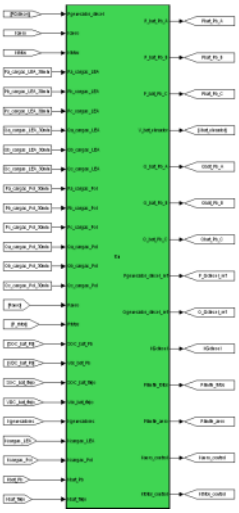

The microgrid control system is set up by the group of management codes of the components in the microgrid, and it is built up in Matlab code. In this control, the necessary lecture parameters are implemented in order to govern the microgrid under the active working mode, and depending on the status of every particular component.

  - Switchers control panel

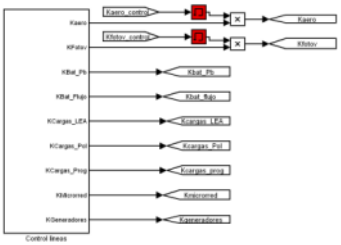

Through this lines control panel, and given the versatility of the simulation platform used, it is possible to connect or disconnect lines at any moment without the need of stopping the simulation. This ability allows to observe and to analyze the performance of the system control, verifying its suitability.

4 MODEL OF MICROGRID AT PORT OF BAYONNE

4.1 Description of the study area

Figure 9 shows the port area of Tarnos. One can be seen the offices, the platform and the cranes.

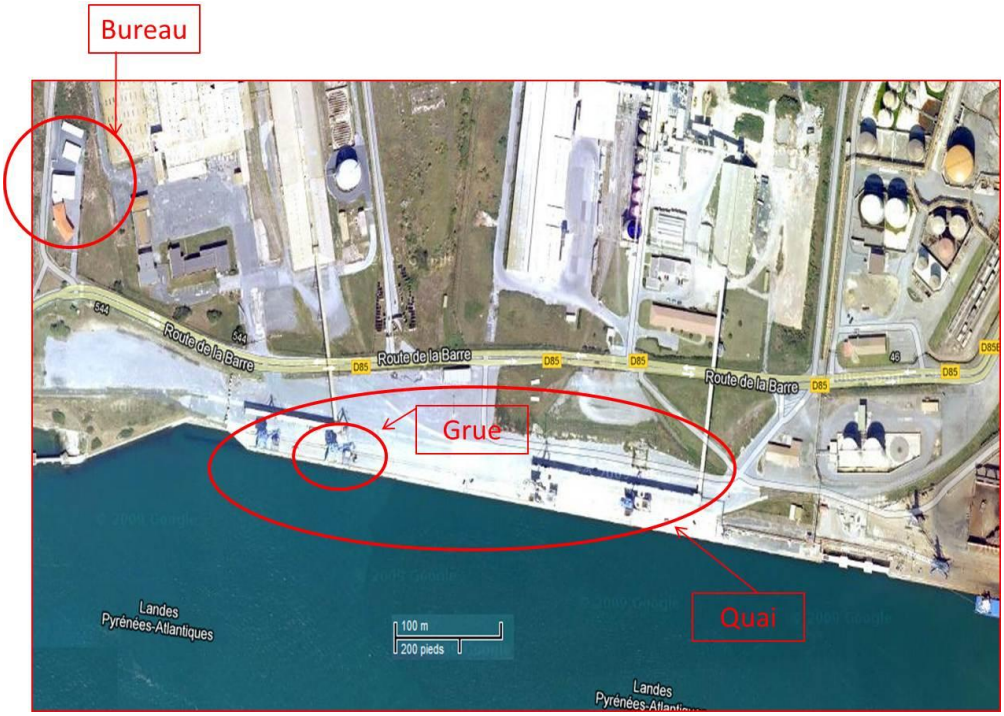

Figure 9. Area port Tarnos

Tarnos port area is composed of a 400m dock and a open area with a technical platform to supply the cranes, and a technical platform with two water pipes, one with freshwater to serve ships and one driven by a fire pump in the Adour. Two railway tracks pass between the open area and the pltform. All is illuminated by spotlights:

- 24 projectors of 1000W;
- 3 projectors of 500W

The material handling is provided by 4 cranes:

- Two 10T cranes to grab and 20T to the hook;
- One 12 T crane to grab and hook;
- One 35 T crane to grab and hook, and exceptional support to 42 T grab;

The cranes supply comes from a private HT 20kV station with as a single EDF supplier:

- 3 cranes 5,5kV;
- 1 crane in 20kV

The power consumption in 2009 was 95989 kWh.
The Figure 10 shows the distribution of consumption of different cranes on the three port areas for the month of July 2011. As can be seen the cranes of the port of Tarnos area are the most used and the crane 12 has been the most used. It should be noted that the 14 crane, is the less used simply because the Regional Council of Aquitaine does not have the license. .

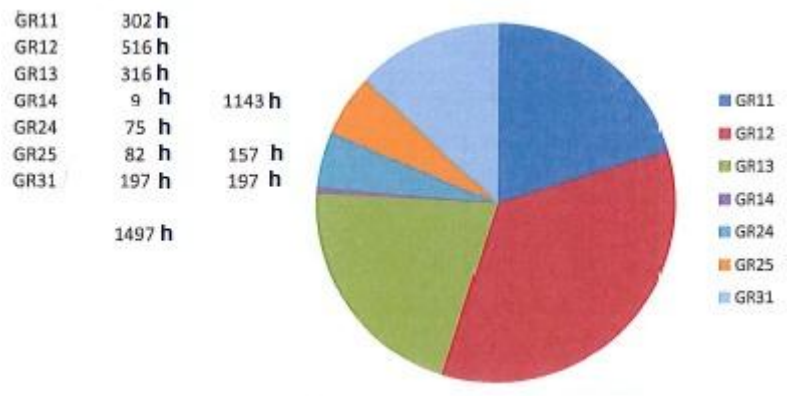

Figure 10. Use of cranes

Various cranes of the port area of Tarnos are presented in Illustration 7.

Illustration 7. Cranes on the wharf.

The 14 crane is the latest installed. To become familiar with how to use a crane considers the 14 crane.

4.1.1 Description of a crane

The crane 14 is designed for lifting of goods, especially for loading and unloading of ships. This crane can do:

- lifting;
- power tools changer or mechanical;
- be moved on rails within the work area, with hook, dump or spreader suspended;
- be safely stopped for maintenance or repairing operations.

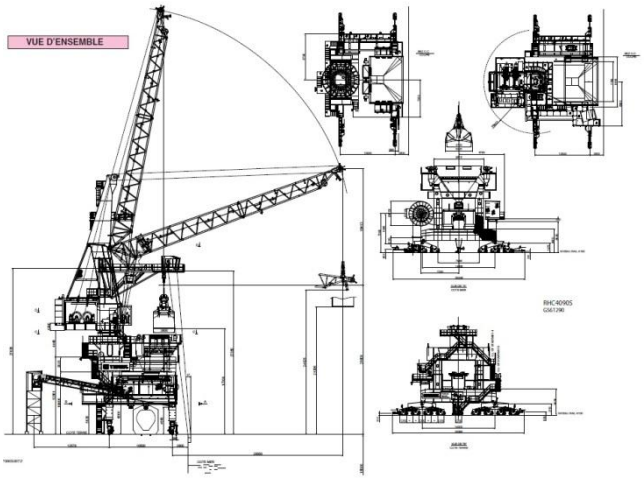

Figure 11. Synthetic view crane 14

Figure 11 shows the dimensions and a detailed description of the structure of the crane 14. Figure 12 shows different positions of a crane.

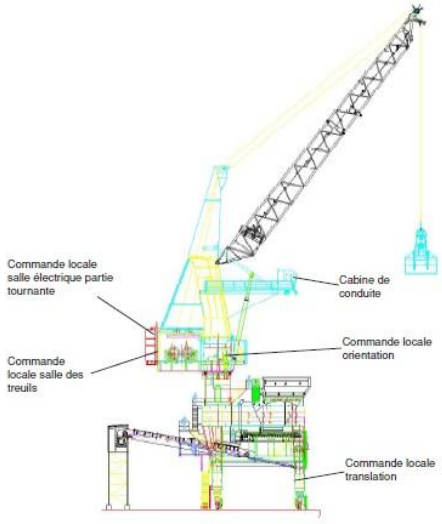

Figure 12. Positions of command

From there, different operation modes can be extrapolated. The five different movements of the crane are:

- Translation;
- Orientation;
- Lifting;
- Closing;
- Suspension.

All crane movements are used simultaneously. The translation is generally an unaccompanied movement. The lifting movement is composed of the closure and of the suspension movements. When the bucket opens and closes, is the closing movement. When the bucket up and down, the movements of closure and suspension are used together (is the lifting). The lifting movement actuates the arrow; it is also called variation range.

4.1.2 Electrical schema for the orientation of a crane

For each of these movements specific engines are used. This is presented for example in figure 13.

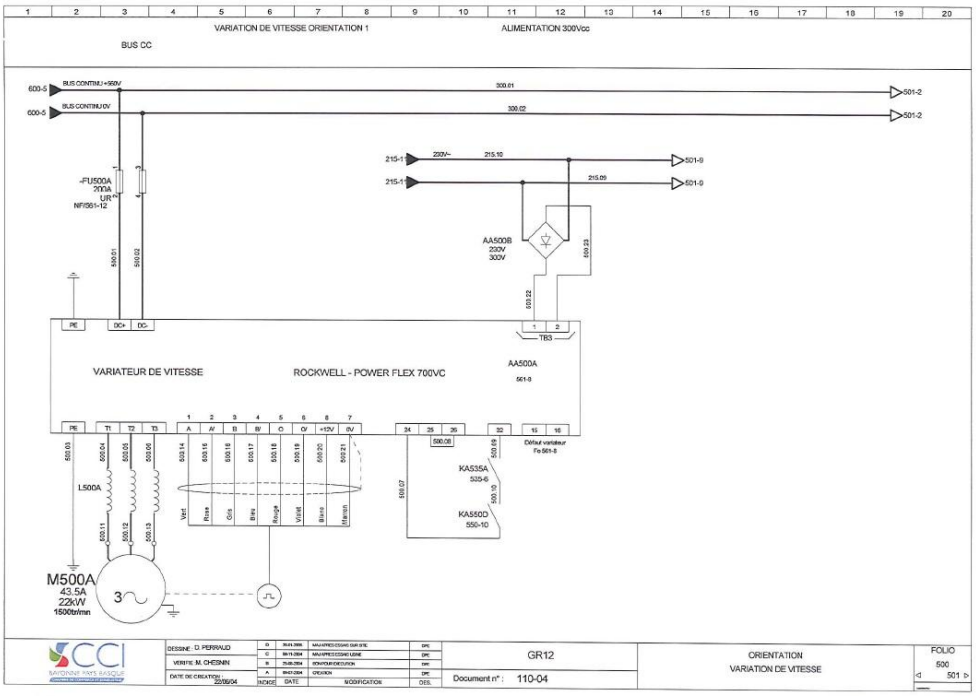

Figure 13. Electrical schema for orientation of a crane electric

In this particular case, to rotate the turret of the crane that supports the arrow, the engine is a three-phase motor with a power of 22 kW, and running at 1500 rpm.

4.1.3 Supply agreement and electrical distribution

The four cranes are powered by an electric connection with a single electrical distributor EDF. The type of supply agreement to EDF is a yellow tariff. The tension associated with the subscription is 22 kV. This power is then distributed by a transformer HT/HT in 5.5 kV to each of the cranes. At the level of the crane there is another transformer HT/LT distributing a voltage of 400 V to each engine. This is illustrated by the figure 14, which is the synoptic of the PCVue supervision which allows the monitoring of the consumption of the different cranes.

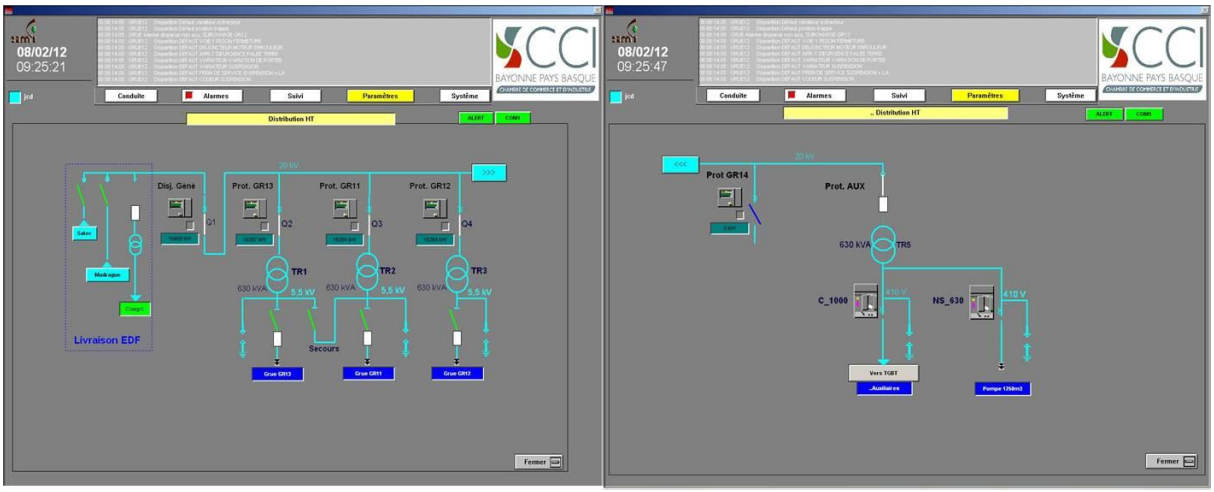

Figure 14. Synoptic of electrical distribution

4.1.4 Supervision and installation of electrical sensors

The usefull data used by the supervision are transmitted by various sensors shown in figure 15.

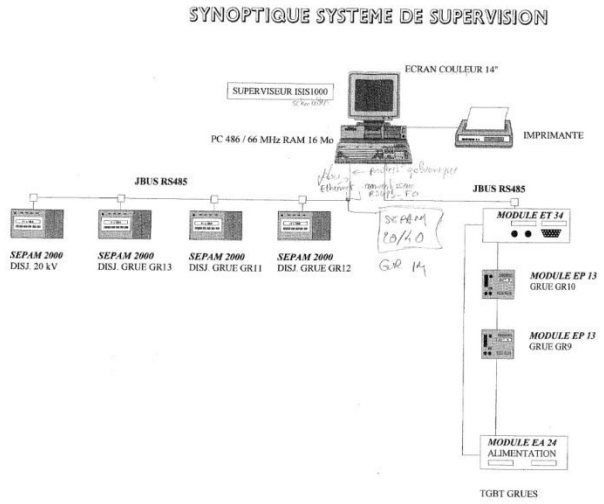

Figure 15. Supervision system synoptic

At the level of the port area of Tarnos different ways of measuring the consumption have been installed. SEPAM 2000 type sensors are installed at the level of circuit breaker on different cranes. These measures are carried by RS485 JBUS to a RS485 optical fiber converter. And then, this optic fiber arrives in the office where a computer is located with PCVue supervision software. These data are accessible by the supervision and/or a VPN tunnel that allows retrieving data from the ESTIA. Figure 16 shows the home page of the supervision where we have a representation of the port area of Bayonne.

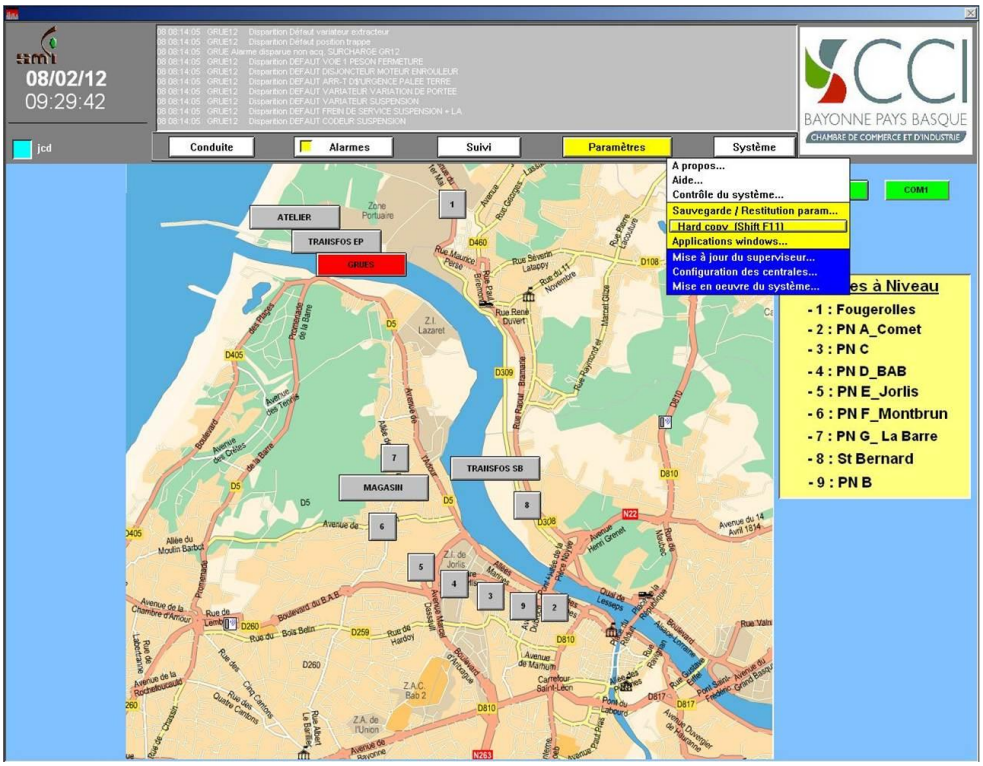

Figure 16. Supervision: synoptic port of Bayonne

4.1.5 Cranes and motors

The following table presents the motors used by the cranes 11, 13 and 12. The crane 11 and 13 are different to the crane 12.

CRANE 11_13:	Motor	Description
	M300A:	THREE PHASE INDUCTION MOTOR
		178A
		90KW
	M400A:	THREE PHASE INDUCTION MOTOR
		178A
		90KW
	M500A:	THREE PHASE INDUCTION MOTOR
		57A
		30KW
		1500 rpm
	M505A:	THREE PHASE INDUCTION MOTOR
		57A
		30KW
	M600A:	THREE PHASE INDUCTION MOTOR
		69A
		37KW
		1000rpm
	M710A/B/C/D:	PHASE MOTOR ROTOR WINDING
		14KW

Table 1. 11 and 13 cranes motors description

CRANE 12:	Motor	Description	Motor	Description
	M300A:	THREE PHASE INDUCTION MOTOR	M501:	THREE PHASE INDUCTION MOTOR
		280A		43.5A
		160KW		22KW
	M310A:	THREE PHASE INDUCTION MOTOR	M600A:	THREE PHASE INDUCTION MOTOR
		1.1KW		95A
		3.4A		55KW
	M310B:	THREE PHASE INDUCTION MOTOR	M701A:	THREE PHASE INDUCTION MOTOR
		0.7KW		7.5KW
		2.2A		17.5A
	M310C:	THREE PHASE INDUCTION MOTOR	M701B:	THREE PHASE INDUCTION MOTOR
		3KW		7.5KW
		6A		17.5A
	M400A:	THREE PHASE INDUCTION MOTOR	M701C:	THREE PHASE INDUCTION MOTOR
		280A		7.5KW
		160KW		17.5A
	M410A:	THREE PHASE INDUCTION MOTOR	M701D:	THREE PHASE INDUCTION MOTOR
		3.4A		7.5KW
		1.1KW		17.5A
	M410B:	THREE PHASE INDUCTION MOTOR	M702A:	THREE PHASE INDUCTION MOTOR
		2.2A		7.5KW
		0.7KW		17.5A
	M410C:	THREE PHASE INDUCTION MOTOR	M702B:	THREE PHASE INDUCTION MOTOR
		6A		7.5KW
		3KW		17.5A
	M500A:	THREE PHASE INDUCTION MOTOR		
		43.5A		
		22KW		
		1500RPM		

Table 2. Crane 12 motor description

4.1.6 Load profile

Sensors on the Tarnos site allow making electrical measurements. These measures are then saved on a server for a temporary duration (a few weeks). This implies that we have measures of load curves from October 2011. These load curves of are saved every month. It should be noted that only the cranes 11, 12 and 13 are currently used on the port of Bayonne.

The measures are made every 10 minutes, this is what is called a 10 minutes point. This type of sampling is used by EDF to charge the port of Bayonne when it exceeds the threshold of power sets in agreed subscription.

The next figures present the power consumption of the crane 11, 12 and 13 during the period January 12 to February 08.

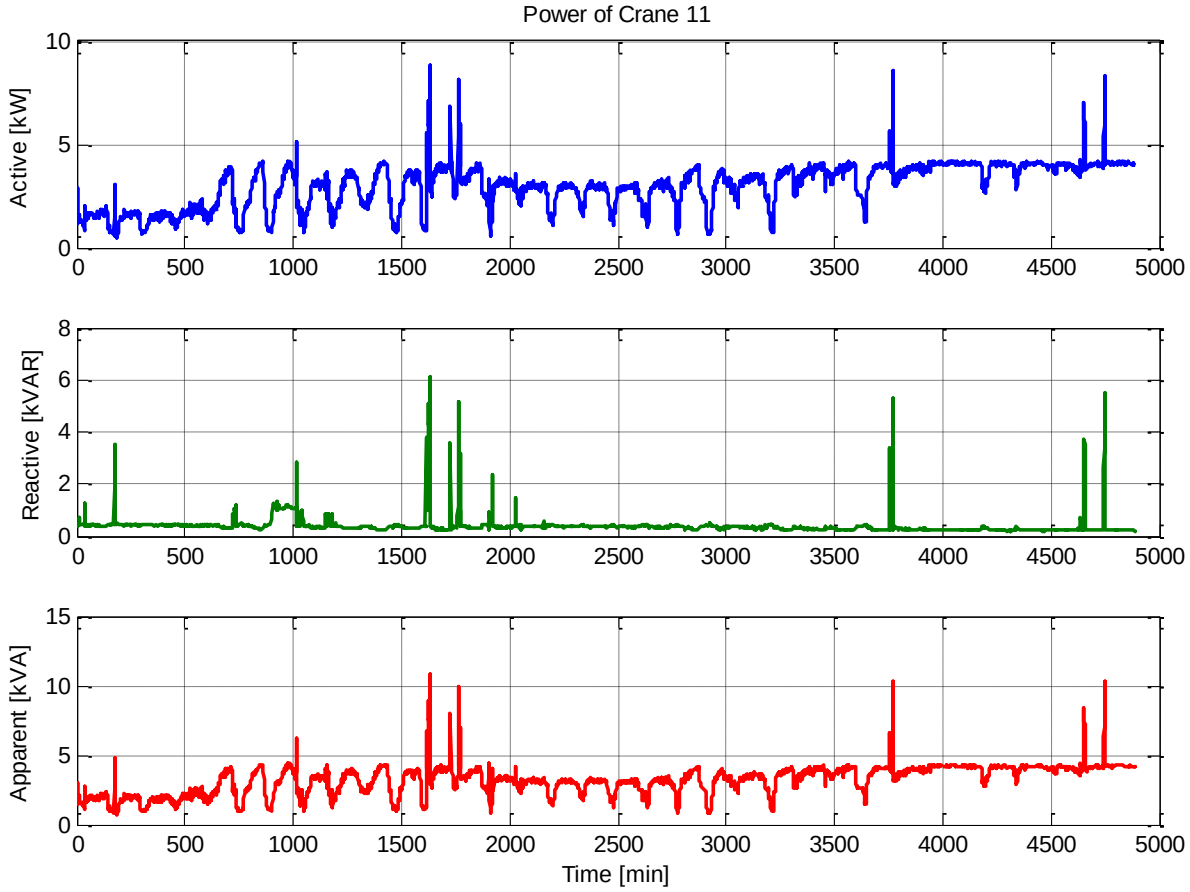

Figure 17. Active, reactive and apparent power of Crane 11

The figure 17, presents the apparent, reactive and active power of the crane 11. Comparing to the motors power this crane has not been fully used during January and February 2012.

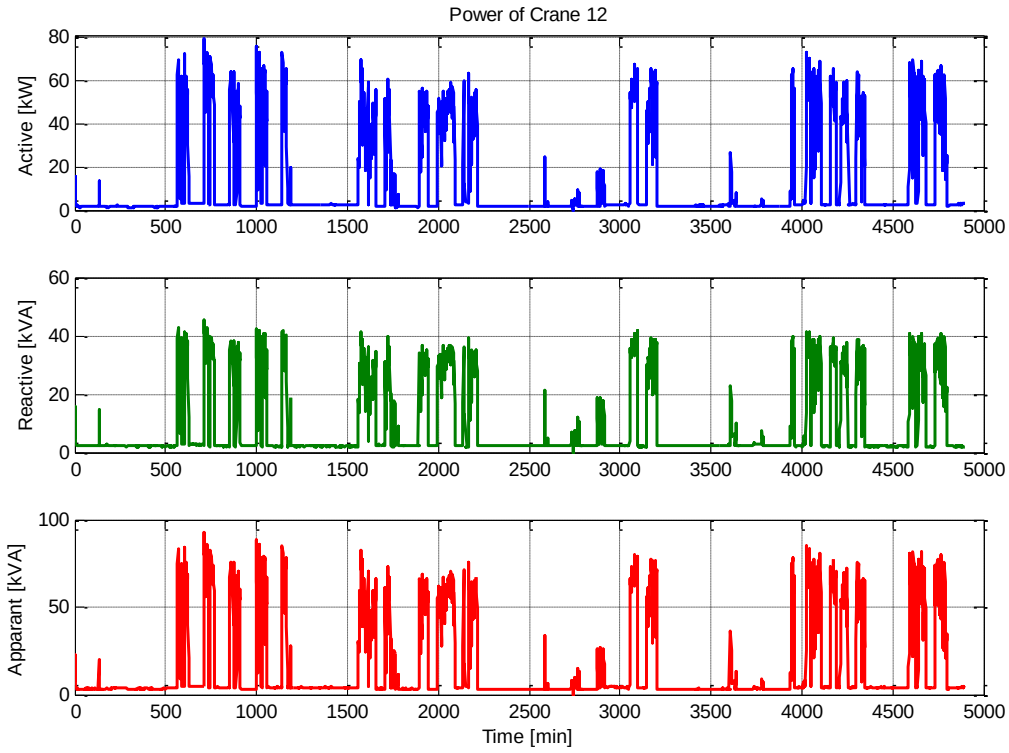

Figure 18. Active, reactive and apparent power of crane 12

The figure 18 presents the power consumption of the crane 12. This crane has been more used tan the crane 11 and we can observe that apparent power corresponds more or less to motors powers have presented before.

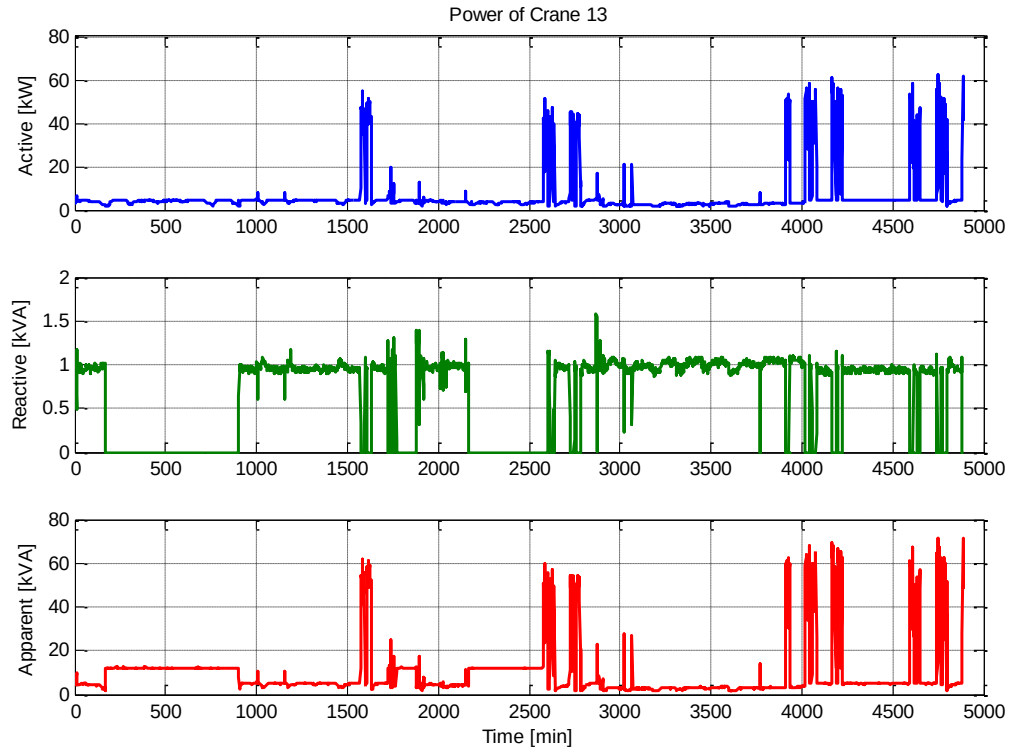

Figure 19. Active, reactive and apparent power of Crane 13

As for the crane 12, this crane has been regularly used during this 6 weeks.

4.2 Tools for modeling

The port contains much obviously electrical equipment connected to the network. An accurate modeling of all these facilities would be very laborious, and of little use. A pre-study on the behaviour of this network can significantly simplify its representation without away excessively from the actual behavior. In this representation simplified, only the following components deserve to be modeled:

- Power sources: the power grid to which the Port is connected.
- Electric charges:
  - Loads more great power and consuming the most energy are electrical machinery related to the cranes. Those are generally asynchronous machines.
  - Electric lighting can be represented as a resistive load.
- Other:
  - Power lines.
  - Transformers.

The next chapter describes the models of these key components. Chapter 3 compares different software simulations in which could be implemented these models. Finally, the last chapter gives the conclusions of this study.

4.2.1 Mathematical models of the main electrical components of the Port of Bayonne.

Sources / grid

The grid can be modelled by lines of inductance L_R and resistance R_R associated to a source of three-phase voltaje ideal u_R.

The parameter S_R and R_R can be used to fix the short-circuit power S_R and the angle ψ_R of the network. More it's resistive, more the angle is small and vice versa. The angle and the power of the network are given by the following expressions:

- $\psi_R = \arctan\left(\frac{\omega_S L_R}{R_R}\right)$
- $S_R = \frac{V_S^2}{\sqrt{R_R^2 + (\omega_S L_R)}}$

This model is generally sufficient to represent, as in the case of the Port of Bayonne, the connection of a subnet to a large interconnected network.

Loads

Modeling of an asynchronous machine

The electrical engines can be an asynchronous machine, whose axis is linked to an axis of rotation of a crane by a gearbox. The asynchronous machine can be provided at the level of the rotor or not. Here is the modeling of a wound rotor asynchronous machine, knowing that to find that a machine induction (thus without power to the rotor), simply short-circuit the rotor, that is considered a voltage zero at its terminals.

To simulate this machine these entries will be the values of the tension in the stator and the rotor (Vs, Vr) and the speed of rotation of the electric machine (ω_m). With these values and equations that model the machine we get (Is,Ir) currents, electric rotation speed (ω) and electromagnetic (Tem) torque.

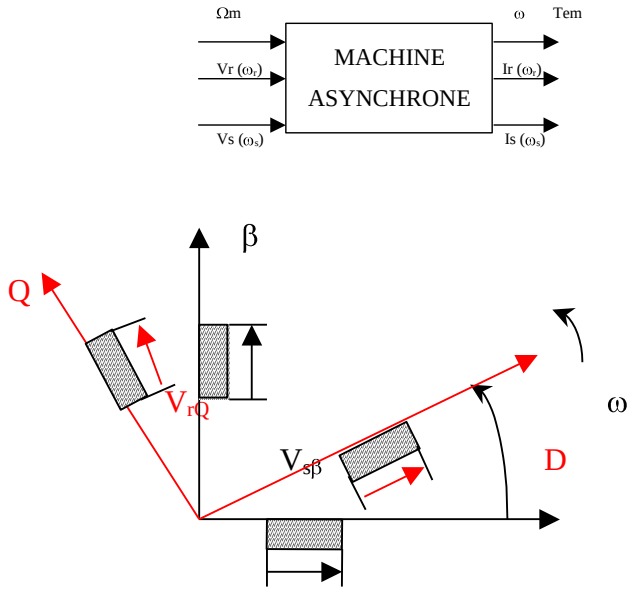

Figure 20. Diagram of blocks and axes for the engine system

As indicated earlier, the model of the machine must allow the simulation of a machine (at induction) squirrel cage and both wound rotor machine. This electric machine is powered with a voltage in the rotor.
This is achieved by designing a model in which the entries are tension in the stator and rotor and exits (corresponding to the state variables) to the rotor and the stator currents.
To simulate the case of a rotor in cage, tensions in the rotor are short-circuited (they have a value of zero). Model of asynchronous machine based on state variables $[i_{\alpha s}, i_{\beta s}, i_{\alpha r}, i_{\beta r}]^t$.

$$\bar{u}_s = R_s \cdot \bar{i}_s + \frac{d\bar{\Psi}_s}{dt}$$

$$\bar{\Psi}_s = L_s \cdot \bar{i}_s + L_h \cdot \bar{i}_r$$

$$\bar{u}_r = R_r \cdot \bar{i}_r + \frac{d\bar{\Psi}_r}{dt} - j \cdot \omega_m \cdot \bar{\Psi}_r$$

$$\bar{\Psi}_r = L_r \cdot \bar{i}_r + L_h \cdot \bar{i}_s$$

By replacing:

$$\bar{u}_s = R_s \cdot \bar{i}_s + L_s \cdot \frac{d\bar{i}_s}{dt} + L_h \cdot \frac{d\bar{i}_r}{dt}$$

$$\bar{u}_r = R_r \cdot \bar{i}_r + L_r \cdot \frac{d\bar{i}_r}{dt} + L_h \cdot \frac{d\bar{i}_s}{dt} - j \cdot \omega_m \cdot L_r \cdot \bar{i}_r - j \cdot \omega_m \cdot L_h \cdot \bar{i}_s$$

Hence the equations of State in which the derivative of each of the variables ($\bar{i}_s, \bar{i}_r$) depends on state variables and inputs (voltage).

$$\frac{d}{dt}\begin{pmatrix}\bar{i}_s\\ \bar{i}_r\end{pmatrix}=\frac{1}{(L_s\cdot L_r-L_h^{\,2})}\begin{pmatrix}-R_s\cdot L_r-j\cdot\omega_m\cdot L_h^{\,2} & L_h\cdot R_r-j\cdot\omega_m\cdot L_h\cdot L_r\\ L_h\cdot R_s+j\cdot\omega_m\cdot L_s\cdot L_h & -R_r\cdot L_s+j\cdot\omega_m\cdot L_s\cdot L_r\end{pmatrix}\cdot\begin{pmatrix}\bar{i}_s\\ \bar{i}_r\end{pmatrix}+$$
$$+\frac{1}{(L_s\cdot L_r-L_h^{\,2})}\begin{pmatrix}L_r & -L_h\\ -L_h & L_s\end{pmatrix}\cdot\begin{pmatrix}\bar{u}_s\\ \bar{u}_r\end{pmatrix}$$

If we take the real and imaginary part:

$$\frac{d}{dt}\begin{pmatrix}i_{\alpha s}\\ i_{\beta s}\\ i_{\alpha r}\\ i_{\beta r}\end{pmatrix}=\frac{1}{(L_s\cdot L_r-L_h^{\,2})}\cdot\begin{pmatrix}-R_s\cdot L_r & \omega_m\cdot L_h^{\,2} & L_h\cdot R_r & \omega_m\cdot L_h\cdot L_r\\ -\omega_m\cdot L_h^{\,2} & -R_s\cdot L_r & -\omega_m\cdot L_h\cdot L_r & L_h\cdot R_r\\ L_h\cdot R_s & -\omega_m\cdot L_s\cdot L_h & -R_r\cdot L_s & -\omega_m\cdot L_s\cdot L_r\\ \omega_m\cdot L_s\cdot L_h & L_h\cdot R_s & \omega_m\cdot L_s\cdot L_r & -R_r\cdot L_s\end{pmatrix}\cdot\begin{pmatrix}i_{\alpha s}\\ i_{\beta s}\\ i_{\alpha r}\\ i_{\beta r}\end{pmatrix}+$$
$$+\frac{1}{(L_s\cdot L_r-L_h^{\,2})}\cdot\begin{pmatrix}L_r & 0 & -L_h & 0\\ 0 & L_r & 0 & -L_h\\ -L_h & 0 & L_s & 0\\ 0 & -L_h & 0 & L_s\end{pmatrix}\cdot\begin{pmatrix}u_{\alpha s}\\ u_{\beta s}\\ u_{\alpha r}\\ u_{\beta r}\end{pmatrix}$$

The solutions of these equations are currents. They will determine at any time the torque developed by the machine with the following equation:

$$T_{em}=\frac{3}{2}pL_h\cdot\left(i_{\alpha s}\cdot i_{\beta r}+i_{\beta s}\cdot i_{\alpha r}\right)$$

The mechanical equation calculates the speed of the axis of the engine:

$$T_{em}-T_{res}-D\cdot\omega_m=J\cdot\frac{d\omega_m}{dt}$$

where there is the presence of load torque, coefficient of friction and inertia of the engine.

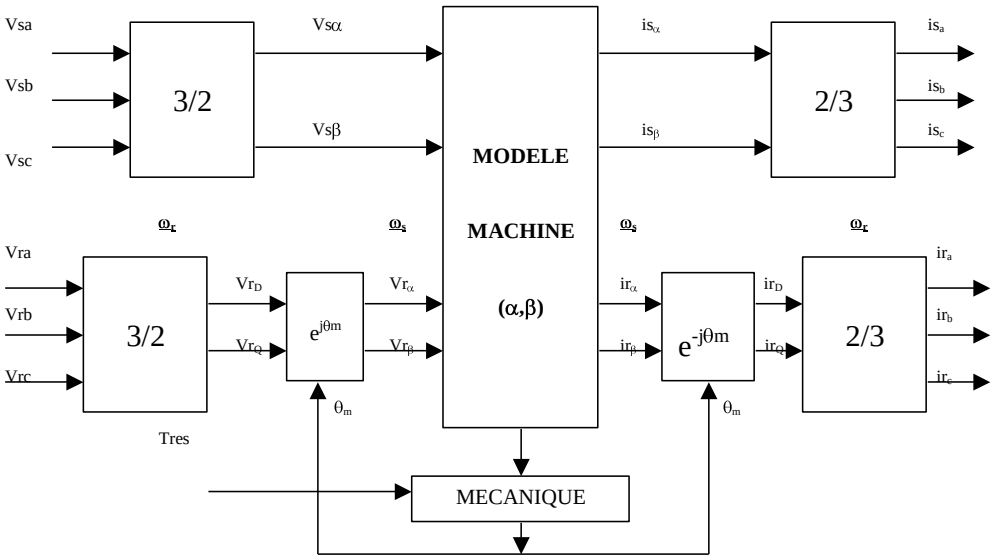

Figure 21. Change of reference axis system

On the other hand, the equivalent circuit of the machine translating static behavior is as follows:

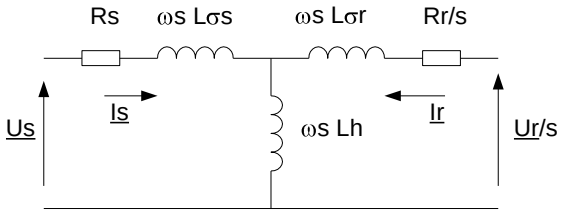

Figure 22. Equivalent circuit of asynchronous machine

Where Lσs is the inductance of leaks and Ls = Lh + Lσs.
A note that in the equivalent circuit all quantities are mentioned in the frequency of synchronization ω_s (Ur is different from V_r, since the last turn with an electrical pulse equal in frequency to the rotor ω_r). Relations between different frequencies are:

- The landslide $s = \frac{\omega_s - \omega_m}{\omega_s}$
- $\omega_s = \frac{2\pi \cdot Ns}{60} = \frac{2\pi}{60} \cdot 60 \cdot f$
- ωr (rotor)= ω_s (synchrony)- ω_m (engine)

The equations of tension of the stator and the rotor by phase are:

$$\begin{cases} Us = Rs \cdot Is + j\omega_s \cdot L\sigma s \cdot Is + j\omega_s \cdot Lh \cdot (Is + Ir) \\ \frac{Ur}{s} = \frac{Rr}{s} \cdot Ir + j\omega_s \cdot L\sigma r \cdot Ir + j\omega_s \cdot Lh \cdot (Is + Ir) \end{cases}$$

- The active powers :

$$\Rightarrow Pmec = \underbrace{-3 \cdot Ur \cdot Ir \cdot \cos\theta \cdot \frac{(1-s)}{s}}_{\text{P dissipated in the source}} + \underbrace{3 \cdot Rr \cdot \frac{(1-s)}{s} \cdot I_r^2}_{\text{P in the load}} = Tem \cdot \omega_m$$

$$\begin{cases} \Pr = -\dfrac{s}{(1-s)} \cdot Pmec \\ Ps = -s \cdot Pmec \end{cases}$$

- The reactive powers:

$$\begin{cases} Qr = \dfrac{3}{2} \cdot (Urq \cdot Ird - Urd \cdot Irq) \\ Qs = \dfrac{3}{2} \cdot (Usq \cdot Isd - Usd \cdot Isq) \end{cases}$$

Modeling of resistive loads

Many loads are resistive type. They can be modelled as a simple resistance whose value depends on the power consumed by the load.

Others

Power lines of Port of Bayonne grid

These lines can be modelled with a resistor and an inductance in series, such as lines of the interconnected network. The distribution system lines are more resistive than those of transport grids. It must be taken into account in the choice of values for the parameters R and L.

Transformer

The transformer is an isolated AC /AC electrical energy converter. The two primary functions are isolated energy transmission and modification of the level of an alternative source.
In an ideal transformer modeling, considering that there is:

- is no losses in conductors;
- losses in the magnetic core is no;
- infinite permeability of the magnetic circuit;
- a magnetic coupling perfect windings.

For a more realistic modelling, is taken into account:

- Losses by Joule effect in conductors;
- Losses in the magnetic core by Eddy current and hysteresis;
- Permeability finite magnetic circuit;

- Imperfect windings magnetic coupling.

In this case, the equivalent circuit of the transformer is as follows:

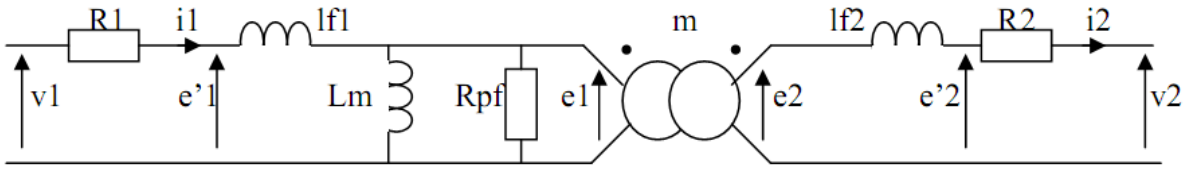

Figure 23. Equivalent circuit of the transformer

5 MODEL OF RURAL MICROGRID FOR IRRIGATION PUMPING

The microgrid to be simulated in detail is an irrigation pumping station with wind power support and storage, located in the Valdabra reservoir (Huesca). In this microgrid there are integrated wind power generation, a reversible hydraulic pump, hydrogen storage and ultracapacitors. The objective of this installation is to support water pumping but in addition to increase the transport capacity of the rural network, avoiding grid extensions in the case of the connection of new consumption.
The pumping station is located at Valdabra, next to the reservoir of the same name, near the town of Huesca (GPS: 42.0680, -0.4427). The installation consists of the following elements:

- AC/DC converter for grid connection (250 kW)
- Chopper with resistors (rated at 250 kW)
- ADES Wind Turbine 250 kW
- Three simple (110.4 kW) and one reversible hydraulic pump (160 kW)
- Energy storage with 260 Maxwell 3 kF ultracaps (700V, 11.5 F)
- Portable energy storage system
- Control and communication system (Measurement, PLC and SCADA)

5.1 Case 1: HOMER model of Irrigation pumping station

This first case is only simulated in HOMER/HOGA, and PSAT. In order to demonstrate how the model might look like, as an example the input variables are given for the case of the model in HOMER. In order to present these input variables, HOMER provides an interesting tool called “HTML Input Summary”, which is used here to create the data presentation.

5.1.1 HOMER Input Summary

File name: Valdabra_template.hmr
File version: 2.81
Author: Hans Bludszuweit
Notes: Optimagrid: Case 1: Valdabra pumping station

AC Load: 490 kW pumps

Data source:	demanda_valdabra.txt
Daily noise:	0.526%
Hourly noise:	2.11%
Scaled annual average:	3.3 MWh/d
Scaled peak load:	487 kW
Load factor:	0.281

Figure 24. Basic parameters of AC load.

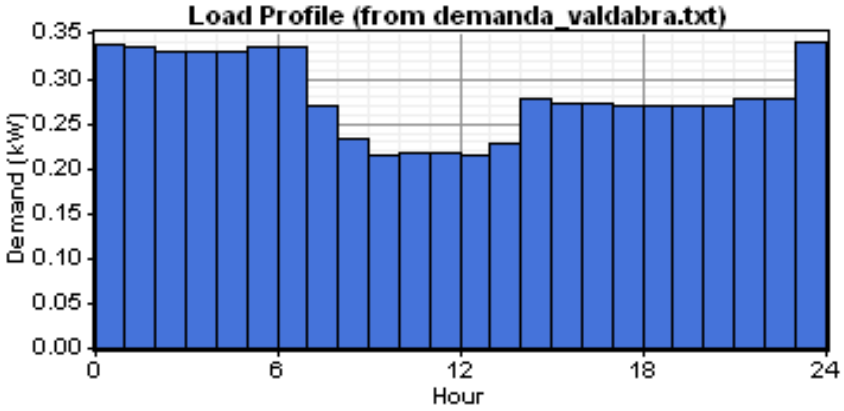

Figure 25. Annual mean load profile of the pumping station, given per unit.

PV

Size (kW)	Capital ($)	Replacement ($)	O&M ($/yr)
1.000	2,000	2,000	5

Sizes to consider: 0, 50, 75 kW
Lifetime: 30 yr
Derating factor: 80%
Tracking system: No Tracking
Slope: 42.6 deg
Azimuth: 0 deg
Ground reflectance: 20%

Solar Resource

Latitude: 42 degrees 35 minutes North
Longitude: 1 degrees 18 minutes West
Time zone: GMT +1:00

Data source: Synthetic

Month	Average Radiation ($kWh/m^2/d$)
Jan	1.670
Feb	2.560
Mar	3.820
Apr	4.450
May	5.380
Jun	6.210
Jul	6.300

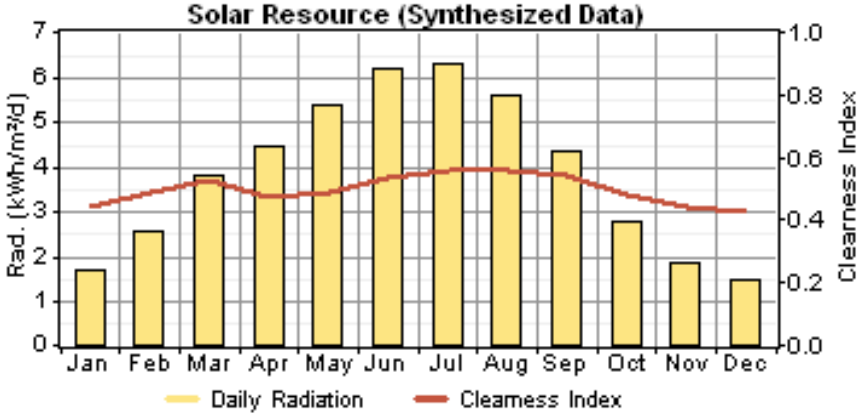

Aug	5.580
Sep	4.320
Oct	2.780
Nov	1.820
Dec	1.450

Figure 26. Monthly solar resource.

Scaled annual average: 3.87 kWh/m²/d

AC Wind Turbine: ADES 250kW

Quantity	Capital ($)	Replacement ($)	O&M ($/yr)
1	300,000	300,000	3,000

Quantities to consider: 0, 1, 2, 5, 10

Lifetime: 25 yr

Hub height: 31 m

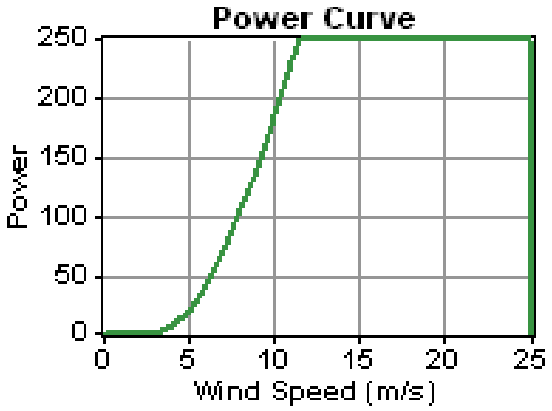

~~Figura~~ Figure 27. ADES 250 kW power curve.

Wind Resource

Data source: wind_walqa.txt

Month	Wind Speed (m/s)
Jan	5.90
Feb	6.14
Mar	5.47
Apr	6.17
May	6.32
Jun	4.46
Jul	5.97
Aug	4.50
Sep	4.48
Oct	5.97

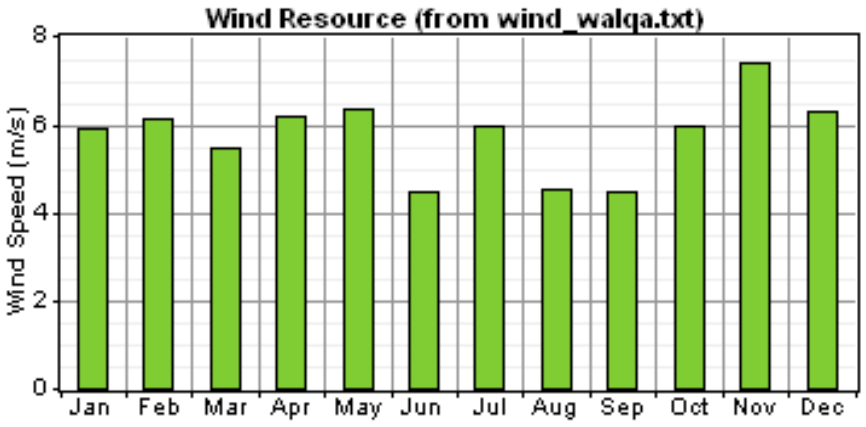

~~Figura~~ Figure 28. Monthly wind resource.

Nov	7.38
Dec	6.29

Weibull k:	1.60	Anemometer height:	50 m
Autocorrelation factor:	0.966	Altitude:	500 m
Diurnal pattern strength:	0.184	Wind shear profile:	Logarithmic
Hour of peak wind speed:	20	Surface roughness length:	0.01 m
Scaled annual average:	5.75 m/s		

AC Hydro

Capital cost:	$ 500,000
Replacement cost:	$ 250,000
O&M cost:	$ 5,000/yr
Lifetime:	40 yr
Available head:	12.5 m
Design flow rate:	2,000 L/s
Min. flow ratio:	50%
Max. flow ratio:	100%
Turbine efficiency:	75%
Pipe head loss:	1.88%

Consider systems without hydro: Yes

Hydro Resource

Data source: Synthetic

Month	Stream Flow (L/s)
Jan	8,700
Feb	10,000
Mar	7,800
Apr	8,200
May	5,000
Jun	2,000
Jul	1,300
Aug	1,100
Sep	1,400
Oct	3,300
Nov	6,000
Dec	9,100

Residual flow: 1,000 L/s
Scaled annual average: 2,000 L/s

Battery: Surrette 4KS25P*

Quantity	Capital ($)	Replacement ($)	O&M ($/yr)
1	2,660	2,660	10.00

Quantities to consider: 50, 100, 200
Voltage: 4 V
Nominal capacity: 1,900 Ah
Lifetime throughput: 10,569 kWh
Min battery life: 4 yr

Converter

Size (kW)	Capital ($)	Replacement ($)	O&M ($/yr)
200.000	187,000	187,000	3,000
2,000.000	1,450,000	1,450,000	22,000

Sizes to consider: 250 kW
Lifetime: 25 yr
Inverter efficiency: 96%
Inverter can parallel with AC generator: Yes
Rectifier relative capacity: 107%
Rectifier efficiency: 95%

Grid

Rate	Power Price	Sellback Rate	Applicable
	$/kWh	$/kWh	
P1	0.113	0.113	Jan-Feb, Dec Weekdays 10:00-13:00, 18:00-21:00 Jun-Jul Weekdays 11:00-19:00
P2	0.095	0.095	Jan-Feb, Dec Weekdays 08:00-10:00, 13:00-18:00, 21:00-24:00 Jun-Jul Weekdays 08:00-11:00, 19:00-24:00
P3	0.08	0.08	Mar, Nov Weekdays 16:00-22:00 Sep Weekdays 09:00-15:00
P4	0.08	0.08	Mar, Nov Weekdays 08:00-16:00, 22:00-24:00 Sep Weekdays 08:00-09:00, 15:00-24:00
P5	0.072	0.072	Apr-May, Oct Weekdays 08:00-24:00
P6	0.056	0.056	Jan-Jul, Sep-Dec Weekdays 00:00-08:00 Jan-Dec Weekends 00:00-24:00

Aug Weekdays 00:00-24:00

Other parameters

Economics

Annual real interest rate: 6%
Project lifetime: 25 yr
Capacity shortage penalty: $ 0/kWh
System fixed capital cost: $ 0
System fixed O&M cost: $ 0/yr

Generator control

Check load following: No
Check cycle charging: Yes
Setpoint state of charge: 80%
Allow systems with multiple generators: Yes
Allow multiple generators to operate simultaneously: Yes
Allow systems with generator capacity less than peak load: Yes

Constraints

Maximum annual capacity shortage: 0%
Minimum renewable fraction: 0%
Operating reserve as percentage of hourly load: 10%
Operating reserve as percentage of peak load: 0%
Operating reserve as percentage of solar power output: 0%
Operating reserve as percentage of wind power output: 0%

6 MODEL OF INDUSTRIAL AREA WITH SMALL WORKSHOPS AND INDUSTRIAL STORES

The generic case describes typical industrial areas where the activity is dominated by small workshops, small factories and industrial stores. This type of industrial areas is very common in the entire zone of SUDOE (Portugal, Spain and south-west France).

In this case, no renewable energy generation is present and the aim of the model is twofold. First, a possible development of distributed generation is simulated as an optimised planning problem with a planning horizon of 20 years. In a second step, the operation of a developed microgrid after 20 years is simulated with the same method as for the real case. It is assumed that solar pv, wind and hydro power resources are available and the corresponding generators may be connected at certain nodes to the grid. The topology of such a microgrid is basically linear, as these industrial areas are distributed along a road. In **¡Error! No se encuentra el origen de la referencia.**, the assumed grid structure is depicted.

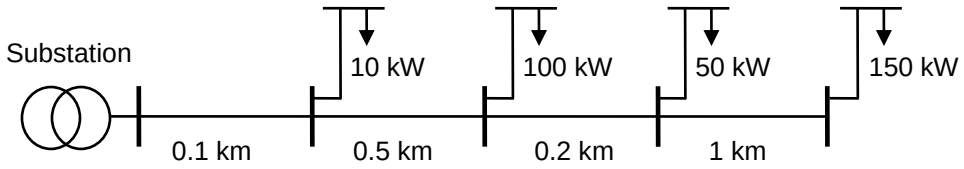

Figure 29. Microgrid structure of assumed industrial area

This case will be simulated with all the above mentioned software tools. As the implementation in HOMER/HOGA, and PSAT is basically a question of parameterization of the network (consumption profiles, generation profiles, power line lengths and parameters), in this section, only the model in GAMS is presented. Although the characterisation of solar and wind resources is the subject of another GT of this project, in order to integrate it into GAMS, some methods are presented here too.

6.1 The objective function

In the model for optimal expansion planning of distributed generation, the objective function $F(x)$ is minimized being subject to a set of constraints $h(x)$ and $g(x)$:

$$F(x) = \min[f(x)] \quad (1)$$

$$h(x) = 0 \quad (2)$$

$$g(x) \leq 0 \quad (3)$$

In the optimization problem presented here, the objective function is the total system cost and restrictions are: balance of power in nodes (Kirchhoff's current law), balance of generation, balance of energy in the storage units (state of charge), power capacity limits of substations, generators and storage units, capacity limits of power lines, voltage limits in nodes.

The probabilistic model of the system provides a large number of deterministic results, representing different expansion scenarios. These results are expressed as histograms expanded in time. The stochastic input variables are: electricity demand, wind generation, photovoltaic generation and hydro generation.

The objective function to be minimized is the total cost C_{total} over the planning horizon, which in this case is 20 years. To do this, annual costs are calculated for the expansion for every year. Project costs are derived by adding the fixed costs and variable costs per day multiplied by 365 and by 20. Finally, the costs are annualized with the so-called "Capital Recovery Factor". As a result, the objective function can be formulated as follows:

$$C_{total} = \min\left[\sum_a \sum_k \left\{ f_{re} CF_{a,k} + CRF \sum_{j=1}^{y} \left(\frac{1+g_k}{1-r}\right)^j \left(CVA_{a,k} + 365 \sum_t CV_{a,k,t} \right) \right\}\right] \quad (4)$$

with

$$CRF = \frac{r\,(1+r)^y}{(1+r)^y - 1} \quad (5)$$

where C is the total cost of the system, CRF is the capital recovery factor, k are the network elements, t are the periods, CF_k is the fixed cost of element k, f_{re} is the reduction factor of installation costs of element k, CVA_k is the annual variable cost of element k, $CV_{k,t}$ is the variable cost of element k as a function of time t, g_k is the rate of increase of variable cost of element k, r is the market interest rate, and y is the project planning horizon in years.

In the first year, the whole distribution system is set up, under the condition that no distributed generation and no storage are present. As a result, lines are sized according to the load flows and the associated annualized costs are calculated. From the second year onwards, the installation of distributed generation and storage is allowed, but no additional lines can be added. The installation cost of the new capacity is annualized and added to the costs originated from the first year, and so on. For every year, the sum of these annualized costs is minimized. If this annual cost is divided by the annual demand of energy, the cost of energy can be calculated for every year of the planning horizon as shown in (6). This way, the evolution of the minimized COE is obtained in €/kWh.

$$COE_a = \frac{C_a}{E_a} \quad (6)$$

where C_a is the cumulated annualized cost after a years, E_a is the energy demand in year a.

Fixed costs

In the following equation, the fixed costs of the network elements are formulated.

$$C_L = \sum_{ij} c_{f,ij}\, P_{ijmax} \quad (7)$$

$$C_W = \sum_i \sum_w c_{f,w}\, P_{wmax,i} \quad (8)$$

$$C_{PV} = \sum_i \sum_w c_{f,pv}\, P_{pvmax,i} \quad (8)$$

$$C_H = \sum_i \sum_w c_{f,mgh}\; P_{mghmax,i} \quad (9)$$

$$C_S = \sum_i \sum_{st} \left\{ c_{fp,st}\, P_{stmax,i} + c_{fe,st}\, E_{stmax,i} \right\} \quad (10)$$

where C_L, C_W, C_{PV}, C_H and C_S are the fixed costs of distribution lines ij, wind generators w, solar generators pv, mini-hydro generators mgh and storage units st, with corresponding fixed cost coefficients c_f in €/kW and for storage $c_{fp,st}$ in €/kW and $c_{fe,st}$ in €/kWh, P_{ijmax}, $P_{wmax,i}$, $P_{pvmax,i}$, $P_{mghmax,i}$, $P_{stmax,i}$ are the installed power of lines and generators and $P_{stmax,i}$ and $E_{stmax,i}$ are de power and energy capacity of the storage unit st at node i.

Variable costs

Next, variable costs are described. The cost related to energy obtained from the grid $C_{E,t}$ in every time period t is given in (11).

$$C_{E,t} = f_{pe} \cdot PE_t \sum_i \sum_q E_{q,i,t} \tag{11}$$

where f_{pe} is the escalation factor of the electricity Price, PE_t in €/kWh at time t, $E_{q,i,t}$ is the energy in kWh imported from the grid at time t through substation q at node i.

In this model, the variable costs are referred as operational costs, which are supposed to be proportional to the investment cost. In case of storage, the cost of energy losses is included too.

One exception is the variable cost of distribution lines, which is assumed to be exclusively the energy loss. If line losses are linearized, the variable cost of the lines at time t $C_{LO,t}$ can thus be written as

$$C_{LO,t} = \sum_{ij} c_{v,ij,t} \cdot P_{ij,t} \cdot P_{ijmax} \tag{12}$$

with

$$c_{v,ij,t} = PE_t \cdot 0.75 \cdot FP_{ij} \cdot \frac{R_{ij}}{U_{n,ij}^2} \cdot p_t \tag{13}$$

where $c_{v,ij,t}$ is the loss cost coefficient of line ij in period t in $€/(kW)^2$, $P_{ij,t}$ is the power in kW transported by line ij in period t, P_{ijmax} is the maximum capacity in kW of line ij, PE_t is the electricity Price in period t in $€/kWh$, FP_{ij} is the loss factor, R_{ij} the phase resistance in Ω, and $U_{n,ij}$ the nominal voltage in V of line ij, p_t is the duration of period t in hours.

The annual operational costs of the renewable generators are calculated as a percentage of the investment cost with a coefficient of variable costs c_v as can be seen in the following equations.

$$C_{WO} = \sum_i \sum_w c_{v,w,i} \cdot C_{w,i} \tag{14}$$

$$C_{PVO} = \sum_i \sum_{pv} c_{v,pv,i} \cdot C_{pv,i} \tag{15}$$

$$C_{HO} = \sum_i \sum_{mgh} c_{v,mgh,i} \cdot C_{mgh,i} \tag{16}$$

where c_v are the annual O&M cost coefficients in p.u. and C are the investment costs with the indices w, pv y mgh for wind, solar pv and mini-hydro generation and i is the node.

In the case of storage, the energy loss has to be added to the variable costs.

$$C_{SO,t} = \sum_i \sum_{st} \{c_{v,st,i} \cdot C_{S,st,i} + 365 \cdot C_{p,st,i}\} \tag{17}$$

with

$$C_{p,st,i} = PE_t \cdot p_t \cdot \left(P_{c,st,i,t}\left(1 - \eta_{c,st,i,t}\right) + P_{d,st,i,t}\left(1 - \eta_{d,st,i,t}\right)\right) \tag{18}$$

where $c_{v,st,i}$ the annual O&M cost coefficient per unit of investment cost $C_{S,st,i}$ and $C_{p,st,i}$ is the daily cost of energy losses for storage unit st at node i, $P_{c,st,i,t}$ and $P_{d,st,i,t}$ are the power of charge and discharge in kW during period t, $\eta_{c,st,i,t}$ and $\eta_{d,st,i,t}$ are the efficiencies of charge and discharge.

Note that for simplification, in the variable costs for storage there are included several quite different costs, such as normal O&M costs and the replacement of lager parts of the storage system, due to a shorter lifetime (inverters, battery packs, etc.)

6.2 Modeling of charge and discharge cycles of the storage

Charge and discharge cycles of the storage units are introduced into the model assuming that they are completed in 24 h, which leads to the condition that SOC is zero at the beginning and at the end of the day. Charge and discharge efficiency is defined separately, including wiring and the inverter. To adequately model the storage it is necessary to introduce a model of the state of charge SOC which provides the energy stored in any moment. This is necessary to model the charge limits. The depth of discharge (DoD) is assumed to be 100%. Possible limitations of the DoD depend on the storage technology and can be taken into account when sizing the storage unit to be installed. Below see the model of SOC:

$$SOC_{st,i,t} = SOC_{st,i,(t-1)} + E_{c,st,i,t} - E_{d,st,i,t} \tag{20}$$

with

$$E_{c,st,i,t} = P_{c,st,i,t} \cdot \eta_{c,st,i,t} \cdot p_t \tag{21}$$

$$E_{d,st,i,t} = \frac{P_{d,st,i,t}}{\eta_{d,st,i,t}} \cdot p_t \tag{22}$$

6.3 Constraints

The restrictions imposed here on the optimization problem for distributed generation planning are: balance of power in nodes (Kirchhoff's Current Law), capacity limits of power flow in lines, maximum generator power capacity, power and energy limits in storage units, substation power limit and voltage limit in nodes.
In (19) the balance in every node is shown. Note that distribution losses $P_{p,ij,t}$ and storage losses $P_{p,st,i,t}$ are included.

$$D_{i,t} = \begin{cases} \sum_{ij} \left[\left(P_{ij,t} - P_{p,ij,t} \right) - \left(P_{ji,t} - P_{p,ji,t} \right) \right] + \sum_{q} P_{q,i,t} \\ + \sum_{w} P_{w,i,t} + \sum_{pv} P_{pv,i,t} + \sum_{mgh} P_{mgh,i,t} \\ + \sum_{st} \left[P_{d,st,i,t} - P_{c,st,i,t} - P_{p,st,i,t} \right] \end{cases} \tag{23}$$

where $D_{i,t}$ is the demand in node i in time period t, $P_{p,ij,t}$ and $P_{p,ji,t}$ are los line losses in directions ij and ji, $P_{p,st,i,t}$ are the storage losses.

Finally, several limits are imposed on the different system elements. Power lines are limited by their thermal limit P_{ijmax} and as power flows in opposite directions are modeled separately ($P_{ij,t}$ and $P_{ji,t}$), no negative power flows are permitted. In (24) the set of restrictions of the distribution power lines is shown.

$$\begin{aligned} 0 \le P_{ij,t} \le P_{ijmax} \\ 0 \le P_{ji,t} \le P_{ijmax} \end{aligned} \tag{24}$$

Finally, the restrictions of the storage are defined. Power limits for charging and discharging are separated and SOC is limited between zero and the maximum storage capacity E_{stmax}.

$$P_{c,st,i,t} \leq P_{c,stmax,i} \quad (28)$$

$$P_{d,st,i,t} \leq P_{d,stmax,i} \quad (29)$$

$$0 \leq SOC_{st,i,t} \leq E_{stmax,i} \quad (30)$$

6.4 Model of intermittent energy sources

In this model, three types of renewable energy sources are considered: solar pv, wind and mini-hydro power. From real world data, probability density functions (pdf) are obtained and translated into a model of states in a Markov chain.

For hydro power, daily mean values are assumed. For solar and wind power, hourly means are modelled.

6.4.1 Mini-hydro power

The pdf of the hydro power resource is obtained by fitting the Generalized Extreme Value Distribution to available data. The pdf $f(x)$ and cdf (cumulative distribution function) $F(x)$ are given in the following equation.

$$f(x) = \frac{1}{\sigma} e^{-(1+kz)^{-\frac{1}{k}}} (1+kz)^{-1-\frac{1}{k}} \quad (6.1)$$

$$F(x) = e^{-(1+kz)^{-\frac{1}{k}}} \quad (6.2)$$

Con

$$z = \frac{x-\mu}{\sigma} \quad (6.3)$$

where σ is the standard deviation, μ the mean and k a parameter which defines the tail of the distribution.

The historical data used in this example is shown in **¡Error! No se encuentra el origen de la referencia.** The cdf of that data and the fitted $F(x)$ are shown in Fig. 31. The obtained parameters in this case are:
k = 0.6, σ = 0.6 and μ =1.05.

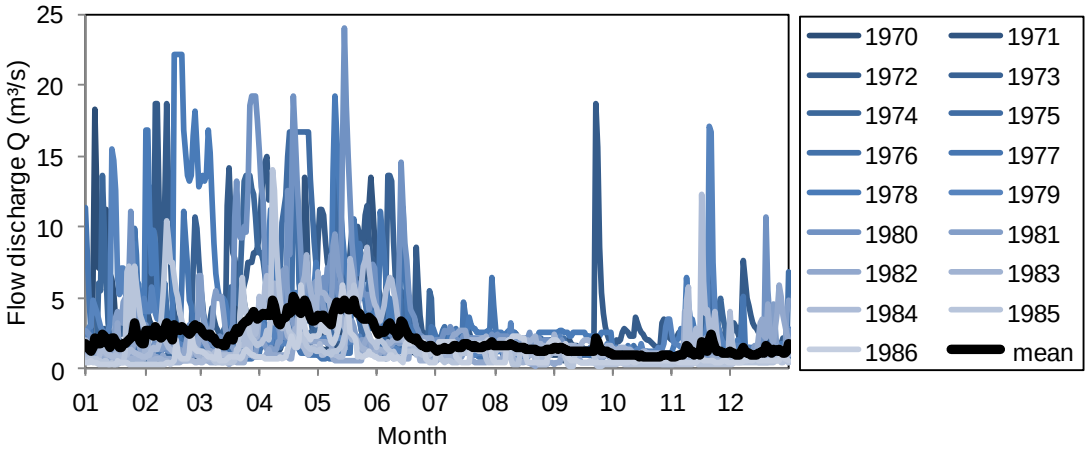

Figure 30. Average daily flow in mountain river for 10 years.

For the simulation, the inverted cdf is used, as shown in the following equation.

$$F^{-1}(u) = \mu + \frac{\sigma}{k}(-\log\, u)^{-k} - \frac{\sigma}{k}, \qquad 0 < u < 1 \qquad (6.4)$$

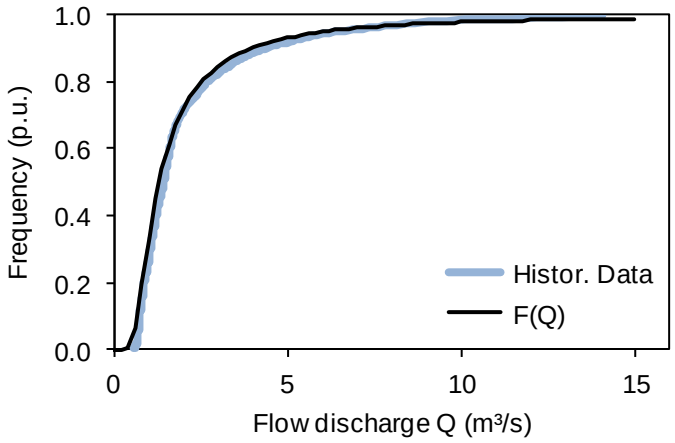

Figure 31. Density function of probability vs. Flow.

6.4.2 Solar PV

In the case of PV power, at least hourly mean values are needed to be modelled, in order to represent properly the intermittent behaviour of the this resource. Therefore, a pdf is developed for every hour of the day. As a simple approximation, the distribution of possible values within a certain hour of the day, the Beta pdf is applied here.

The Beta pdf is defined as follows:

$$f(x) = \frac{1}{B(a,b)} \cdot x^{a-1} \cdot (1-x)^{b-1} \cdot I(0,1)(x) \qquad (6.5)$$

$$B(a,b) = \int_0^1 x^{a-1} \cdot (1-x)^{b-1} dx \qquad (6.6)$$

where $B(a,b)$ is the Beta function and I(x) the Indicator función

As can be seen above, the integral, represented by $B(a,b)$ normalizes $f(x)$ to the interval [0,1]. The Indicator function assures that all values of x outside the interval [0,1] have probability zero.
The parameters a and b can be obtained directly from the mean μ and standard deviation σ of the data. The corresponding relationships are shown below.

$$\mu = \frac{a}{a+b} \qquad \sigma^2 = \frac{a \cdot b}{(a+b+1) \cdot\ a+b^2} \qquad (6.7)$$

$$a = \frac{(1-\mu) \cdot \mu^2}{a^2} - \mu \qquad b = \frac{1-\mu}{\mu} \cdot a \qquad (6.8)$$

One limitation of the Beta distribution is that all values must be different from zero and one. While solar pv generation seldom reaches nominal power (P = 1 p.u.), the percentage of zero values is elevated, due to the variable length of the days during the year. Therefore, in order to obtain acceptable values with that approximation, zero values must be treated separately. Here, before fitting the Beta distribution, zero values are counted for every hour

of the day and divided by the total number of samples in that hour. The result is ratio of zero values n_0. After that, zeros are removed from the dataset and the parameters of the Beta distribution are obtained with betafit (function in Matlab).

The resulting pdf, assuming zero values writes as follows:

$$f(x) = \begin{cases} \frac{1-n_0}{B(a,b)} \cdot x^{a-1} \cdot (1-x)^{b-1} \cdot I(0,1)(x) & ; \text{x} > 0 \\ n_0 & ; \text{x} = 0 \end{cases} \qquad (6.9)$$

Fitting results for an example from Zaragoza, are shown in **¡Error! No se encuentra el origen de la referencia.** The hourly values were obtained from monthly means which were introduced to HOMER. It can be observed, that the problem of zero values only occurs during three hours in the morning and three hours in the evening. But in other latitudes, this may change drastically. While in the tropics, the problem would disappear, in the polar region, there might be 24 hours with some zero values (but not all zero).

Hour	μ	σ	a	b	n_0
4	0	0	0	0	1
5	0.002	0.005	0.322	142.908	0.737
6	0.028	0.042	0.254	9.138	0.482
7	0.093	0.100	0.332	3.489	0.236
8	0.208	0.150	1.207	4.674	0
9	0.344	0.174	2.343	4.471	0
10	0.468	0.196	2.612	2.960	0
11	0.558	0.207	2.289	1.751	0
12	0.592	0.220	1.728	1.099	0
13	0.601	0.216	1.954	1.225	0
14	0.546	0.204	2.449	2.031	0
15	0.454	0.194	2.457	2.978	0
16	0.329	0.172	2.224	4.539	0
17	0.186	0.148	0.937	4.205	0
18	0.086	0.096	0.310	3.571	0.277
19	0.024	0.039	0.252	10.410	0.507
20	0.001	0.003	0.357	232.464	0.759
21	0	0	0	0	1

Table 3. Parameters for the approximation with the Beta distribution, including percentage of cero values.

In **¡Error! No se encuentra el origen de la referencia.**, cumulative probability functions are shown for the hours 6, 8, 10 and 12, in order to illustrate the quality of approximation. Solid lines show the curves, based on the cumulative histogram and dashed lines the results using Beta distributions and zero values using the parameters exposed in **¡Error! No se encuentra el origen de la referencia.**. The general approximation is quite good, but there are some shortcomings.

It can be observed that there is a visible deviation for the curve at noon. As a result, solar power at noon is slightly over estimated. Another shortcoming of the Beta distribution is that it has a quite long tail. That means that for

example for hour six, the probability of solar power >0.2 p.u. is not zero, although this is a contradiction to the observation. As a result, maximum power values at early morning and late evening are slightly over estimated.

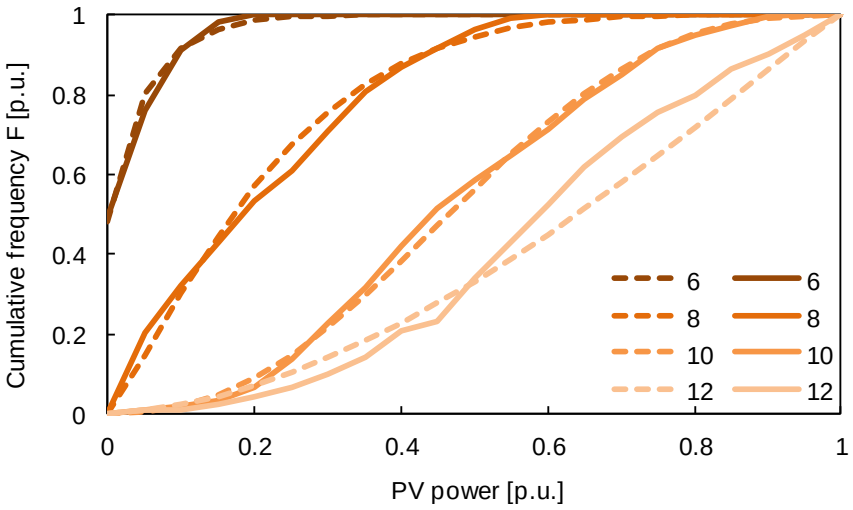

Figure 32. Cumulative distributions from data (Hist) and modeled with Beta pdf (Beta) for hours 6, 8, 10, and 12 of the day.

In **¡Error! No se encuentra el origen de la referencia.**, probability intervals are shown, based on the cumulative histograms obtained from the data.

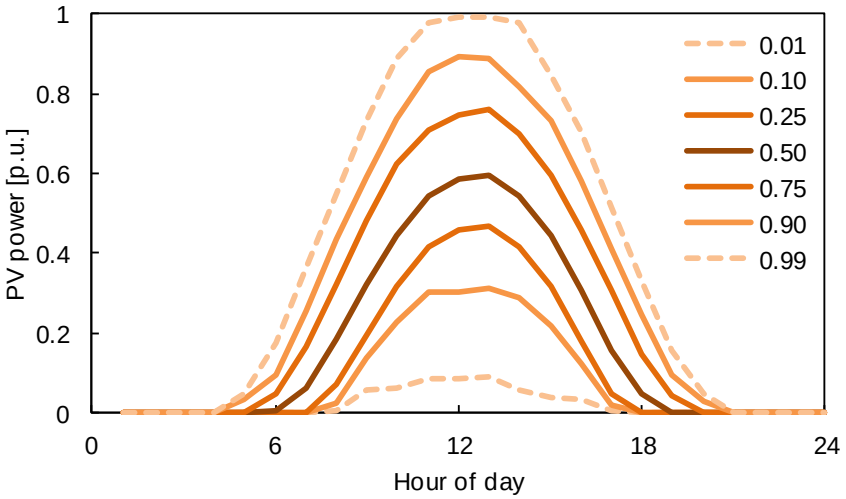

Figure 33. Probability intervals of daily solar radiation based on hourly data generated with HOMER from monthly means from Zaragoza, Spain.

It can be observed that only for 1% of all daily curves, maximum power output is achieved. In general, the expected variability over the year is represented clearly. Therefore, in order to model correctly the solar resource, seasonal differences should be taken into account, using the information of monthly mean values.

6.4.3 Wind

For the description of the wind energy resource, classical Weibull distribution is used. If hourly mean values are available for at least one year, HOMER produces several useful curves, such as monthly box plots (see **¡Error! No se encuentra el origen de la referencia.**) and probability density (histogram) with best fit of a Weibull distribution (see **¡Error! No se encuentra el origen de la referencia.**). In **¡Error! No se encuentra el origen de la referencia.** a DMap is shown, where hourly wind speeds are represented for every day of the year.

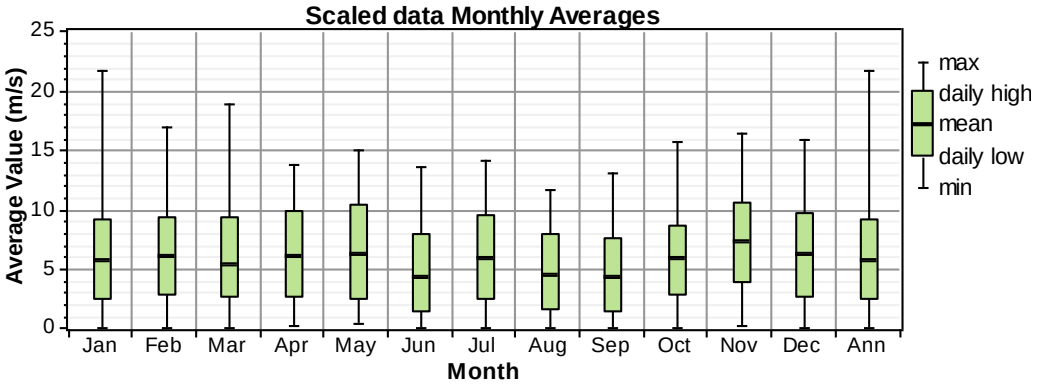

Figure 34. Monthly box plots generated with HOMER from hourly mean wind speed data from Walqa (Huesca), Spain.

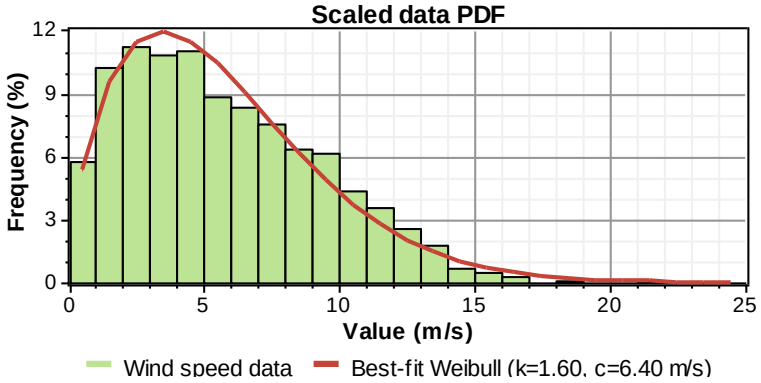

Figure 35. Histogram and best-fit Weibull distribution generated with HOMER from hourly mean wind speed data from Walqa (Huesca), Spain.

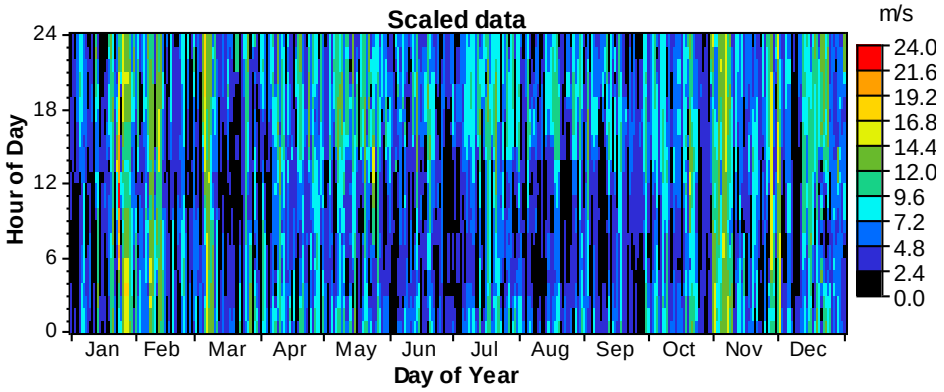

Figure 36. DMap of hourly wind speed generated with HOMER.

7 MODEL OF AICIA MICROGRID FACILITY

The AICIA micro-grid is located at the laboratory building in Engineering School of the University of Seville. The system includes renewable energy simulators, an electrolyser, hydrogen storage, batteries, a fuel cell and also plug-in hybrid vehicles.

The plant is equipped with a 6 kW programmable power supply to simulate cycles of electricity generation from various renewable sources (wind speed curves of wind turbines, radiation curves in photovoltaic and solar thermal plants, etc.), a PEM electrolyser (1 kW) for hydrogen production, a hydride tank for H_2 storage, a PEM Fuel cell of 1,5 kW, electronic loads of 2,5 kW to simulate different use conditions of the grid use and finally various auxiliary systems required for the operation of the plant: waste water, cooling water, hot water, nitrogen inerting, gas detection, etc..

In **¡Error! No se encuentra el origen de la referencia.** a picture of facility is shown.

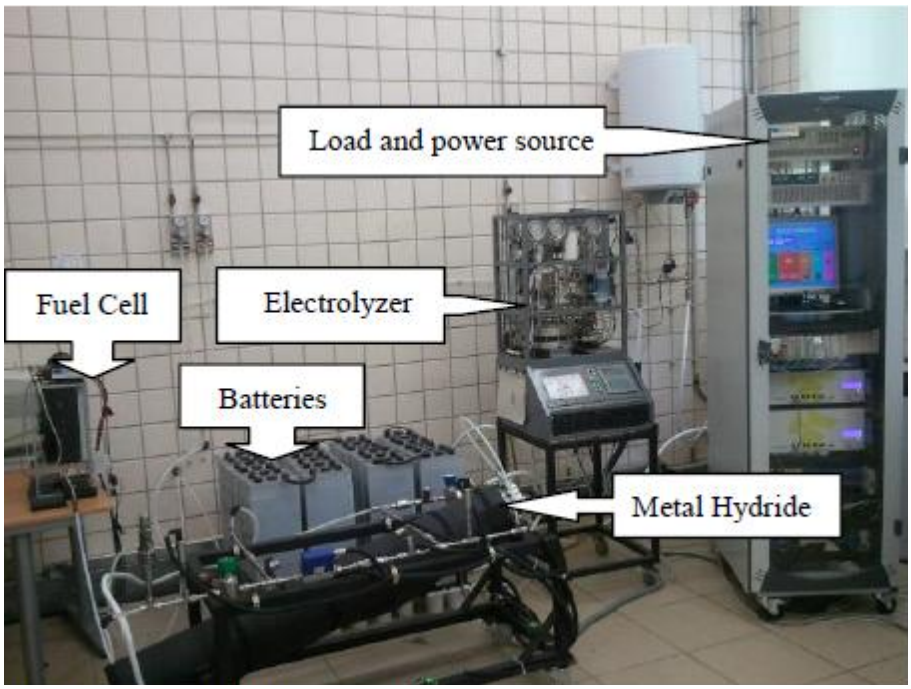

Figure 37. AICIA Micro-Grid Facility.

As an example of model implementation, in next sections several models of ESSFER tool are described. In particular, models presented are: Wind turbine model, electrolyzer model and PEMFC model.

7.1 Wind turbine model

The wind turbine model is based on a methodology developed to characterize its real behavior in a specific location [1]. The methodology is applied in three steps:

1) Get the real power curve for the site, processing measured operating data by following the steps outlined in norm UNE 61400-12.

2) For each wind speed, calculate the normalized power difference points, according to equation 1, where the normalized power difference is equal to the difference of power according to manufacturer power curve and the real curve divided by the maximum power of the wind turbine. This calculation should be performed for several wind speeds within the operation range.

$$DP_{nom}=(P_{wt,man}-P_{wt,real})/P_{wt,max} \quad (1)$$

3) Adjust the normalized power differences points of the previous step by means of a fitted curve (power difference curve). An equation for the curve, based on a 4-parameter Weibull (a, b, c and d) depending on the type of wind turbine, location and operating conditions, is proposed. The mathematical expression of the Weibull curve is shown in equation 2. The selected curve adjusts satisfactorily with experimental points (obtained in the previous step) and allows to be standardized for other wind turbines.

$$DP_{nom,mod} = a\left(\frac{d-1}{d}\right)^{\frac{1-d}{d}}\left(\frac{v-b}{c}+\left(\frac{d-1}{d}\right)^{\frac{1}{d}}\right)^{d-1} exp\left(-\left(\frac{v-b}{c}+\left(\frac{d-1}{d}\right)^{\frac{1}{d}}\right)^{d}+\frac{d-1}{d}\right) \quad (2)$$

The Power generated by wind turbine, for each wind speed, is calculated, according to the proposed model ($P_{wt,mod}$) as the difference between manufacturer power curve ($P_{wt,man}$) and the maximum power ($P_{wt,max}$) multiplied by the power difference curve ($DP_{nom,mod}$). Equation 3 shows the curve for the proposed model curve:

$$P_{wt,mod} = P_{wt,man} - P_{wt,max} \cdot DP_{nom,mod} \quad (3)$$

7.2 Electrolyzer model

The electrolyzer model is based on an electrical mathematical equations. Globally, the electrolyzer model calculates the hydrogen production ($n_{H2,prod}$) from the electric power consumed ($P_{elec,AC}$).
The electrical module is based on the electrolytic cell current-voltage characteristic curve. The equation proposed by Ulleberg [2] is modified in order to improve the adjustment between operating data and model results [1]. A current-voltage curve equation is developed, and its dependence on electrolyzer temperature, has the following expression:

$$U = U_{rev} + \frac{r_0+r_1T}{A} I + \mathrm{s}\log\left(\frac{t_0+t_1T+t_2T^2}{A} I + 1\right) \quad (4)$$

U_{rev} is the reversible voltage, calculated from the thermodynamic of the process. The parameters ri and ti are determined from measured experimental data, following the methodology indicated in Pino [3].
Hydrogen production is directly proportional to the current circulating in the cells, and it is calculated from Faraday's equation (equation 5). Faraday's performance (equation 6) depends on two parameters which are also determined from measured experimental data [4].

$$\dot{n}_{H_2} = \varepsilon_F \frac{nc\, I}{z\, F} \quad (5)$$

$$\varepsilon_F = f_2 \frac{(I/A)^2}{(I/A)^2+f_1} \quad (6)$$

The electrolyzer operation temperature is considered constant in simulations. Pino [3] demonstrated that the difference of results, obtained from simulations of an electrolyzer with a time step of one hour when the operating temperature is constant or variable, is negligible.

7.3 Fuel cell model

Fuel cell model is based in formulation proposed by Mann et al. [4] and Corrêa [5][6] where the single cell voltage (U_{FC_cell}) from stack is calculated using next equation:

$$U_{FC\_cell} = U_{Nerst} - U_{act} - U_{ohm} - U_{con} \qquad (7)$$

Where: U_{Nerst} is the Nesrt Potential, and U_{act}, U_{ohm} and U_{act} are respectively the activation, ohmic and concentration voltage losses. The Nerst Potential and voltage losses are modelled using equations of Mann's model [4].
Fuel cell stack voltage is calculated multiplying the number of cell with the single cell voltage (U_{FC_cell})
As electrolyzer model, fuel cell operating temperature will be considered constant when simulations with a time of one hour are done.

8 DESCRIPTION OF THE SOFTWARE

For each one of the test cases each of the research centers or companies involved in the project will use different software and programs. It is not compulsory to use the same program and even is more valuable to use different systems to compare results and to obtain a technological transfer between partners of Optimagrid project.

The software use for each of the partners or in each of the test cases to analyze could be seen in the following table:

Software usado para modelización y dimensionamiento

Case	Partner	Software for Sizing	Software to Model
Microgrid at Walqa Technological Park	FHA	HOMER	Matlab Simulink, PSAT
Microgrid at Sangüesa (CENER installations)	CENER	HOMER	Matlab Simulink
Microgrid at Port of Bayonne	ESTIA	HOMER	Matlab Simulink, Eurostag
Rural Microgrid for Irrigation Pumping	CIRCE	HOGA, HOMER	PSAT
Industrial Area with Small Workshops and Industrial Stores	CIRCE	HOGA, HOMER	PSAT
AICIA microgrid facility	AICIA	HOMER	ESSFER Tool

Table 4. Software used in each of the test cases

A brief description of the software used could be seen as follows.

8.1 Matlab Simulink

MATLAB (matrix laboratory) is a fourth-generation programming language and a development environment. It is used for purposes of computation. Developed by The MathWorks, MATLAB allows the manipulation of matrices, the display of the curves and data, implementation of algorithms, creation of user interfaces. It may in addition to interface with other languages such as C, C++, Java, and Fortran. Users of MATLAB are very different environments such as engineering, science and the economy in a context as well industrial to research. MATLAB can if use alone or with a toolbox (Toolbox). Simulink is a platform of multi-domain simulation and modelling of dynamic systems. It provides a graphical environment and a set of libraries containing the modeling blocks allowing accurate design, simulation, the implementation and the control of communications and signal processing systems. Simulink is integrated with MATLAB, providing immediate access to many algorithmic development tools, visualization and analysis of data from MATLAB.

MATLAB® is a high-level technical computing language and interactive environment for algorithm development, data visualization, data analysis, and numerical computation. Using MATLAB, you can solve technical computing problems faster than with traditional programming languages, such as C, C++, and Fortran.

You can use MATLAB in a wide range of applications, including signal and image processing, communications, control design, test and measurement, financial modeling and analysis, and computational biology. Add-on toolboxes (collections of special-purpose MATLAB functions) extend the MATLAB environment to solve particular classes of problems in these application areas.

MATLAB provides a number of features for documenting and sharing your work. You can integrate your MATLAB code with other languages and applications, and distribute your MATLAB algorithms and applications.
Simulink® is an environment for multidomain simulation and Model-Based Design for dynamic and embedded systems. It provides an interactive graphical environment and a customizable set of block libraries that let you design, simulate, implement, and test a variety of time-varying systems, including communications, controls, signal processing, video processing, and image processing.

Add-on products extend Simulink software to multiple modeling domains, as well as provide tools for design, implementation, and verification and validation tasks.
Simulink is integrated with MATLAB®, providing immediate access to an extensive range of tools that let you develop algorithms, analyze and visualize simulations, create batch processing scripts, customize the modeling environment, and define signal, parameter, and test data.

Additionally, SimPowerSystems™ extends Simulink® with tools for modeling and simulating the generation, transmission, distribution, and consumption of electrical power. It provides models of many components used in these systems, including three-phase machines, electric drives, and libraries of application-specific models such as Flexible AC Transmission Systems (FACTS) and wind-power generation. Harmonic analysis, calculation of Total Harmonic Distortion (THD), load flow, and other key power system analyses are automated. SimPowerSystems models can be discretized to speed up simulations.

8.2 EUROSTAG

Developed by EDF and TRACTEBEL, is used by electricity companies, academics and builders for the simulation of the dynamic behavior of electrical networks (http://www.eurostag.be).

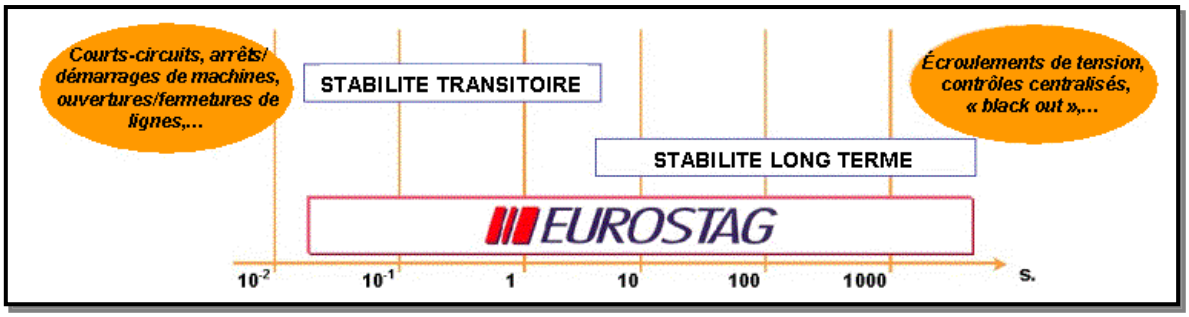

Figure 38. The extent of the phenomena studied by EUROSTAG

8.3 HOMER and HOGA for renewable energy system sizing

HOMER **¡Error! No se encuentra el origen de la referencia.** (Hybrid Optimization Model for Electric Renewables) is a simulation tool which was originally designed at the National Renewable Energy Laboratory (NREL). Now it is licensed to HOMER Energy. A basic version (called “HOMER legacy”) can be downloaded for free. It is version 2.68 and is no longer improved. To obtain a new version with the latest tools, a license must be purchased.

HOMER is a simple computer model, developed for the task of designing distributed generation (DG) systems (on and off-grid). HOMER's optimization and sensitivity analysis algorithms allow for an evaluation of the economic and technical feasibility of a large number of technology options and to account for variations in technology costs and energy resource availability.
HOMER is based on a chronological simulation (one year). HOMER can provide an important overview that compares the cost and feasibility of different configurations; then designers can use more specialized software to model the technical performance.
An interesting feature of HOMER is its sensitivity analysis. It helps determine the potential impact of uncertain factors such as fuel prices or mean wind speed. On the web pages of HOMER, a screen shot is presented which shows a possible representation of such a sensitivity analysis (see Fig. 39)
The intuitive user interface permits to obtain results quickly. The drawback of this program is that no actual optimization algorithm is implemented. The user must provide ALL possible options and HOMER just tries out all combinations and gives as result all feasible solution, sorted by the cost of energy (COE) in $/kWh. As a result, of the search space is too large simulations can quickly take very long time.
HOMER has been chosen in this project as reference simulation tool, in order to make results of different project members comparable.
An interesting alternative to HOMER is a software, developed at the University of Zaragoza, named HOGA, which will be described briefly in the next paragraphs.

HOGA [7] stands for “Hybrid Optimization by Genetic Algorithms” and aims to solve very similar problems as HOMER. But the main difference is that it actually uses optimization algorithms which make it much more effective searching for an optimum solution. A screen shot (see Fig. 40) from HOGA web page shows the main screen where the hybrids system is developed.

Comparison of HOGA and HOMER
It can be stated that these two software tools are complementary. In order to obtain best results, the following strategy may be used:

- Simulation of consumption profiles with HOGA in order to optimize the sizing of System elements and control strategies
- Sensitivity analysis with HOMER, using as base case the configuration found with HOGA. Possible variables for this analysis: annual mean values of wind speed and solar radiation, height of the wind turbine, interest rates, prices of the elements

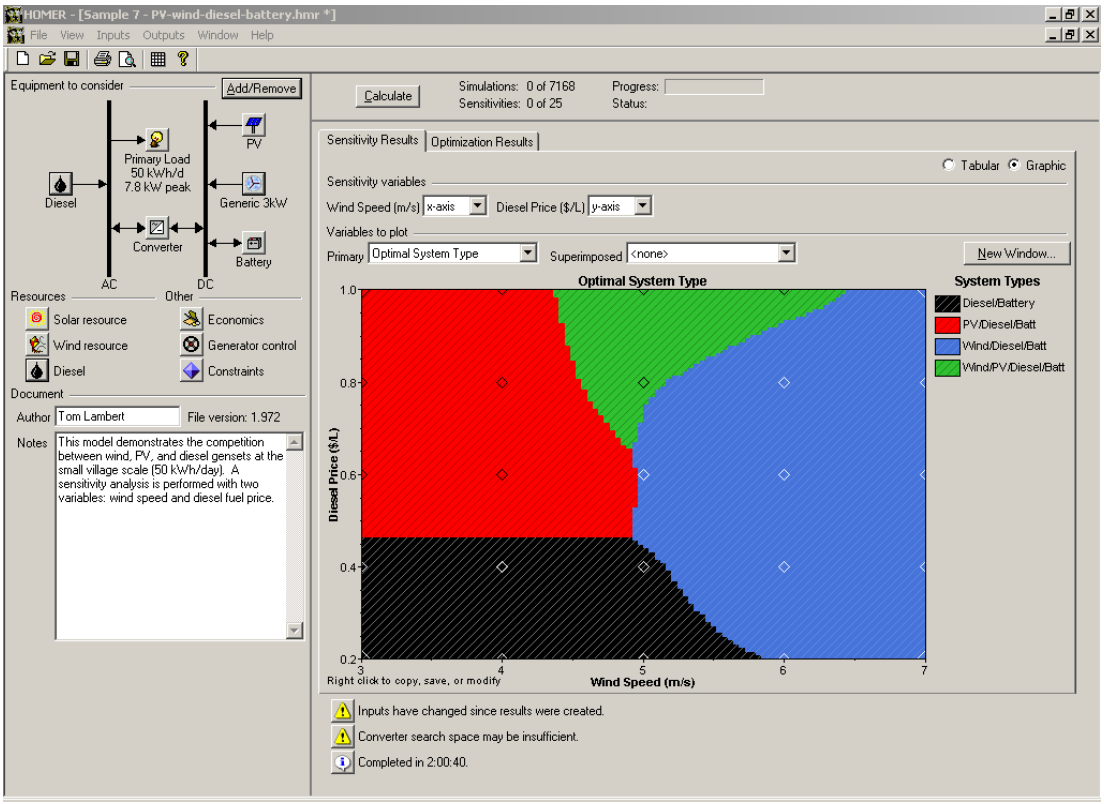

Figure 39. Screenshot from HOMER webpage, with graphical representation of a sensitivity analysis.

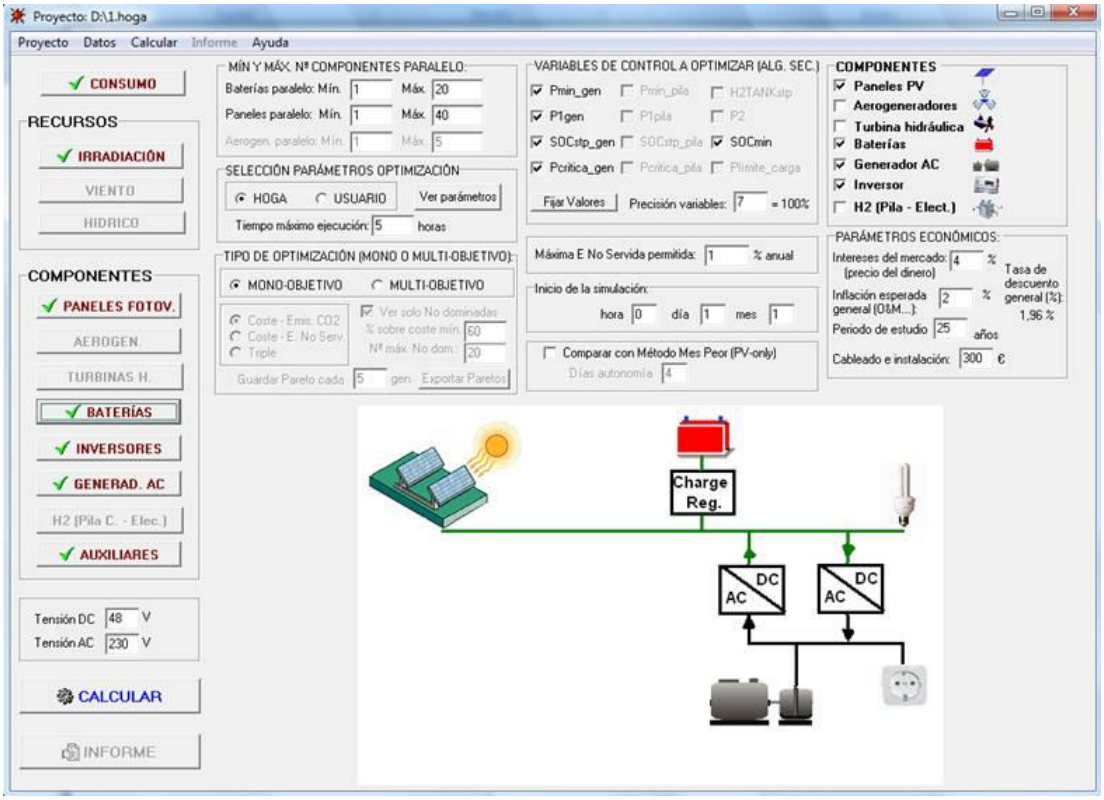

Figure 40. Screenshot from HOGA webpage, with main screen of the software.

HOGA tends to propose larger system elements. Thus, a sensitivity study with HOMER might be useful to obtain a solution with lower system costs.

As a result of the simulation with HOGA and HOMER will stand a proposal for an optimized configuration in order to introduce distributed generation into the industrial areas under study.
But this is just one solution, assuming a certain cost of the renewable energy. But a more realistic scenario is to assume that costs, especially of solar pv will be reduced in the near future, and thus a gradual implementation may be expected, depending on the configuration of the system. May be that in a beginning, no energy storage is installed, because it is still very costly, but at a certain moment in the future, it will become interesting to install such systems, because they make excess energy generation useful and thus directly lower the overall cost of energy. Such a model is presented in the next subsection.

8.4 GAMS for planning

GAMS (General Algebraic Modeling System) [8] is a modeling language, rather than a program to solve optimisation problems. It contains a modeling package, along with several solvers for LP (linear programming), MIP (Mixed Integer Programming), NLP (Non-Linear Programming), MINLP (Mixed Integer Non-Linear Programming), etc.
This language is a flexible and powerful modeling instrument. A good introduction to GAMS is given in [10] where some interesting examples are given. Another good introduction to GAMS is given in Spanish language in [10]. The GAMS Data Exchange (GDX) module permits reading data from Excel or directly from Matlab [11].
GAMS is a commercial software, which is offered in several versions. The basic student version is limited to 1000 non-zero elements (for LP and NLP) and 20 integer variables.
In order to solve any problem with GAMS, a command file must be created. This is a simple text file with the extension *.GMS. Here, the entire model is created, including the interfaces with other programs such as Excel or Matlab. The file is divided in several blocks. In **¡Error! No se encuentra el origen de la referencia.**, the structure of a GAMS optimization model is shown.

Definition	Purpose
Set (s)	Declaration of names and values of counting indices
Scalar (s)	Declaration of names and values of scalar variables
Parameter (s)	Declaration of names and values of vectors
Table (s)	Declaration of names and values of matrices
Variable (s)	Declaration of variables and their type
Equation (s)	Definition of the objective function and constraints
Model	Assign model name and list of constraints
Solve	Indicate the solver which GAMS should use
Display	Indicate elements to show in the list of results

Table 5. Block structure of a GAMS model.

8.5 PSAT for load flow analysis

PSAT (Power System Analysis Toolbox) [12] is a Matlab toolbox for electric power system analysis and simulation. It is freely available software, developed by Dr. Federico Milano of the University of Castilla – La Mancha, Spain. The latest version (2.1.6) can be downloaded at the web page of PSAT [12]. The main features of PSAT are:

Continuation Power Flow (CPF)
Optimal Power Flow (OPF)
Small Signal Stability Analysis
Time Domain Simulation

A screen shot of the main window can be seen in **¡Error! No se encuentra el origen de la referencia.**.

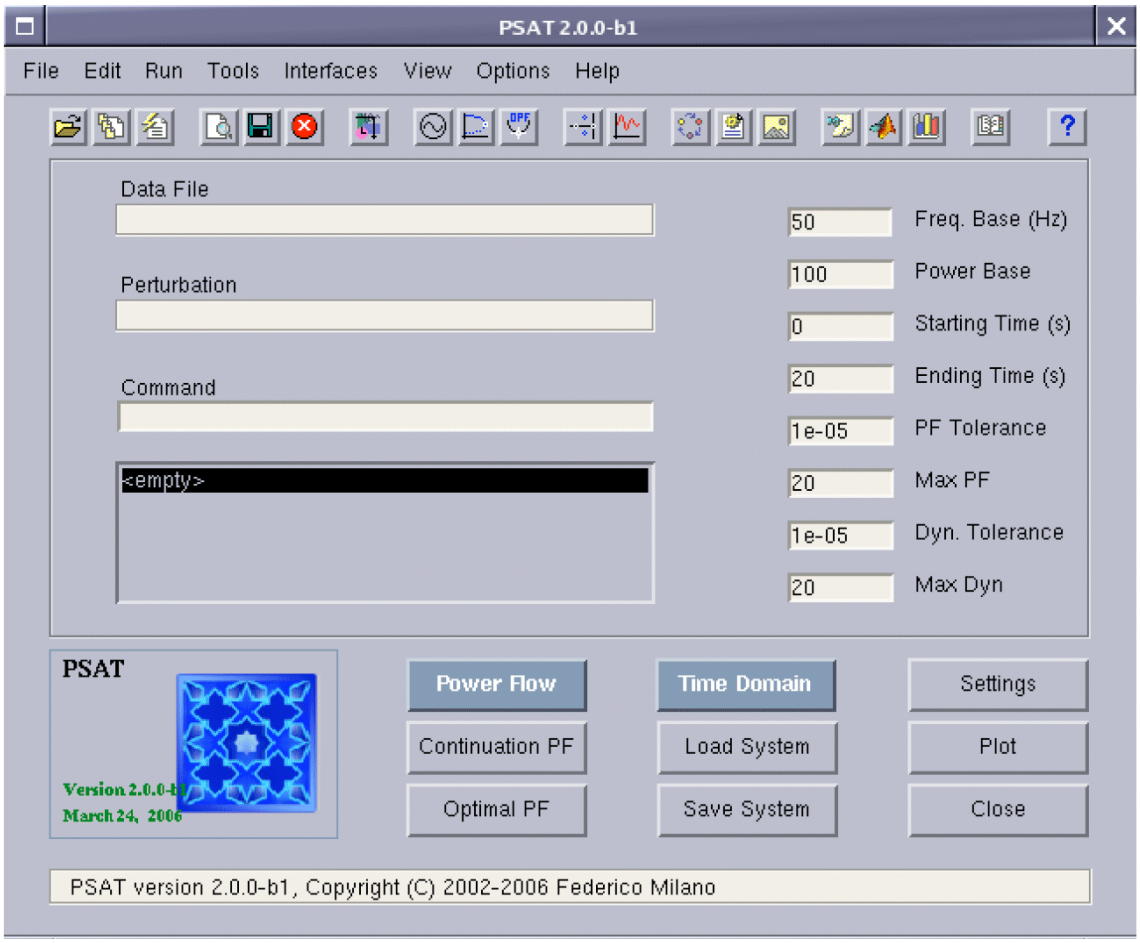

Figure 41. Screenshot from PSAT main screen.

At the PSAT web page [12] a presentation is available which contains a brief introduction to PSAT. In this document, an interesting comparison is provided between several Matlab-based software packages (see **¡Error! No se encuentra el origen de la referencia.**). The abbreviations in that table are describes below:

Power system analysis tools:

- EST: Educational Simulation Tool

- MatEMTP: Electromagnetic Transients Program in Matlab
- MatPower: Matlab Power System Simulation Package
- PAT: Power Analysis Toolbox
- PSAT: Power System Analysis Toolbox
- PST: Power System Toolbox
- SPS: SimPowerSystems
- VST: Voltage Stability Toolbox

Feartures illustrated in the table below:

- PF: Power flow
- CPF-VS: Continuation power flow and/or voltage stability analysis
- OPF: Optimal power flow
- SSA: Small signal stability analysis
- TD: Time domain simulation
- EMT: Electromagnetic Transients
- GUI: Graphical user interface
- GNE: Graphical network editor

Package	PF	CPF	OPF	SSA	TD	EMT	GUI	GNE
EST	✓			✓	✓			✓
MatEMTP					✓	✓	✓	✓
MatPower	✓		✓					
PAT	✓			✓	✓			✓
PSAT	✓	✓	✓	✓	✓		✓	✓
PST	✓	✓		✓	✓			
SPS	✓			✓	✓	✓	✓	✓
VST	✓	✓		✓	✓		✓	

Table 6. Comparison of Matlab-based power system analysis software [11].

From **¡Error! No se encuentra el origen de la referencia.** it can be seen that PSAT covers all features, except EMT. In addition, PSAT exploits Matlab vectorized computations and sparse Matrix functions in order to optimize performances. Finally, PSAT also contains interfaces to GAMS for example, which extends its ability to solve optimization problems.

CIRCE vision of the software

In the present report, a basic description of the simulation software is given. It is foreseen that HOMER, HOGA, PSAT and GAMS will be applied, each with a different purpose. HOMER and HOGA are suitable for a preliminary sizing of a hybrid system. GAMS is a platform were many different optimization problems can be solved. In this case, a least cost strategy for the successive installation of renewable energy sources into industrial areas will be implemented. The objective is to obtain a vision of a possible timeline in the next 20 years. Finally, PSAT is used to perform several power system analysis simulations.

Case 1 (irrigation pumping station) will be simulated with HOMER, HOGA and PSAT, while case 1 (generic industrial area with small workshops) will be simulated with HOMER, HOGA and GAMS.
In order to introduce the variability of renewable resources into the model of GAMS, some addition statistical models need to be developed.
At the end, results from HOMER and HOGA may be compared directly, as these programs have very similar objectives. Then, some of the results can be used in PSAT and GAMS to define possible scenarios of the system configuration.

8.6 ESSFER TOOL

ESSFER tool (Environment Simulation Tool for Renewable Energy Sources Systems) is a library of components, which it is possible to simulate and analyze systems based on renewable energy and hydrogen technology. It has been developed in several stages by various departments of Engineering School of University of Seville (www.us.es) and AICIA since 2002. Currently, the tool is an own-software of Thermal Engineering Group (Department of Energy Engineering). The modules have been developed for using them in simulation environment Matlab Simulink.
The tool has a library of modules (see Figure 1) to evaluate several integrated systems with renewable energy sources and hydrogen technology from an energy point of view. The system configuration is completely definable by user. The tool incorporates economic calculations. Time step can change from seconds to hours and time horizon is open to user preferences [1].
Modules used are improvement modules of TOPIC tool developed in Task 11 of the Hydrogen Implementing Agreement of the International Energy Agency.
In bibliography they are found two articles: first about an analysis of the increase in the rate of penetration of wind energy in the electrical system of Andalusia by integrating hydrogen technology in wind farms [2], and second about new model approaches to real behavior of facilities [1].

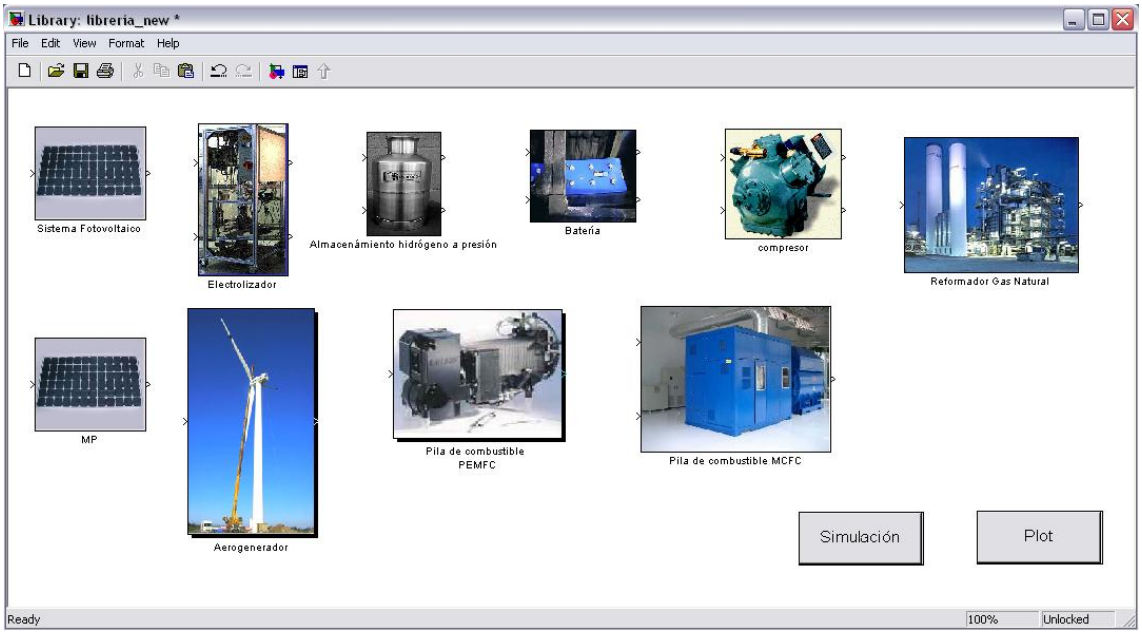

Figure 42. ESSFER Library.

Equipments implemented in tool are:

- POWER SOURCES: Solar Photovoltaic, Wind turbines, Electric grid.
- FUEL CELLS: PEM, MCFC and SOFC.
- STORAGE: Hydrogen and Baterries.
- HYDROGEN PRODUCTION: Alkaline Electrolyzers and Natural Gas reformers.

9 REFERENCES

[1] Pino FJ, Valverde L, Rosa F, Influence of wind turbine power curve and electrolyzer operating temperature on hydrogen production in wind-hydrogen systems. Journal of Power Sources 2011; 196:4418-26.

[2] Ulleberg O, Modeling of advanced alkaline electrolyzers: a system simulation approach, International Journal of Hydrogen Energy 2003; 28:21-33.

[3] Pino FJ, Analysis of hydrogen production in integrated wind-hydrogen systems. Contributions to dynamic system modelling PhD, University of Seville, Seville, 2010. ISBN: 978-84-693-9283

[4] Mann RF et al., Development and application of a generalized steady-state electrochemical model for a PEM fuel cell. Journal of Power Sources 2000; 86:173-80.

[5] Corrêa JM, Farret FA, Canha LN, Simulations of fuel-cell stack using a computer-controller power rectifier with the purposes of actual high-power injection applications. IEEE Transactions on Industry Applications 2003; 4:1136-42.

[6] Corrêa JM, Farret FA, Canha LN, Simões MG, An electrochemical-based fuel-cell model suitable for electrical engineering automation approach. IEEE Transactions on Industrial Electronics 2004; 51:1103-12.

[7] HOMER, Energy Modelling Software for Hybrid Renewable Energy Systems, online available: http://homerenergy.com

[8] HOGA – Hybrid Optimization by Genetic Algorithms, University of Zaragoza, Free download: http://www.unizar.es/rdufo/hoga.htm

[9] GAMS – General Algebraic Modeling System, online available: http://www.gams.com

[10] Castillo, E. *et al.* "Building and Solving Mathematical Programming Models in Engineering and Science" Wiley, 2002, Spanish version available: http://www.investigacion-operaciones.com/ARCHIVOS_LIBRO/LibroCompleto.pdf

[11] Casasus, T.M. *et al*., "Optimización económica con GAMS", Actas de V Jornadas ASEPUMA, 1997, available online: http://www.uv.es/asepuma/V/11.pdf

[12] GAMS. "On-line Documentation", available at: http://www.gams.com/docs/ document.htm, last visited 2012

[13] PSAT – Power System Analysis Toolbox, Federico Milano, Free download: http://www.uclm.es/area/gsee/web/Federico/psat.htm.

- SINTER project, http://www.sinter.es
- CNE, "Propuesta final de metodología para establecer tarifas de acceso a redes eléctricas", available online: http://www.cne.es/cne/doc/sesiones/ cne128_01.pdf
- Idoia Ederra Gil y Pilar Larumbe Martín, "Primera fase del 'Proyecto de eficiencia energética en los regadíos de Navarra' ", Servicio de Asesoramiento al Regante de Riegos de Navarra, S.A., available online: http://www.riegosdenavarra.com/ publica/publicaciones.htm
- Town council (Ayuntamiento) of Zaragoza, "Los polígonos industriales en Zaragoza y su entorno metropolitano: Deficiencias y potencialidades"

TITLE OF THE PROJECT: OPTIMAGRID SOE2/P2/E322

GT < 3 >: Implementation of micro-grids with high penetration of renewable energies

DELIVERABLE < 8 >: Evaluation of natural resources

ABSTRACT

This report comprises an analysis of the existing renewable resource available in the selected locations for the case studies, including wind, solar, hydraulic and biomass resource. This study is necessary in order to simulate the performance of the renewable generation equipments in the case studies in a realistic manner.

INDEX

LIST OF FIGURES

LIST OF TABLES

1. CASE STUDIES

Within the GT3 of the Optimagrid project, model simulations are planned in different industrial areas. The selected case studies should cover different climatic conditions in order to study different existing conditions of the SUDOE region in the simulations.

Figure 1. SUDOE region

The 5 selected case studies are detailed below and can be seen in Figure 2.

- Port of Bayonne (Decimal Coordinates 43.505, -1.495)
- Landaben industrial area (Decimal Coordinates 42.810, -1.710)
- Walqa technology park (Decimal Coordinates 42.112, -0.457)
- Valdabra pumping station (Decimal Coordinates 42.068, -0.443)
- Huelva chemical park (Decimal Coordinates 37.230, -6.940)

Figure 2. Location of the case studies

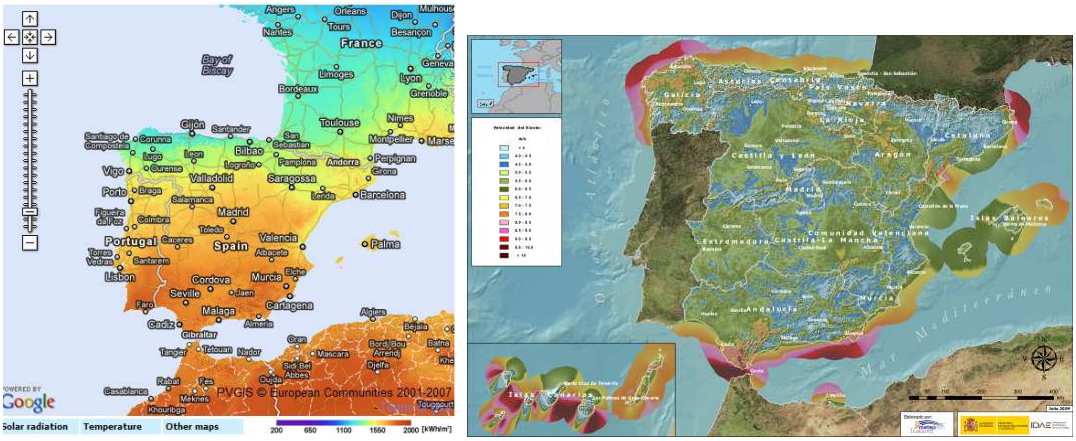

Figure 3. a) Map of solar resource in the SUDOE region; b) wind resource in Spain. Source: PVGIS; IDAE

2. WIND RESOURCE

CENER, in collaboration with the University of Athens, developed a methodology for the calculation of wind maps at regional scale from the skiron mesoscale model. These wind maps allow identifying the areas with the best conditions for the installation of wind farms, as well as simulating virtual wind measuring stations in any point of the simulated area. These virtual stations are useful to carry out calculations of energy production from a wind farm, as well as to have a wind data reference for the long term.

From this simulation tool, virtual wind data at a height of 50 metres for the last 7 years has been taken. The average parameters for the selected locations are shown in Table 1.

Table 1. Wind resource in the selected locations

Location	Bayonne	Landaben	Walqa-Valdabra	Huelva	**Typically**
Mean velocity (m/s)	5.21	5.30	5.81	5.10	
Weibull k	1.71	1.97	1.60	2.01	**1.50 - 2.50**
Autocorrelation factor	0.95	0.96	0.97	0.96	**0.80 - 0.95**
Diurnal pattern strength	0.07	0.10	0.15	0.11	**0.00 - 0.40**
Hour of peak windspeed	21	13	16	17	**14 - 16**

- Weibull k – The Weibull shape factor, which describes the breadth of the distribution of wind speeds over the year. A higher value means a more stable wind speed (less variability).
- Autocorrelation factor – A measure of how strongly the wind speed in one hour depends (on average) on the wind speed in the previous hour. A higher value means a stronger dependency on the previous hour (less variability).
- Diurnal pattern strength – A measure of how strong the wind speed depends on the time of day. A higher value means a stronger dependency on the time of day.
- Hour of peak windspeed – The time of day that tends to be windiest on average throughout the year.

Taking into account the resolution of the wind map, the same wind data is used for Walqa and Valdabra locations so the number of locations in the wind map is reduced to four.

In Table 1 we can see that Huelva has the weakest wind resource with an average of 5.10 m/s. Regarding the Weibull curve, every location has a different Weibull factor so there are locations with different wind speed distributions. Finally, the diurnal pattern strength is difficult to identify in an annual scope, as it changes a lot throughout the year as is shown in the next figures.

Most of the simulating tools ask for a one year wind data file, so we would have to select just one among the different years of virtual wind data. Thus, one representative year has been taken for each location and different figures have been pictured with “HOMER Energy” software which are shown below.

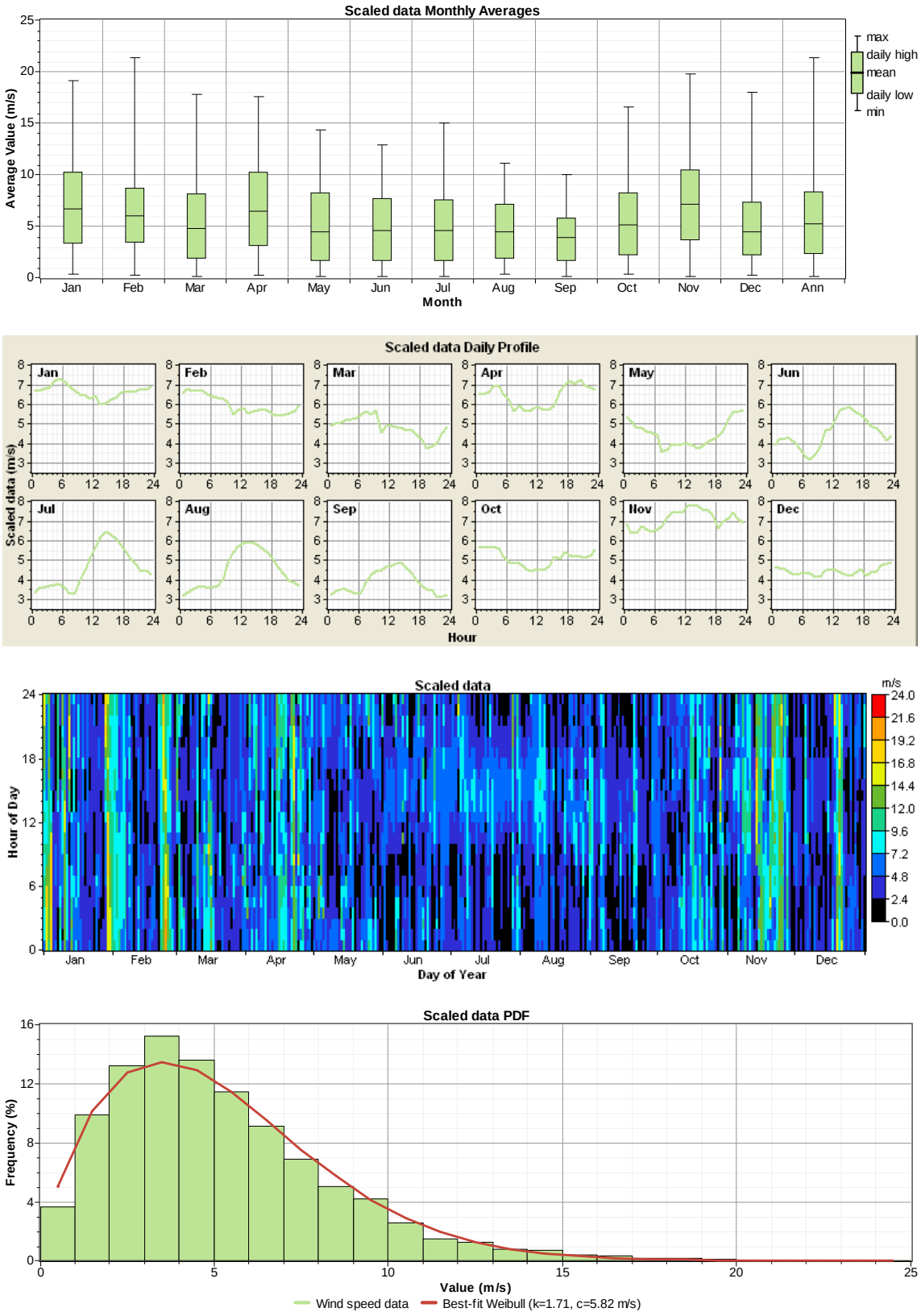

Figure 4. Wind speed in Bayonne in 2005

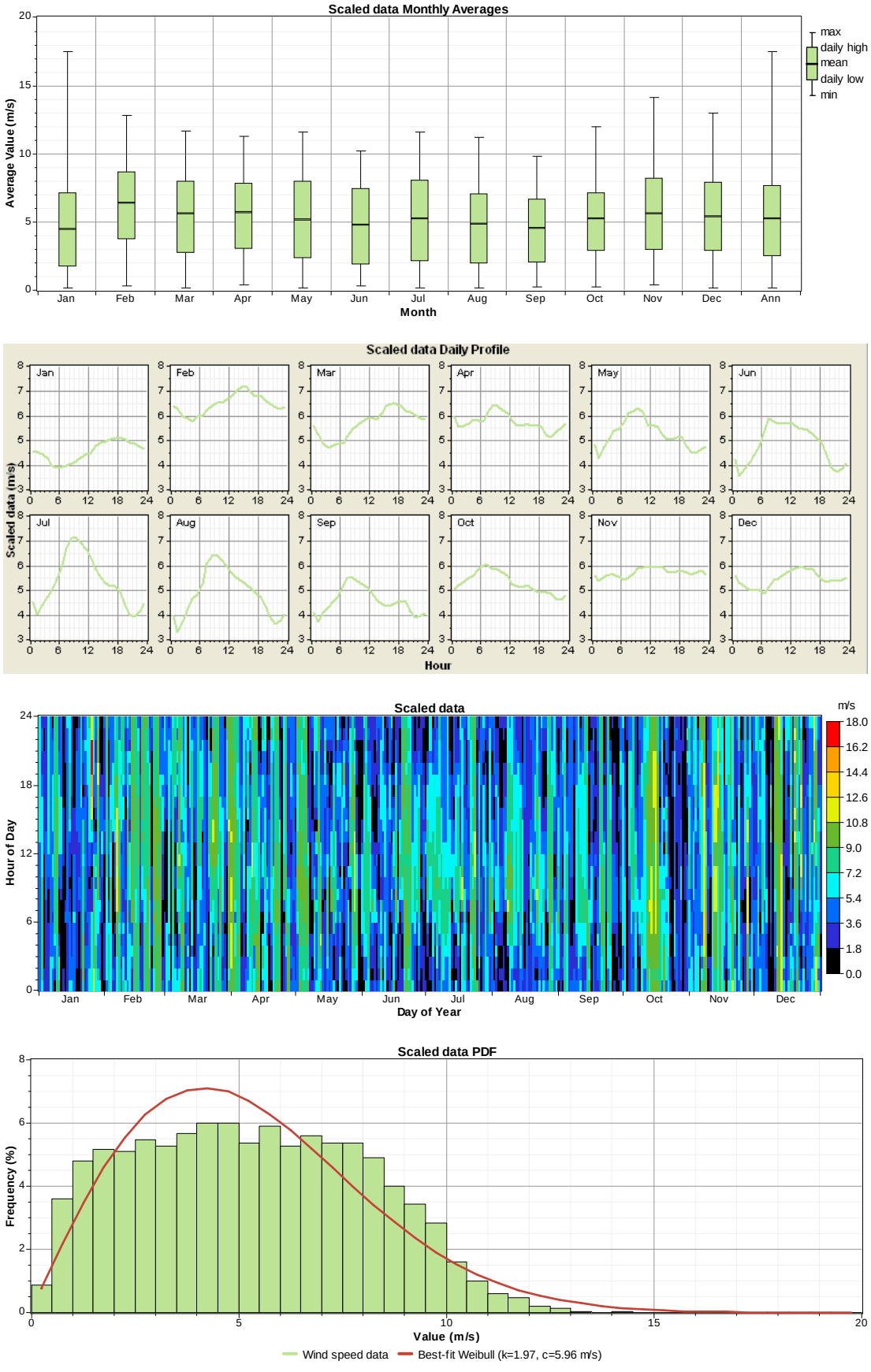

Figure 5. Wind speed in Landaben in 2009

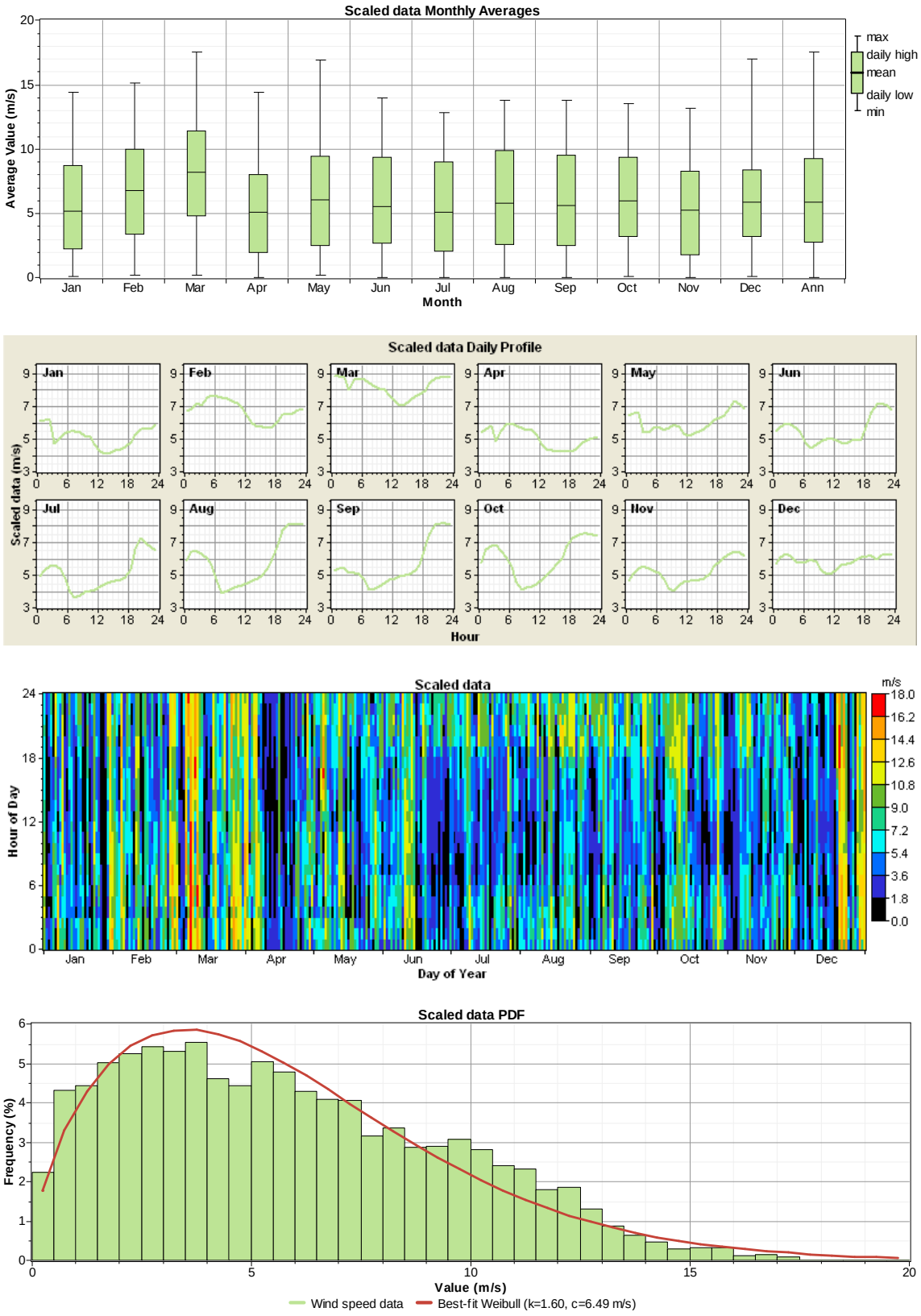

Figure 6. Wind speed in Walqa-Valdabra in 2004

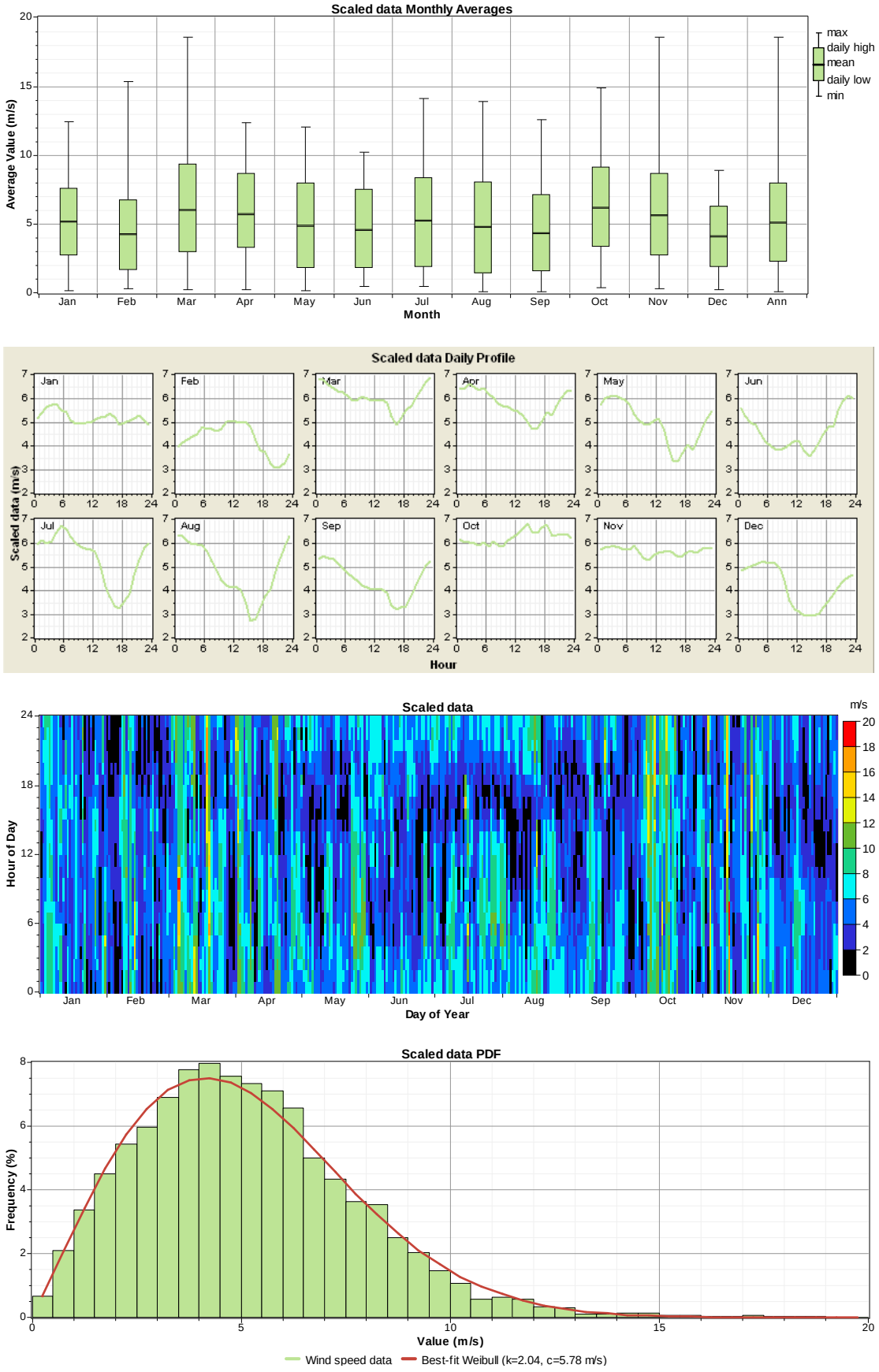

Figure 7. Wind speed in Huelva in 2006

3. SOLAR RESOURCE

The solar radiation data, has been obtained by AICIA through two different simulation tools:

- For Andalusia region (Spain), AMT-A, developed by AICIA, has been used. This tool used 10 years historical measured radiation in different locations and a methodology for estimating the radiation at any point. This tool is well suited for analysing the potential of Low Temperature or High temperature Solar Energy Systems.

- For the rest of regions of SUDOE Area, METEONORM tool has been used. This tool has been developed by Meteotest, and the radiation series are calculated from the monthly values (station data, interpolated data or imported data). Meteonorm calculates hourly values of all parameters using a stochastic model. The resulting time series correspond to "typical years" used for system design.

In this case, the solar radiation used in all the case studies has been the one from the nearest city for a typical year. Thus, in Figure 8 the average solar resource for the case studies is shown. Depending on the geographical situation the resource can vary enormously. As an example, the solar resource in Huelva is a 42% higher than in Bayonne.

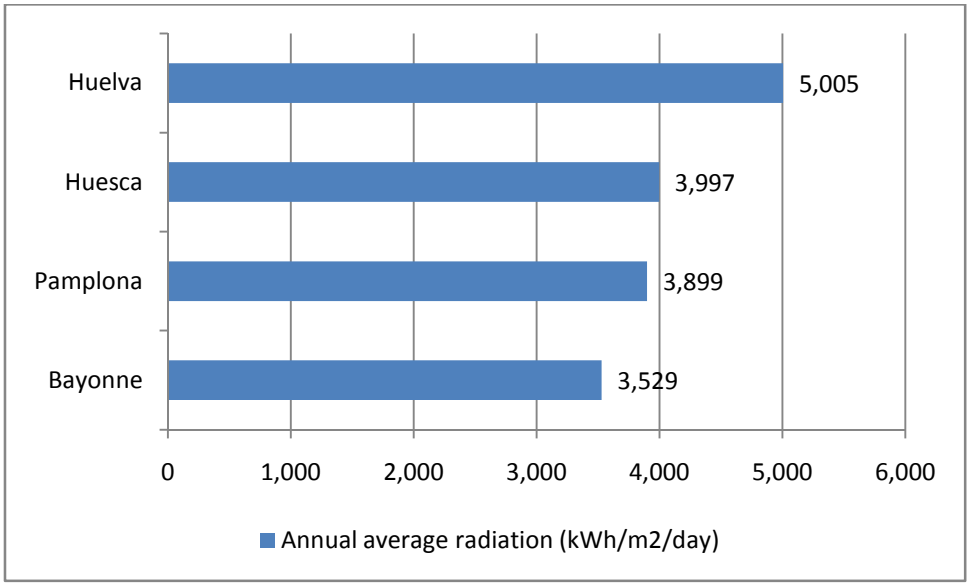

Figure 8. Solar resource in the selected locations

In the next figures, the distribution of the solar resource throughout the year is shown for the different locations studied.

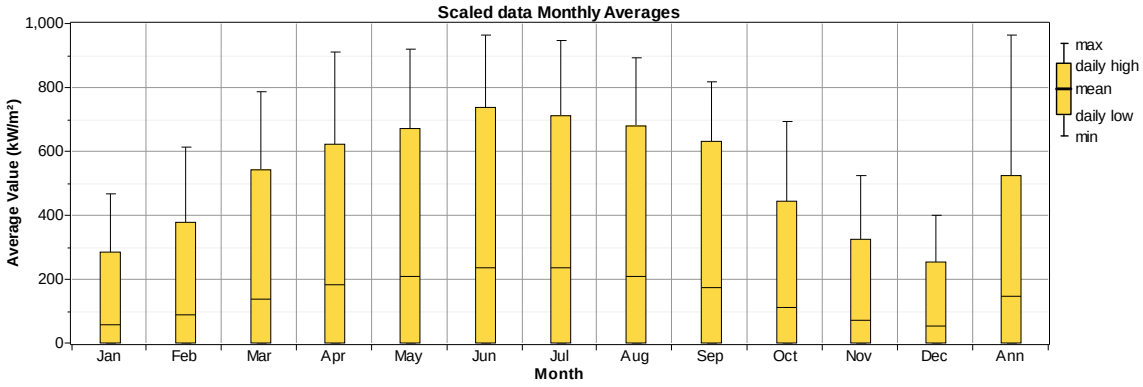

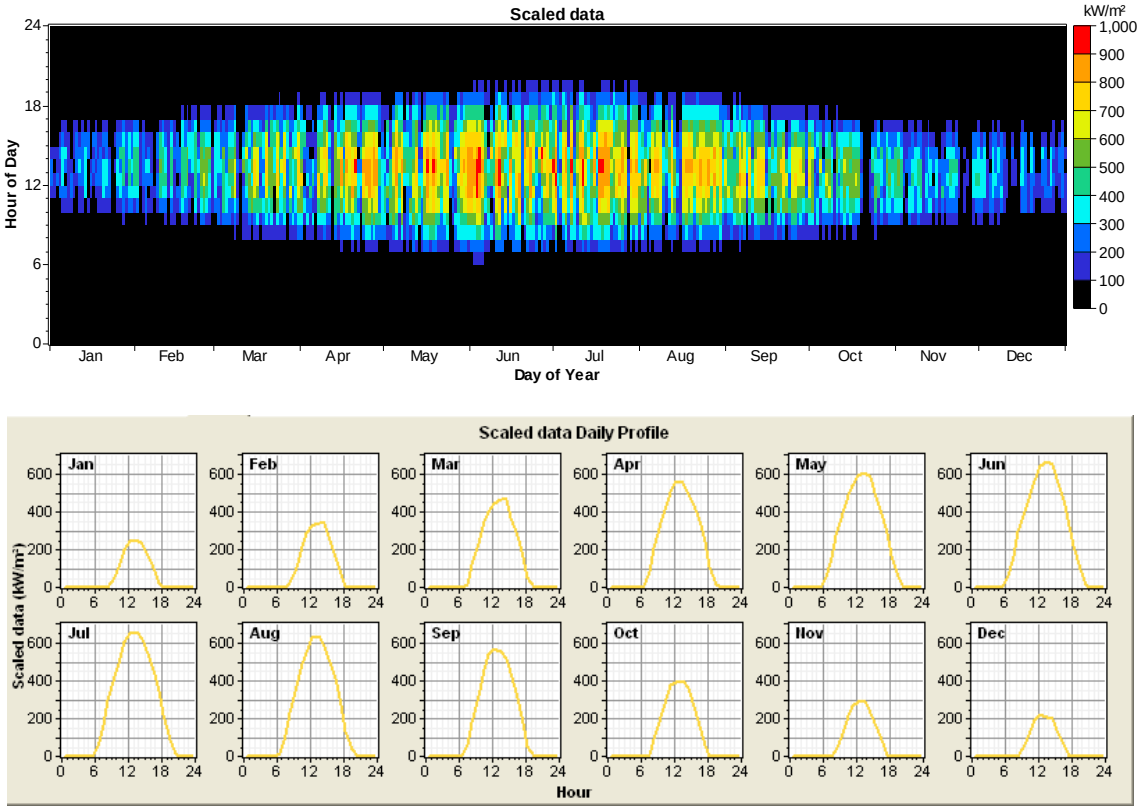

Figure 9. Solar resource in Bayonne

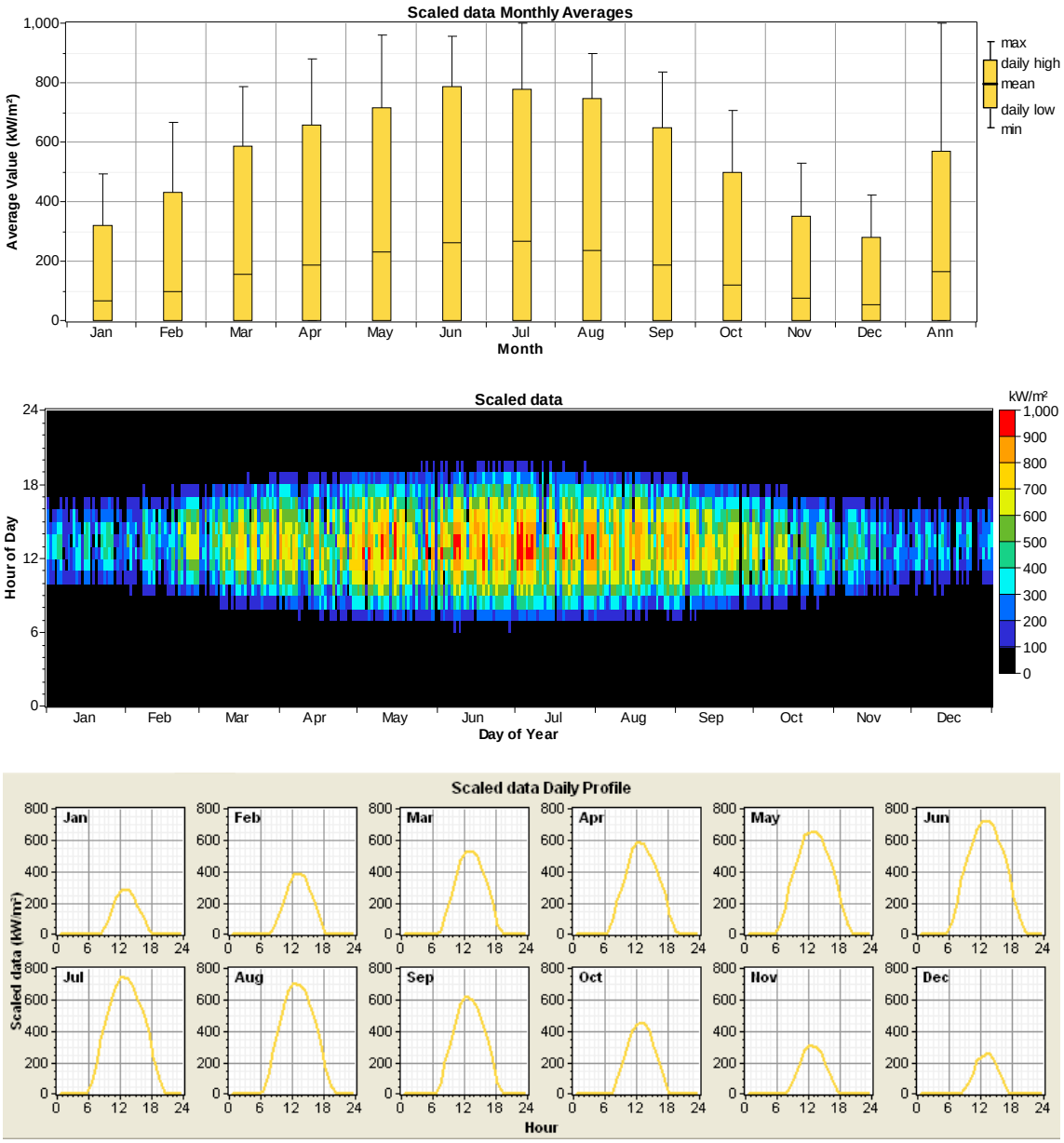

Figure 10. Solar resource in Pamplona

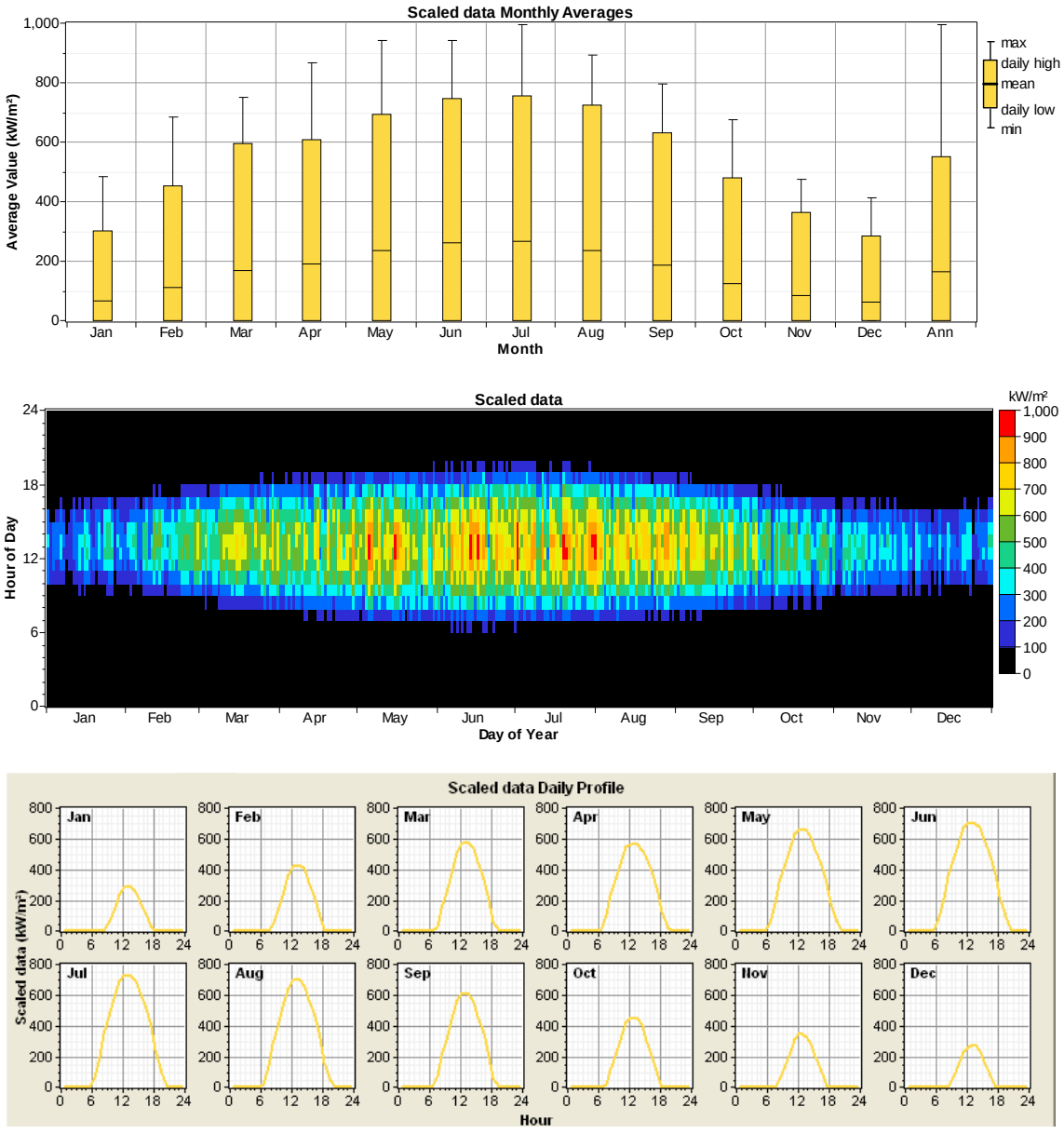

Figure 11. Solar resource in Huesca

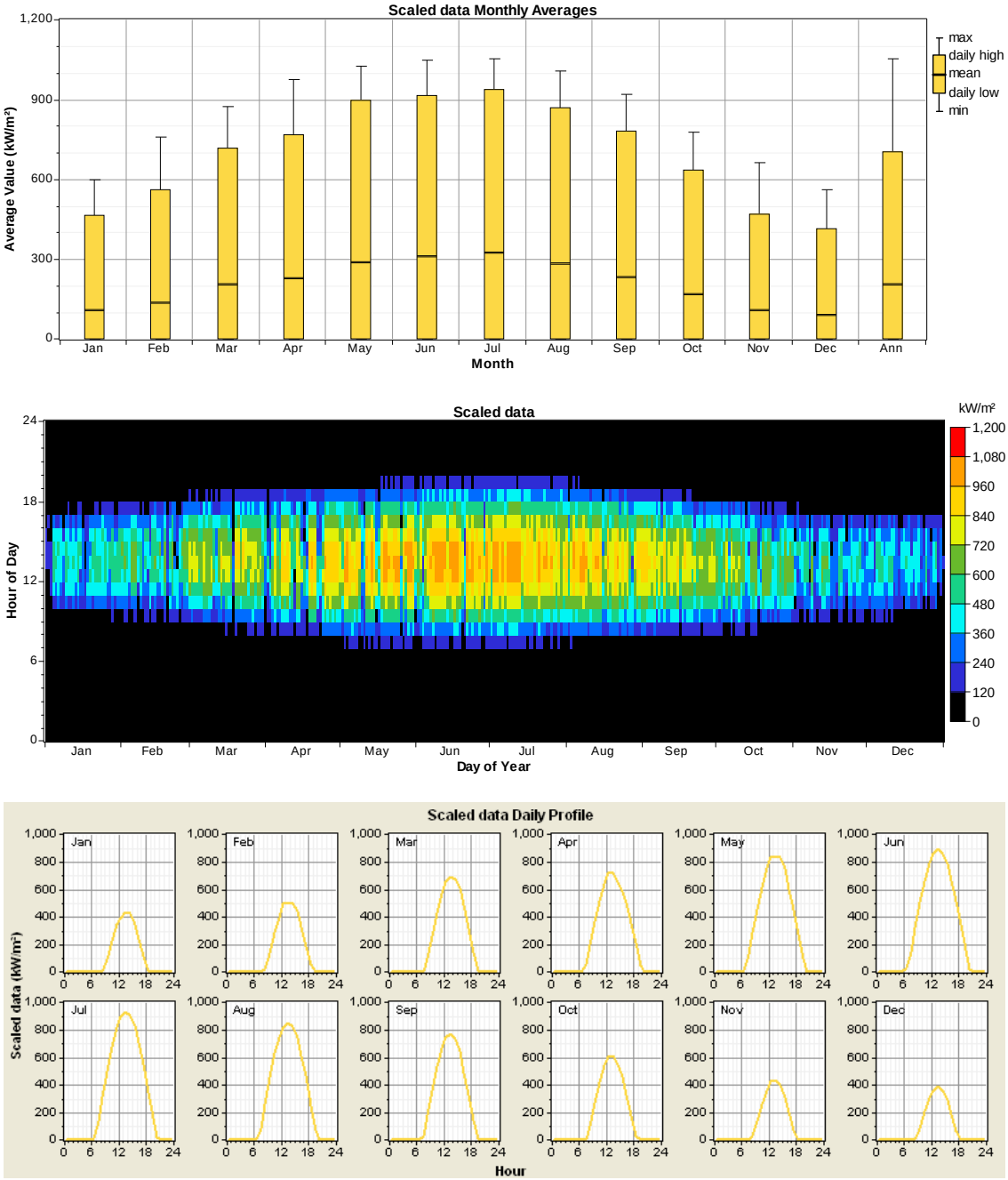

Figure 12. Solar resource in Huelva

4. WATER RESOURCE

While wind turbines and photovoltaic panels can be installed almost everywhere, hydroelectric power presents specific orographic requirements. Thus, few industrial areas will be able to take advantage from this kind of renewable resource.

Regarding the case study of Landaben, river Arga surrounds the industrial estate so depending on the slope of the terrain a hydroelectric station could be an option. In

Table 2, the historical data of water resource in the closest measuring station (Huarte) is shown. According to the annual resource distribution (see Figure 15), this hydro power station would probably have to stop during the summer. This way, the hydro power generation would be limited to some months given that a water reservoir is not feasible in this case.

Figure 13. River Arga surrounding Landaben

Table 2. Historical data of Arga river flow in Huarte station

YEAR	MONTH AVERAGE											
	OCT	NOV	DIC	JAN	FEB	MAR	APR	MAY	JUN	JUL	AUG	SEP
	m^3/s											
1965/66				10.1	12.2	11.7	12.5	9.7	2.3	0.9	0.5	0.3
1966/67	5.3	22.7	26.2	10.5	4.3	4.2	9.6	4.4	1.3	0.3	0.3	0.3
1967/68	0.9	12.0	17.1	23.7	10.8	9.1	7.3	6.7	2.3	0.6	0.8	0.9
1968/69	0.7	3.8	13.0	7.9	9.2	14.4	14.2	6.3	3.7	0.8	0.4	5.3
1969/70	0.7	0.7	30.3	15.3	18.0	13.9	9.4	11.0	2.6	1.0	0.6	0.6
1970/71	0.7	2.2	2.8	6.6	13.2	14.8	8.8	5.6	5.5	2.3	0.8	1.0
1971/72	1.2	6.1	9.9	16.9	23.7	7.9	11.7	9.7	0.9	0.5	0.4	1.2
1972/73	2.2	3.1	7.2	7.6	18.4	6.5	8.9	2.1	3.3	3.8	3.9	4.8
1973/74	6.5	6.1	6.9	7.4	19.6	18.9	12.0	7.2	4.1	4.1	4.1	4.1
1974/75	20.6	24.0	8.3	6.0	6.1	12.7	13.5	5.0	4.6	2.0	2.0	1.7
1975/76	1.2	8.9	7.1	1.8	17.2	7.2	6.8	2.3	1.3	1.4	1.4	1.4
1976/77	4.1	8.6	7.9	4.0	6.5	2.5	6.9	8.8	4.7	2.2	3.7	1.2
1977/78	1.4	5.2	3.0	10.1	31.2	14.7	13.6	11.5	1.7	1.4	1.2	1.2
1978/79	1.3	1.2	1.7	14.7	14.8	5.8	20.3	5.3	2.4	1.3	1.2	1.2
1979/80	3.4	13.4	4.7	8.9	4.2	14.2	3.1	7.6	2.3	1.3	1.2	1.2
1980/81	8.2	6.2	24.1	23.2	8.0	5.5	5.7	7.6	0.9	2.0	1.8	1.9
1981/82	2.3	2.2	18.9	11.6	12.6	17.5	1.8	1.2	1.0	0.7	0.7	0.7
1982/83	3.2	8.7	20.8	4.3	11.0	12.4	13.0	1.6	0.7	0.8	0.5	0.5
1983/84	0.4	0.5	1.5	12.2	12.6	2.6	6.3	7.8	3.6	0.2	0.2	0.2
1984/85	0.9	9.8	5.3	9.3	3.4	6.4	2.7	8.6	0.3	0.2	0.2	0.3
1985/86	0.7	0.8	0.8	7.1	11.6	8.1	11.0	3.3	1.2	1.0	0.9	0.7
1986/87	0.8	1.7	5.1	6.8	13.1	3.5	8.8	0.9	0.7	0.4	0.4	0.4
1987/88		4.1	4.6									
1988/89		0.8	1.2	1.1	1.6	1.5						
1989/90	0.6	1.2	0.8	1.0	2.2	0.7						
1990/91												
1991/92	3.0	8.4	3.7	2.4	2.3	3.1	12.9	2.2	3.4	3.3	1.5	1.7
1992/93	16.4	9.5	14.1	1.9	1.4	1.9	4.7	4.8	1.6	1.0	1.1	3.5
1993/94	4.9	2.8	13.1	11.3	9.6	3.5	15.1	2.6	1.1	0.7	0.6	0.8
1994/95	1.0	1.8	4.0	12.9	4.6	10.1	2.3	1.3	0.8	0.7	0.7	0.8
1995/96	0.7	0.5	1.8	3.4	12.0	5.6	1.7	1.8	0.7	1.3	1.1	1.5
1996/97	3.0	11.9	17.0	12.2	3.3	1.1	0.8	2.1	2.3	1.7	1.2	0.6
1997/98	0.8	3.2	8.4	7.0	2.7	5.3	6.6	2.8	1.8	0.6	0.5	1.4
1998/99	6.0	6.8	8.7	8.6	13.2	8.2	5.7	6.4	1.1	0.5	0.4	0.6
1999/00	0.9	4.6		2.8	6.1	2.0	8.8	2.1	1.9	2.7	0.8	0.7
2000/01	5.9	10.3	5.9	10.6	4.8	8.2	5.3	5.9	0.6	0.5	0.5	1.1
2001/02	1.0	1.3	1.0	1.4	4.6	5.3	2.9	2.7	2.4	1.5	1.3	1.6
2002/03	1.4	6.6	16.7	9.8	19.7	8.3	2.0	2.8	0.7	0.5	0.5	0.9
2003/04					5.8	11.4	7.9	5.8	0.6	0.5	1.3	1.6
2004/05		1.8	4.9	9.0	6.1	7.2	11.0	2.7	0.5	0.5		
AVERAGE	**3.3**	**6.0**	**9.1**	**8.7**	**10.0**	**7.8**	**8.2**	**5.0**	**2.0**	**1.3**	**1.1**	**1.4**

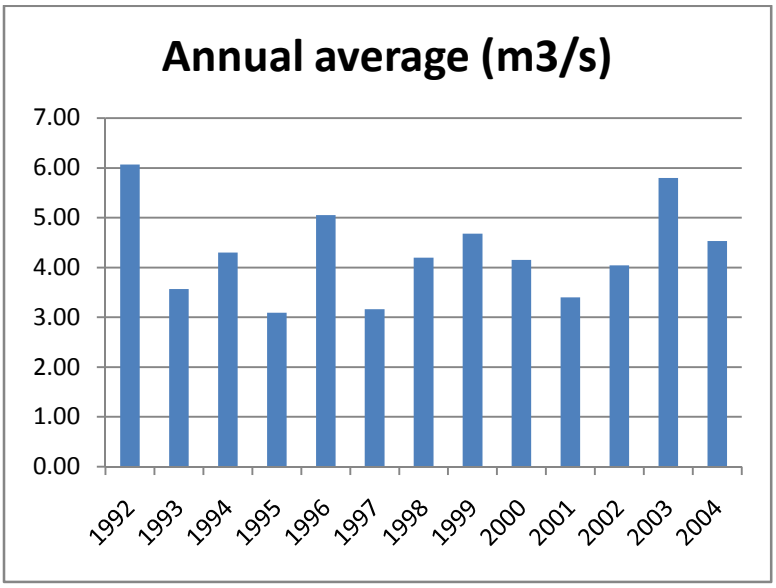

Figure 14. Annual average water resource in river Arga (Huarte)

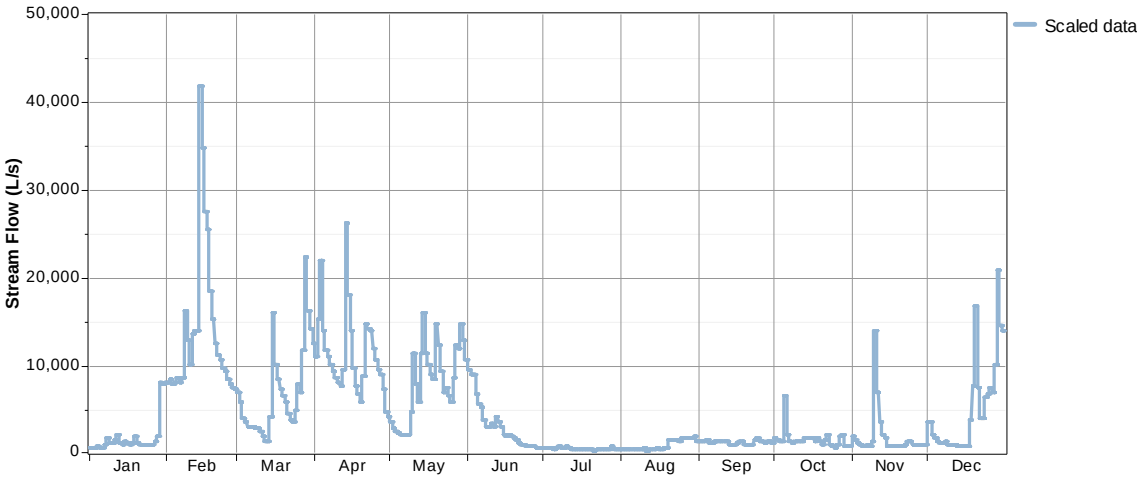

Figure 15. Water flow in river Arga (Huarte) in 2004

As an example, a real hydro station in Landaben surroundings is explained. In the Echauri station, a 10 m height difference is used. The turbine installed with nominal flow of 15 m^3/s can supply 1 MW power, producing around 4 GWh/year of electricity.

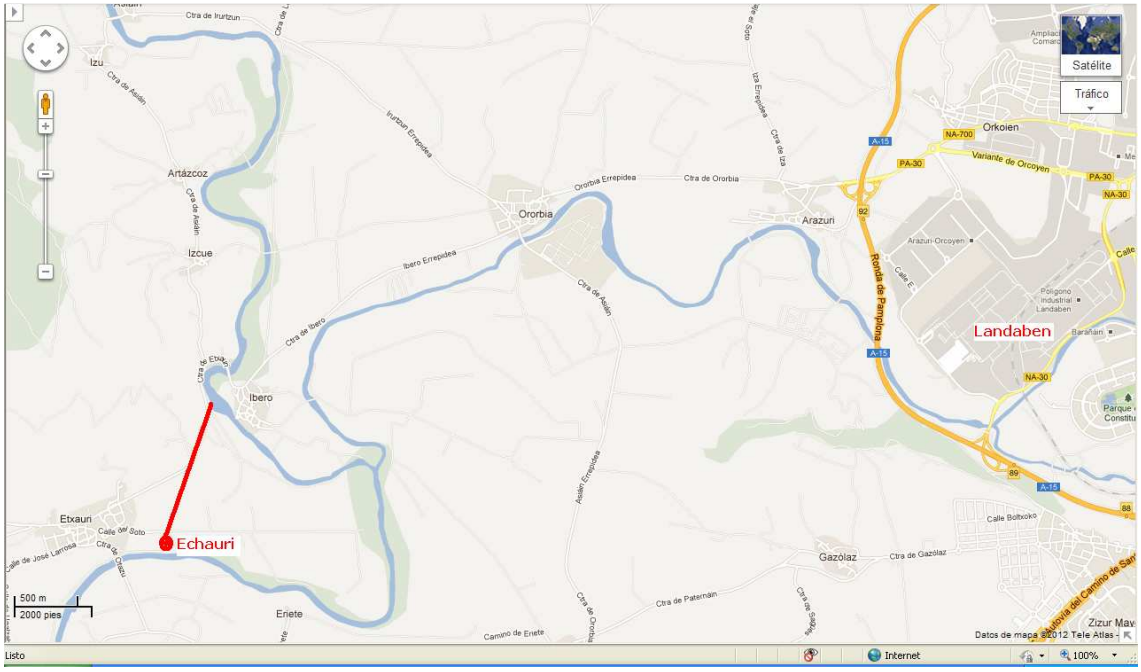

Figure 16. Echauri 1 MW hydro power station

5. BIOMASS RESOURCE

Within this task of the project, no specific biomass resource studies have been carried out for the selected case studies, as this is out of the scope of the project. Nevertheless, the general case of the Navarra region is analyzed as an example of a possible biomass resource use.

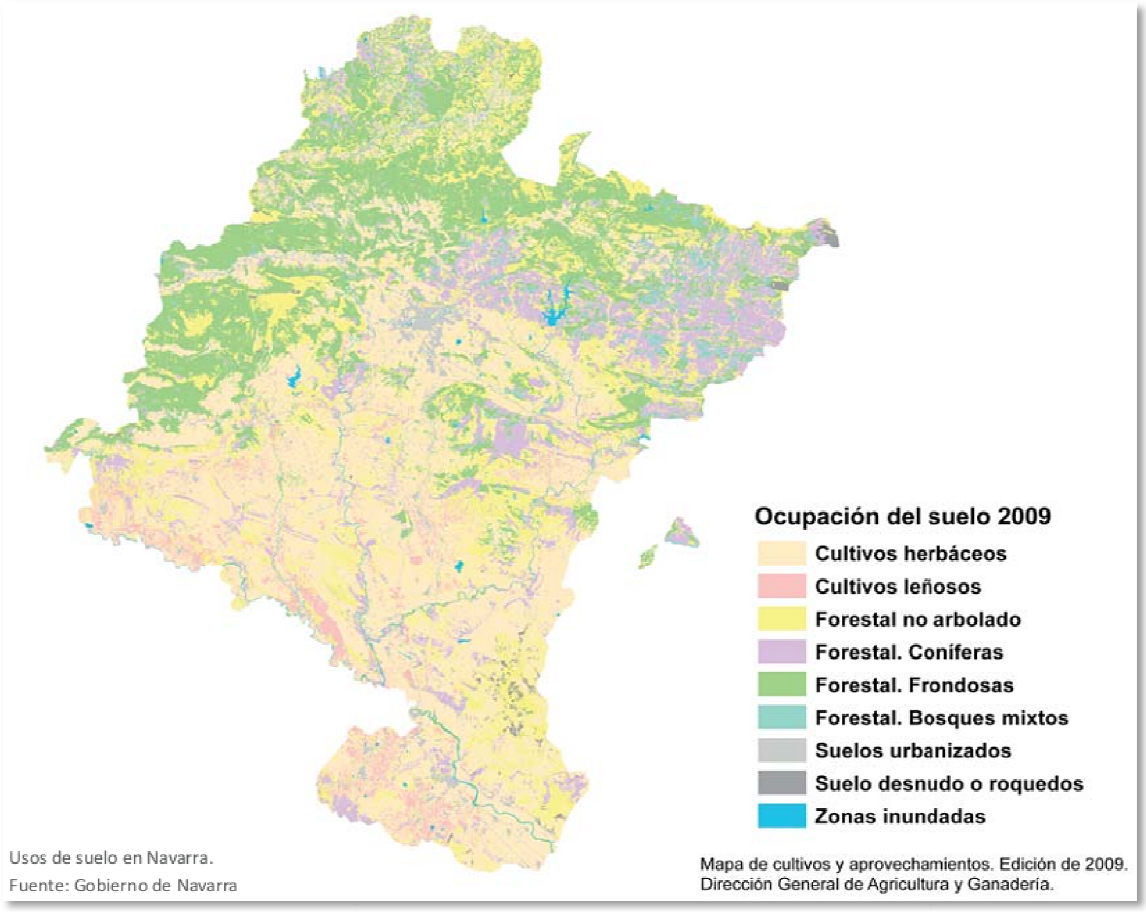

Figure 17. Land use in Navarre in 2009

Origen		Superficie (ha)		Valoración (t/año)	Tep/año	Aplicaciones
Biomasa residual vegetal	Forestal arbolado	462.664	Cortas de madera *	284.881	35.180	Eléctrica Térmica
			Leña hogares	38.586		Térmica
	Residuos agrícolas	291.580	Cultivos herbáceos	623.172	249.267	Eléctrica
			Podas	53.242	17.671	Eléctrica Térmica
	Industria maderera			55.721	18.493	Eléctrica Térmica
Cultivos energéticos		1.654	Cultivos leñosos	10.721,35	3.537,69	Eléctrica Térmica
		40	Cultivos herbáceos	400		Eléctrica
Cultivo energético (Biocombustible)		500	Herbáceos	5.000	4.370	Biocombustible

* Dato referido al total de cortas de madera en Navarra. El destino de dicha madera es la industria forestal. Este valor de madera aprovechada supone un 24% del crecimiento de las masas forestales arboladas en Navarra, por lo que existe potencial para incremental el aprovechamiento sostenible de la biomasa forestal con fines energéticos, sin perjuicio de otros sectores.

Figure 18. Biomass potential in Navarre. Source: Plan Energético Navarra Horizonte 2010

As an example, the main data about the biomass (straw) power plant placed in the industrial area of Rocaforte in Sangüesa is shown in Table 3. Taking into account the potential of herbaceous crops in Navarre (623,172 t/year) and the consumption of this kind of power plant (160,000 t/year), that means that in Navarre could exist up to 3-4 biomass plant of this size without importing straw from other regions.

Table 3. Data of a biomass power plant in Sangüesa

Electric power	25 MW
Occupied area	107,000 m^2
Feedstock	160,000 t/year
Electricity generation	200 GWh/year (6.5 % of Navarra's consumption)
Investment	51 M€
Staff	135 workers

According to the developer the reasons for the site selection, useful to decide whether this solution is feasible for a specific location or not, were the following:

- Well located in relation with straw production sites
- An industrial area is not a pollution sensitive area like a city, and is well connected by road for truck delivery
- Close to an electrical substation, enabling a reduced and buried connection
- There is a water channel available for refrigeration of the power plant

ANNEX 1. IRRADIATION INFORMATION

In this annex, radiation data from different locations of Spain and Portugal are shown.

The information considered in tables are: global and diffuse irradiation on horizontal surface, solar beam irradiation and average temperature in each month.

1.1. SPAIN

MONTH	Solar global irradiation on horizontal surface (kWh/m2·day)	Solar beam irradiation (kWh/m2·day)	Solar diffuse irradiation on horizontal surface (kWh/m2·day)	Temperature (°C)
January	2,315	1,301	1,014	5,3
February	2,965	2,319	1,293	6,3
March	4,196	3,281	1,829	8,6
April	5,365	4,215	2,299	10,9
May	6,473	5,123	2,700	15,4
June	7,514	6,290	2,448	19,9
July	7,431	6,236	2,390	24,2
August	6,575	5,465	2,220	23,8
September	4,773	3,773	2,001	19,5
October	3,060	2,296	1,529	13,9
November	2,534	2,031	1,006	8,5
December	1,965	1,501	0,927	5,4

Table 4. Albacete.

MONTH	Solar global irradiation on horizontal surface (kWh/m2·day)	Solar beam irradiation (kWh/m2·day)	Solar diffuse irradiation on horizontal surface (kWh/m2·day)	Temperature (°C)
January	2,575	1,542	1,033	10,6
February	3,331	2,689	1,285	11,0
March	4,724	3,873	1,703	12,1
April	5,566	4,329	2,475	13,9
May	6,587	5,314	2,546	17,3
June	7,005	5,520	2,969	20,8
July	7,162	5,894	2,535	24,0
August	6,197	4,942	2,509	24,6
September	5,030	4,023	2,015	21,9
October	3,750	2,982	1,536	18,1
November	2,470	1,912	1,115	13,6
December	2,241	1,778	0,927	11,0

Table 5. Alicante.

MONTH	Solar global irradiation on horizontal surface (kWh/m2·day)	Solar beam irradiation (kWh/m2·day)	Solar diffuse irradiation on horizontal surface (kWh/m2·day)	Temperature (°C)
January	2,583	1,522	1,061	13,8
February	3,449	2,776	1,347	13,8
March	4,664	3,751	1,828	14,7
April	5,649	4,418	2,461	15,5
May	6,608	5,361	2,494	18,3
June	7,029	5,661	2,738	21,5
July	7,233	5,911	2,644	25,2
August	6,212	4,939	2,546	26,0
September	5,030	3,997	2,066	24,1
October	3,703	2,940	1,526	20,4
November	2,420	1,869	1,102	16,6
December	2,248	1,729	1,038	14,5

Table 6. Almería.

MONTH	Solar global irradiation on horizontal surface (kWh/m2·day)	Solar beam irradiation (kWh/m2·day)	Solar diffuse irradiation on horizontal surface (kWh/m2·day)	Temperature (°C)
January	2,271	1,147	1,125	8,9
February	2,915	2,160	1,511	10,0
March	4,628	3,798	1,659	12,0
April	5,231	4,173	2,117	14,0
May	6,518	5,227	2,583	17,9
June	7,262	6,033	2,458	21,8
July	7,597	6,528	2,138	25,3
August	6,823	5,853	1,941	25,1
September	5,229	4,306	1,846	21,9
October	3,660	2,885	1,551	17,0
November	2,297	1,682	1,230	11,7
December	1,857	1,401	0,913	9,0

Table 7. Badajoz.

MONTH	Solar global irradiation on horizontal surface (kWh/m2·day)	Solar beam irradiation (kWh/m2·day)	Solar diffuse irradiation on horizontal surface (kWh/m2·day)	Temperature (°C)
January	1,755	0,835	0,921	9,7
February	2,507	1,836	1,344	10,4
March	3,759	2,829	1,860	12,1
April	4,699	3,428	2,542	13,8
May	5,339	3,925	2,829	17,4
June	6,202	4,664	3,075	20,7
July	6,480	5,021	2,917	24,2
August	5,636	4,403	2,466	23,8
September	4,394	3,386	2,017	21,2
October	2,996	2,296	1,401	17,4
November	1,973	1,461	1,024	13,0
December	1,566	1,150	0,832	10,7

Table 8: Barcelona.

MONTH	Solar global irradiation on horizontal surface (kWh/m2·day)	Solar beam irradiation (kWh/m2·day)	Solar diffuse irradiation on horizontal surface (kWh/m2·day)	Temperature (°C)
January	1,485	0,588	0,896	8,9
February	2,128	1,504	1,249	9,3
March	3,415	2,496	1,837	10,6
April	4,281	3,056	2,451	11,8
May	5,232	3,798	2,867	15,4
June	5,600	4,053	3,095	17,9
July	5,531	3,990	3,082	20,3
August	4,874	3,615	2,518	20,6
September	4,021	3,019	2,004	18,7
October	2,630	1,893	1,474	15,6
November	1,641	1,146	0,989	11,1
December	1,227	0,888	0,678	9,3

Table 9. Bilbao.

MONTH	Solar global irradiation on horizontal surface (kWh/m2·day)	Solar beam irradiation (kWh/m2·day)	Solar diffuse irradiation on horizontal surface (kWh/m2·day)	Temperature (°C)
January	1,605	0,691	0,915	2,6
February	2,426	1,794	1,265	3,9
March	3,799	2,915	1,769	5,8
April	4,593	3,390	2,407	7,6
May	5,803	4,452	2,702	11,1
June	6,581	5,248	2,665	14,9
July	6,694	5,343	2,702	18,4
August	5,878	4,700	2,356	18,3
September	4,597	3,713	1,767	15,2
October	2,977	2,244	1,466	10,7
November	1,794	1,270	1,048	5,8
December	1,342	0,944	0,796	3,2

Table 10. Burgos.

MONTH	Solar global irradiation on horizontal surface (kWh/m2·day)	Solar beam irradiation (kWh/m2·day)	Solar diffuse irradiation on horizontal surface (kWh/m2·day)	Temperature (°C)
January	2,601	1,547	1,053	12,0
February	3,361	2,654	1,415	12,2
March	4,894	4,038	1,711	12,6
April	5,465	4,232	2,466	13,9
May	6,831	5,632	2,397	16,3
June	7,350	6,167	2,366	19,0
July	7,597	6,534	2,127	22,4
August	6,693	5,571	2,244	23,5
September	5,499	4,518	1,963	22,1
October	3,960	3,185	1,551	18,7
November	2,579	1,942	1,274	14,5
December	2,192	1,660	1,064	12,5

Table 11. Cádiz.

MONTH	Solar global irradiation on horizontal surface (kWh/m2·day)	Solar beam irradiation (kWh/m2·day)	Solar diffuse irradiation on horizontal surface (kWh/m2·day)	Temperature (°C)
January	2,126	1,127	0,998	11,3
February	2,856	2,114	1,485	12,0
March	4,191	3,221	1,941	13,8
April	5,353	4,156	2,393	15,7
May	6,425	4,974	2,902	18,9
June	7,040	5,525	3,030	22,1
July	6,992	5,548	2,889	25,7
August	6,125	4,805	2,640	25,4
September	4,722	3,653	2,138	22,6
October	3,407	2,620	1,574	18,8
November	2,214	1,668	1,092	14,3
December	1,807	1,321	0,974	11,4

Table 12. Castellón de la Plana.

MONTH	Solar global irradiation on horizontal surface (kWh/m2·day)	Solar beam irradiation (kWh/m2·day)	Solar diffuse irradiation on horizontal surface (kWh/m2·day)	Temperature (°C)
January	2,498	1,463	1,034	9,3
February	3,273	2,532	1,481	10,6
March	4,714	3,774	1,878	12,8
April	5,418	4,208	2,419	14,6
May	6,675	5,411	2,530	19,1
June	7,176	5,837	2,678	22,6
July	7,565	6,463	2,202	26,7
August	6,507	5,425	2,165	26,5
September	5,371	4,487	1,769	23,0
October	3,864	3,112	1,504	18,0
November	2,483	1,945	1,075	12,5
December	2,151	1,657	0,988	9,5

Table 13. Córdoba.

MONTH	Solar global irradiation on horizontal surface (kWh/m2·day)	Solar beam irradiation (kWh/m2·day)	Solar diffuse irradiation on horizontal surface (kWh/m2·day)	Temperature (°C)
January	2,738	1,728	1,010	5,2
February	3,605	2,941	1,327	6,6
March	4,759	3,877	1,764	9,1
April	5,456	4,273	2,367	10,7
May	6,128	4,817	2,622	15,6
June	7,505	6,233	2,544	19,7
July	7,548	6,464	2,167	23,5
August	6,784	5,700	2,169	23,0
September	5,354	4,417	1,875	18,9
October	3,708	2,929	1,557	14,0
November	2,748	2,150	1,196	8,5
December	2,535	2,079	0,912	5,3

Table 14. Granada.

MONTH	Solar global irradiation on horizontal surface (kWh/m2·day)	Solar beam irradiation (kWh/m2·day)	Solar diffuse irradiation on horizontal surface (kWh/m2·day)	Temperature (°C)
January	2,633	1,607	1,027	10,5
February	3,367	2,618	1,496	11,6
March	4,841	3,946	1,790	13,6
April	5,551	4,419	2,265	15,4
May	6,872	5,709	2,325	19,0
June	7,493	6,306	2,375	22,1
July	7,696	6,593	2,205	25,4
August	6,806	5,782	2,046	25,7
September	5,566	4,635	1,863	22,9
October	4,014	3,258	1,512	18,6
November	2,594	1,961	1,266	14,0
December	2,210	1,699	1,023	11,1

Table 15. Huelva.

MONTH	Solar global irradiation on horizontal surface (kWh/m2·day)	Solar beam irradiation (kWh/m2·day)	Solar diffuse irradiation on horizontal surface (kWh/m2·day)	Temperature (°C)
January	1,611	2,062	0,895	1,8
February	2,731	3,112	1,199	2,5
March	4,070	4,228	1,741	5,2
April	4,619	4,122	2,447	6,9
May	5,624	5,040	2,720	10,7
June	6,340	5,700	2,899	14,4
July	6,412	5,987	2,703	17,7
August	5,608	5,281	2,447	17,5
September	4,492	4,504	1,908	14,3
October	2,947	3,088	1,430	9,9
November	1,954	2,237	1,036	5,0
December	1,486	1,830	0,798	2,2

Table 16. Huesca.

MONTH	Solar global irradiation on horizontal surface (kWh/m2·day)	Solar beam irradiation (kWh/m2·day)	Solar diffuse irradiation on horizontal surface (kWh/m2·day)	Temperature (°C)
January	2,563	1,553	1,010	7,4
February	3,356	2,606	1,499	8,9
March	4,680	3,761	1,839	11,3
April	5,530	4,390	2,279	12,9
May	6,477	5,111	2,732	17,9
June	7,057	5,686	2,743	21,9
July	7,362	6,178	2,367	25,8
August	6,390	5,305	2,170	25,2
September	5,251	4,358	1,786	21,1
October	3,808	3,059	1,499	16,3
November	2,459	1,910	1,098	10,7
December	2,194	1,706	0,974	7,5

Table 17. Jaén.

MONTH	Solar global irradiation on horizontal surface (kWh/m2·day)	Solar beam irradiation (kWh/m2·day)	Solar diffuse irradiation on horizontal surface (kWh/m2·day)	Temperature (°C)
January	1,245	0,398	0,847	12,0
February	2,420	1,791	1,259	11,6
March	3,469	2,545	1,847	11,8
April	4,552	3,331	2,443	11,9
May	5,833	4,388	2,891	14,0
June	5,531	4,022	3,018	16,2
July	5,883	4,396	2,974	18,8
August	4,977	3,594	2,767	19,4
September	4,376	3,342	2,069	18,7
October	3,175	2,489	1,373	16,6
November	1,400	0,915	0,970	13,4
December	0,599	0,365	0,468	12,3

Table 18. La Coruña.

MONTH	Solar global irradiation on horizontal surface (kWh/m2·day)	Solar beam irradiation (kWh/m2·day)	Solar diffuse irradiation on horizontal surface (kWh/m2·day)	Temperature (°C)
January	2,931	1,473	1,458	19,0
February	4,936	4,217	1,439	18,6
March	6,327	5,553	1,548	18,7
April	6,876	5,848	2,055	18,2
May	6,533	5,216	2,634	19,4
June	5,073	3,600	2,945	20,8
July	5,630	4,117	3,024	23,3
August	6,735	5,469	2,532	24,3
September	6,152	5,148	2,007	24,1
October	4,955	4,058	1,794	23,2
November	3,557	2,748	1,618	21,0
December	2,275	1,648	1,253	19,7

Table 19. Las Palmas de Gran Canarias.

MONTH	Solar global irradiation on horizontal surface (kWh/m2·day)	Solar beam irradiation (kWh/m2·day)	Solar diffuse irradiation on horizontal surface (kWh/m2·day)	Temperature (°C)
January	1,806	0,901	0,904	3,8
February	2,624	2,064	1,121	5,6
March	4,089	3,259	1,660	7,7
April	4,817	3,765	2,104	9,7
May	5,925	4,612	2,626	13,1
June	6,962	5,592	2,740	17,1
July	7,414	6,230	2,368	20,3
August	6,486	5,449	2,074	20,2
September	4,877	3,991	1,771	17,1
October	3,102	2,372	1,459	12,2
November	1,852	1,317	1,071	7,2
December	1,338	0,966	0,745	4,3

Table 20. León.

MONTH	Solar global irradiation on horizontal surface (kWh/m2·day)	Solar beam irradiation (kWh/m2·day)	Solar diffuse irradiation on horizontal surface (kWh/m2·day)	Temperature (°C)
January	2,628	2,023	0,605	6,0
February	2,886	2,236	1,301	8,0
March	5,441	5,013	0,856	11,5
April	6,452	5,571	1,761	14,1
May	7,283	6,151	2,264	18,3
June	7,441	6,172	2,538	22,0
July	7,305	6,022	2,565	25,6
August	6,582	5,516	2,131	24,8
September	5,346	4,507	1,678	20,5
October	3,739	3,088	1,301	16,1
November	2,109	1,567	1,084	9,2
December	1,774	1,345	0,858	6,2

Table 21. Lérida.

MONTH	Solar global irradiation on horizontal surface (kWh/m2·day)	Solar beam irradiation (kWh/m2·day)	Solar diffuse irradiation on horizontal surface (kWh/m2·day)	Temperature (°C)
January	1,645	0,736	0,908	5,5
February	2,485	1,875	1,221	6,8
March	3,841	2,844	1,994	8,8
April	4,511	3,277	2,468	10,7
May	5,767	4,310	2,915	14,3
June	6,462	5,099	2,728	17,9
July	6,586	5,238	2,696	21,2
August	5,682	4,453	2,458	21,2
September	4,502	3,555	1,894	18,1
October	2,929	2,203	1,454	13,8
November	1,806	1,287	1,039	8,6
December	1,340	0,930	0,820	5,9

Table 22. Logroño.

MONTH	Solar global irradiation on horizontal surface (kWh/m2·day)	Solar beam irradiation (kWh/m2·day)	Solar diffuse irradiation on horizontal surface (kWh/m2·day)	Temperature (°C)
January	2,150	1,205	0,945	6,1
February	2,764	2,070	1,389	7,9
March	4,607	3,744	1,726	10,2
April	5,129	3,990	2,278	12,4
May	6,575	5,239	2,672	16,7
June	7,448	6,210	2,474	21,3
July	7,343	6,217	2,251	25,3
August	6,460	5,401	2,118	24,8
September	4,999	4,115	1,769	20,5
October	3,339	2,577	1,526	14,9
November	2,106	1,587	1,038	9,2
December	1,585	1,134	0,902	6,5

Table 23: Madrid.

MONTH	Solar global irradiation on horizontal surface (kWh/m2·day)	Solar beam irradiation (kWh/m2·day)	Solar diffuse irradiation on horizontal surface (kWh/m2·day)	Temperature (°C)
January	2,503	1,436	1,067	12,0
February	3,336	2,596	1,480	12,5
March	4,684	3,770	1,829	13,6
April	5,293	3,962	2,661	15,2
May	6,717	5,419	2,596	18,5
June	7,289	6,074	2,430	21,4
July	7,596	6,555	2,083	24,5
August	6,532	5,401	2,262	25,0
September	5,378	4,397	1,962	22,2
October	3,887	3,063	1,648	18,5
November	2,483	1,844	1,278	14,4
December	2,161	1,654	1,016	12,3

Table 24. Málaga.

MONTH	Solar global irradiation on horizontal surface (kWh/m2·day)	Solar beam irradiation (kWh/m2·day)	Solar diffuse irradiation on horizontal surface (kWh/m2·day)	Temperature (°C)
January	2,533	1,466	1,067	9,4
February	3,424	2,705	1,439	10,8
March	4,685	3,800	1,771	12,5
April	5,641	4,521	2,240	14,6
May	6,559	5,235	2,648	18,4
June	7,031	5,694	2,674	22,2
July	7,137	5,823	2,628	25,5
August	6,115	4,936	2,359	25,6
September	5,076	4,128	1,896	22,1
October	3,707	2,902	1,609	18,0
November	2,496	1,908	1,177	12,8
December	2,248	1,803	0,890	9,8

Table 25. Murcia.

MONTH	Solar global irradiation on horizontal surface (kWh/m2·day)	Solar beam irradiation (kWh/m2·day)	Solar diffuse irradiation on horizontal surface (kWh/m2·day)	Temperature (°C)
January	1,884	0,913	0,972	7,5
February	2,702	2,106	1,192	8,2
March	4,199	3,378	1,641	9,5
April	4,877	3,650	2,453	10,7
May	6,012	4,642	2,740	13,1
June	7,038	5,732	2,610	15,9
July	7,304	6,081	2,446	18,4
August	6,511	5,486	2,050	18,4
September	4,908	4,004	1,809	16,8
October	3,106	2,393	1,425	13,8
November	1,875	1,380	0,990	10,0
December	1,378	0,972	0,810	7,9

Table 26. Orense.

MONTH	Solar global irradiation on horizontal surface (kWh/m2·day)	Solar beam irradiation (kWh/m2·day)	Solar diffuse irradiation on horizontal surface (kWh/m2·day)	Temperature (°C)
January	1,487	0,602	0,885	8,2
February	2,063	1,461	1,203	9,1
March	3,391	2,415	1,953	9,9
April	4,263	3,103	2,319	10,5
May	5,126	3,771	2,711	13,2
June	5,529	4,131	2,796	16,0
July	5,564	4,135	2,858	18,5
August	4,830	3,546	2,567	18,8
September	3,999	2,995	2,010	17,3
October	2,602	1,868	1,469	14,2
November	1,636	1,108	1,055	10,9
December	1,225	0,836	0,778	9,2

Table 27. Oviedo.

MONTH	Solar global irradiation on horizontal surface (kWh/m2·day)	Solar beam irradiation (kWh/m2·day)	Solar diffuse irradiation on horizontal surface (kWh/m2·day)	Temperature (°C)
January	2,102	1,080	1,022	8,6
February	2,856	2,152	1,408	9,3
March	4,044	3,033	2,023	10,9
April	5,308	4,104	2,409	12,9
May	6,338	4,866	2,944	17,1
June	6,939	5,391	3,095	20,8
July	6,873	5,468	2,810	24,2
August	5,963	4,615	2,696	24,4
September	4,615	3,540	2,149	20,9
October	3,361	2,584	1,553	17,1
November	2,181	1,648	1,064	12,4
December	1,841	1,371	0,940	9,7

Table 28. Palma de Mallorca.

MONTH	Solar global irradiation on horizontal surface (kWh/m2·day)	Solar beam irradiation (kWh/m2·day)	Solar diffuse irradiation on horizontal surface (kWh/m2·day)	Temperature (°C)
January	1,587	0,722	0,865	6,0
February	2,350	1,743	1,214	7,0
March	3,815	2,896	1,836	9,7
April	4,569	3,308	2,521	11,2
May	5,552	4,135	2,834	15,0
June	6,395	4,850	3,090	18,2
July	6,347	5,036	2,621	21,1
August	5,659	4,414	2,490	21,8
September	4,495	3,529	1,934	18,7
October	2,866	2,167	1,398	14,7
November	1,768	1,275	0,986	8,8
December	1,329	0,957	0,743	6,3

Table 29. Pamplona.

MONTH	Solar global irradiation on horizontal surface (kWh/m2·day)	Solar beam irradiation (kWh/m2·day)	Solar diffuse irradiation on horizontal surface (kWh/m2·day)	Temperature (°C)
January	1,948	0,914	1,035	3,7
February	2,721	2,001	1,440	5,3
March	4,300	3,449	1,703	7,0
April	4,954	3,739	2,429	9,3
May	6,206	4,875	2,661	13,3
June	7,132	5,964	2,337	17,4
July	7,469	6,398	2,141	20,9
August	6,527	5,467	2,119	20,2
September	4,946	4,014	1,864	16,9
October	3,192	2,446	1,491	11,8
November	1,997	1,482	1,029	6,7
December	1,454	1,007	0,894	4,1

Table 30. Salamanca.

MONTH	Solar global irradiation on horizontal surface (kWh/m2·day)	Solar beam irradiation (kWh/m2·day)	Solar diffuse irradiation on horizontal surface (kWh/m2·day)	Temperature (°C)
January	1,468	0,569	0,898	10,6
February	2,209	1,596	1,225	10,5
March	3,395	2,476	1,837	11,6
April	4,345	3,128	2,433	12,7
May	5,105	3,570	3,071	15,4
June	5,699	4,166	3,066	18,1
July	5,692	4,174	3,035	20,9
August	5,008	3,681	2,656	21,3
September	4,165	3,182	1,964	20,3
October	2,638	1,950	1,377	17,0
November	1,683	1,185	0,996	12,7
December	1,244	0,854	0,779	11,2

Table 31. San Sebastián.

MONTH	Solar global irradiation on horizontal surface (kWh/m2·day)	Solar beam irradiation (kWh/m2·day)	Solar diffuse irradiation on horizontal surface (kWh/m2·day)	Temperature (°C)
January	2,822	1,354	1,468	16,9
February	4,398	3,522	1,751	17,0
March	6,129	5,305	1,647	17,7
April	6,171	4,972	2,398	17,8
May	6,133	4,692	2,881	19,3
June	5,383	4,253	2,261	20,5
July	6,226	4,924	2,605	22,9
August	6,807	5,622	2,369	23,7
September	5,517	4,384	2,265	22,8
October	5,166	4,402	1,529	21,7
November	3,424	2,650	1,549	19,4
December	3,022	2,327	1,390	17,8

Table 32. Santa Cruz de Tenerife.

MONTH	Solar global irradiation on horizontal surface (kWh/m2·day)	Solar beam irradiation (kWh/m2·day)	Solar diffuse irradiation on horizontal surface (kWh/m2·day)	Temperature (°C)
January	1,476	0,573	0,902	9,7
February	2,051	1,451	1,201	9,9
March	3,310	2,355	1,909	11,2
April	4,234	3,020	2,427	12,2
May	5,267	3,863	2,808	15,2
June	5,517	4,036	2,964	17,5
July	5,494	4,050	2,888	19,9
August	4,686	3,367	2,637	20,1
September	3,990	2,933	2,112	18,7
October	2,612	1,910	1,404	15,7
November	1,638	1,149	0,979	11,5
December	1,220	0,854	0,731	10,3

Table 33. Santander.

MONTH	Solar global irradiation on horizontal surface (kWh/m2·day)	Solar beam irradiation (kWh/m2·day)	Solar diffuse irradiation on horizontal surface (kWh/m2·day)	Temperature (°C)
January	2,502	1,483	1,019	10,5
February	3,324	2,575	1,498	11,7
March	4,698	3,836	1,724	13,9
April	5,434	4,199	2,468	15,9
May	6,673	5,335	2,675	19,8
June	7,232	5,946	2,572	23,2
July	7,460	6,287	2,346	26,7
August	6,489	5,350	2,278	26,8
September	5,378	4,411	1,935	23,7
October	3,835	3,125	1,422	19,0
November	2,482	1,894	1,176	14,1
December	2,157	1,661	0,991	11,0

Table 34. Sevilla.

MONTH	Solar global irradiation on horizontal surface (kWh/m2·day)	Solar beam irradiation (kWh/m2·day)	Solar diffuse irradiation on horizontal surface (kWh/m2·day)	Temperature (°C)
January	2,565	1,807	0,759	10,0
February	3,250	2,620	1,259	10,9
March	4,934	4,193	1,482	12,5
April	5,227	4,025	2,403	14,4
May	6,204	4,813	2,782	17,7
June	7,026	5,596	2,860	21,2
July	6,409	4,913	2,991	24,7
August	5,921	4,697	2,447	24,7
September	4,606	3,579	2,054	21,8
October	3,259	2,513	1,491	18,0
November	2,231	1,728	1,007	13,1
December	2,147	1,762	0,769	10,7

Table 35. Tarragona.

MONTH	Solar global irradiation on horizontal surface (kWh/m2·day)	Solar beam irradiation (kWh/m2·day)	Solar diffuse irradiation on horizontal surface (kWh/m2·day)	Temperature (°C)
January	2,194	1,185	1,008	10,5
February	2,932	2,192	1,479	11,3
March	4,260	3,298	1,924	13,0
April	5,409	4,217	2,384	14,6
May	6,435	5,018	2,834	18,1
June	6,995	5,542	2,906	21,4
July	6,972	5,589	2,766	24,6
August	6,096	4,809	2,574	24,9
September	4,743	3,653	2,181	22,1
October	3,449	2,679	1,541	18,0
November	2,268	1,677	1,183	13,4
December	1,905	1,442	0,926	10,8

Table 36. Valencia.

MONTH	Solar global irradiation on horizontal surface (kWh/m2·day)	Solar beam irradiation (kWh/m2·day)	Solar diffuse irradiation on horizontal surface (kWh/m2·day)	Temperature (°C)
January	1,901	1,040	0,860	4,0
February	2,683	2,005	1,356	5,7
March	4,266	3,518	1,499	7,7
April	4,793	3,557	2,472	9,7
May	5,960	4,500	2,919	13,4
June	7,125	5,863	2,524	17,4
July	7,463	6,349	2,228	21,3
August	6,513	5,495	2,035	20,9
September	4,915	3,995	1,841	17,6
October	3,138	2,402	1,471	12,6
November	1,900	1,358	1,086	7,1
December	1,388	0,950	0,875	4,3

Table 37. Valladolid.

MONTH	Solar global irradiation on horizontal surface (kWh/m2·day)	Solar beam irradiation (kWh/m2·day)	Solar diffuse irradiation on horizontal surface (kWh/m2·day)	Temperature (°C)
January	1,628	0,730	0,898	4,9
February	2,432	1,776	1,313	5,4
March	3,845	2,955	1,779	7,3
April	4,549	3,433	2,231	8,8
May	5,726	4,293	2,866	12,4
June	6,417	5,034	2,765	15,3
July	6,525	5,103	2,844	18,4
August	5,741	4,569	2,345	18,7
September	4,517	3,519	1,996	16,4
October	2,947	2,217	1,460	12,7
November	1,787	1,264	1,047	7,7
December	1,333	0,949	0,769	5,3

Table 38. Vitoria.

MONTH	Solar global irradiation on horizontal surface (kWh/m2·day)	Solar beam irradiation (kWh/m2·day)	Solar diffuse irradiation on horizontal surface (kWh/m2·day)	Temperature (°C)
January	1,598	0,660	0,938	6,4
February	2,473	1,856	1,234	8,0
March	3,750	2,903	1,693	10,5
April	4,616	3,355	2,522	12,9
May	5,634	4,233	2,801	17,1
June	6,422	4,955	2,934	20,9
July	6,448	5,011	2,875	24,3
August	5,731	4,455	2,552	23,7
September	4,428	3,426	2,003	20,1
October	2,874	2,179	1,389	15,2
November	1,778	1,257	1,041	9,8
December	1,337	0,925	0,825	6,8

Table 39. Zaragoza.

1.2. PORTUGAL

MONTH	Solar global irradiation on horizontal surface (kWh/m2·day)	Solar beam irradiation (kWh/m2·day)	Solar diffuse irradiation on horizontal surface (kWh/m2·day)	Temperature (°C)
January	2,712	1,407	1,305	16,8
February	3,451	2,623	1,656	16,6
March	4,553	3,570	1,965	16,6
April	5,324	4,127	2,396	16,6
May	5,907	4,521	2,771	17,8
June	5,386	3,913	2,946	19,3
July	6,156	4,600	3,113	21,5
August	5,808	4,555	2,505	22,7
September	4,903	3,691	2,425	22,7
October	3,827	2,924	1,806	21,2
November	2,935	2,175	1,521	19,3
December	2,600	2,001	1,198	17,9

Table 40. Funchal.

MONTH	Solar global irradiation on horizontal surface (kWh/m2·day)	Solar beam irradiation (kWh/m2·day)	Solar diffuse irradiation on horizontal surface (kWh/m2·day)	Temperature (°C)
January	2,119	0,974	1,145	12,2
February	2,862	2,182	1,360	12,4
March	4,701	3,795	1,812	13,5
April	5,270	4,050	2,439	14,5
May	6,401	4,889	3,023	16,8
June	7,224	5,807	2,833	19,4
July	7,259	5,993	2,533	22,1
August	6,620	5,585	2,071	22,5
September	5,165	4,144	2,042	21,4
October	3,596	2,859	1,473	18,4
November	2,123	1,552	1,141	14,6
December	1,868	1,378	0,980	12,4

Table 41. Lisboa.

MONTH	Solar global irradiation on horizontal surface (kWh/m2·day)	Solar beam irradiation (kWh/m2·day)	Solar diffuse irradiation on horizontal surface (kWh/m2·day)	Temperature (°C)
January	1,945	0,989	0,956	10,7
February	2,578	1,868	1,420	11,1
March	4,151	3,297	1,708	11,8
April	4,987	3,951	2,072	12,7
May	6,254	4,848	2,810	14,8
June	6,985	5,594	2,784	17,4
July	6,697	5,334	2,727	19,7
August	6,188	5,170	2,036	19,7
September	4,863	3,924	1,879	18,8
October	3,230	2,509	1,441	16,6
November	2,004	1,447	1,114	12,8
December	1,538	1,095	0,885	11,1

Table 42. Oporto.

MONTH	Solar global irradiation on horizontal surface (kWh/m2·day)	Solar beam irradiation (kWh/m2·day)	Solar diffuse irradiation on horizontal surface (kWh/m2·day)	Temperature (°C)
January	2,128	0,971	1,157	10,6
February	2,808	2,109	1,399	11,3
March	4,683	3,770	1,825	13,2
April	5,275	3,974	2,602	14,7
May	6,442	4,987	2,910	17,2
June	7,219	5,832	2,773	19,8
July	7,260	6,015	2,491	22,2
August	6,660	5,542	2,236	22,3
September	5,123	4,176	1,892	20,8
October	3,596	2,793	1,607	17,5
November	2,198	1,654	1,089	13,6
December	1,876	1,420	0,911	10,9

Table 43. Setúbal.